Effect of Confinement from Lateral Restraints in Circular Steel-free Concrete Deck Models Under Static and Fatigue Loading

by

Md. Rashedul Alam

A Thesis submitted to the Faculty of Graduate Studies of

The University of Manitoba

in partial fulfilment of the requirements of the degree of

Master of Science

Department of Civil Engineering

Faculty of Engineering

University of Manitoba

Winnipeg, Manitoba, Canada

THE UNIVERSITY OF MANITOBA

FACULTY OF GRADUATE STUDIES

*****

COPYRIGHT PERMISSION

Effect of Confinement from Lateral Restraints in Circular Steel-free Concrete Deck Models Under Static and Fatigue Loading

By

Md. Rashedul Alam

A Thesis/Practicum submitted to the Faculty of Graduate Studies of The University of Manitoba in partial fulfillment of the requirement of the degree

Of

Master of Science

Abstract

The bridge decks, especially in harsh cold weather, are prone to deterioration due to corrosion of internal reinforcing steels as a result of environmental effects and the application of de-icing salts. The concept of a steel-free bridge deck slab design was proposed to resolve this corrosion problem in the reinforcing steel of conventionally designed bridge deck slabs. This steel-free deck design concept is based on the internal arching action of the concrete deck slab subjected to concentrated loading. As a comparatively new concept, the steel-free bridge deck slab demands more experiment to understand its mechanics of behaviour and to enhance its performance. Researchers have proposed that a small-scale circular physical model similar to the rational mechanics model of steel-free deck slab can be used to study the behaviour of full-scale steel-free deck slabs. This small-scale circular steel-free deck models will save cost and time compared to building the full-scale deck models.

The primary objective of this research project was to investigate the static and fatigue behaviour of circular steel-free concrete bridge deck slabs. In addition, the effects of confinement on circular steel-free concrete decks subjected to freeze-thaw cycles were also studied in this research program. In total, three circular steel-free concrete deck slabs were constructed and tested under static and fatigue load until failure. All the slabs were designed according to the guidelines provided by Canadian Highway Bridge Design

Code. Among those three slabs, two slabs were confined with external wrap of CFRP sheets and six radial steel straps. The other slab was confined with only six radial steel straps and no circumferential CFRP wrap was provided on it.

The experimental results and analytical models indicated that confinement played an important role in punching shear failure of the steel-free deck slabs. The slabs confined with both CFRP wraps and radial straps failed in punching mode and the crack patterns were similar to that of full-scale steel-free concrete deck slabs. The experimental results suggested that the static and fatigue behaviour of small-scale circular steel-free deck slabs were similar to that of full-scale steel-free deck slabs. The strains in the steel straps and circumferential CFRP wrap indicate that at the beginning of fatigue tests, both the radial steel straps and circumferential CFRP wrap provided the lateral restrain to the slab. With progression of fatigue tests, the circumferential CFRP wrap rather than the radial steel straps provided the major confinement.

Acknowledgments

I would like to express my deepest gratitude to Dr. Aftab A. Mufti for his ideas, guidelines, supervision, continuous encouragement and financial support throughout this research project. The financial support from the University of Manitoba and ISIS Canada, A Network of centres of Excellence, are gratefully acknowledged.

I am very much thankful to Dr. Ehab El-Salakawy and Dean K. McNeill for their comprehensive assistance in reviewing and editing this thesis, and their helpful suggestions on improving the final outcome.

I would like to express my appreciations to Chad Klowak, Hughes Vogel, Amr El Ragaby and Grant Whiteside for their technical support and valuable assistance during fabrication, construction and testing of the specimens. I am also grateful to Mrs. Evangeline Murison and Mrs. Liting Han for their technical assistance to install the strain gauges and to setup DAQ for acquisition of test data. Special thanks are extended to all the staffs of ISIS Canada to provide the valuable administrative and clerical assistance. Help from all the fellow graduate students is also greatly appreciated.

Finally, I would like to thank FORTA© Corporation for supplying polypropylene fibers and Specialty Construction for supplying supporting instruments to do pull-off tests of the CFRP wrap of circular steel-free concrete bridge deck specimens.

Dedication

This thesis report is dedicated to my parents *Md. Shamsul Alam* and *Niru Raihan Ara Begum* for their loving support throughout my years as a student.

Contents

List of Tables

List of Figures

List of Copyrighted Materials

Title of copyright items	Source	Page No. in this thesis
Effect of Confinement from Lateral Restraints in Steel-Free Circular Deck Models Under Static Loading. By: Geethani Mediwake.	M.Sc. Thesis. University of Manitoba, Winnipeg, Manitoba, Canada. Date of Publication: 2006.	27, 28
A Study of Externally Reinforced Fibre-Reinforced Concrete Bridge Decks on Steel Girders. By: Lorna Jane Thorburn	Ph.D. Thesis. Dalhousie University, Halifax, Nova Scotia, Canada. Date of Publication: 1998.	112, 113, 114, F-2
The Behaviour of Steel-Free Concrete Bridge Deck Slabs Under Static Loading Conditions. By: John Patrick Newhook	Ph.D. Thesis. Technical University of Nova Scotia, Halifax, Nova Scotia, Canada. Date of Publication: 1997.	F-2
Experimental Investigation of Fibre-Reinforced Concrete Deck Slabs Without Internal Steel Reinforcement. By: Aftab A. Mufti, Leslie G. Jaeger, Baidar Bakht, Leon D, Wegner	Canadian Journal of Civil Engineering. 20(3). pp. 398-406, 1993.	F-2
Deck Slabs of Skew Girder Bridges. By: Baidar Bakht, Akhilesh C. Agaewal	Canadian Journal of Civil Engineering. 22(3), pp. 514-523, 1995	F-2

List of Symbols

A	Area of tire print
A_s	Cross sectional area of steel straps
d	Depth of slab
D	Longitudinal distance from wheel load to nearest strap
D_g	External diameter of specimen
E	Modulus of elasticity of the material of strap
f'_c	Compressive stress of concrete
f_{frpu}	Tensile strength in FRP sheet
f_{lfrp}	Ultimate confinement pressure due to FRP strengthening
F_s	A factor equal to 6 for outer panels and 5 for inner panels of steel-free deck slab
k	Concrete confinement constant
K	Elastic axial stiffness of strap
N	Number of load cycles

N_b Number of layers of FRP sheets

P Applied cyclic load

P_u Static fatigue load

S Spacing of supporting beams

S_g Clear span between girders

S_l Spacing of straps

t Thickness of slab

t_{frp} Thickness of one layer of FRP sheet

Φ_{frp} Resistance factor for FRP

List of abbreviations and Acronyms

AASHTO American Association of State Highway and Transportation Officials

ASTM American Society for Testing and Materials

CFRP Carbon Fibre-Reinforced Polymer

CHBDC Canadian Highway Bridge Design Code

CSA Canadian Standard Association

DAQ Data Acquisition System

FRC Fibre-Reinforced Concrete

LVDT Linear Variable Displacement Transducers

Chapter 1

Introduction

1.1 Overview

This thesis report describes the static and fatigue behaviour of three steel-free concrete bridge deck slabs. There are six chapters in this report. In Chapter 1, a brief discussion about the background of this research project is discussed. The objective and scope of this research project are also presented in this chapter. Chapter 2 describes a brief literature review followed by summary of a relative research projects. The detail of the experimental models, along with the experimental program including casting of circular steel-free concrete bridge decks, wrapping of circumferential CFRP sheet, freeze-thaw cycles, test setup and test procedure are explained in Chapter 3. The experimental results are presented in Chapter 4. At the end of this chapter, the experimental and theoretical results of circular steel-free concrete bridge deck obtained from this research program are compared with that of a full-scale steel-free slab to justify the logic behind using circular steel-free concrete bridge deck models to understand the mechanics of behaviour of the steel-free bridge deck concept. In Chapter 5, the major research findings along with conclusion and some recommendations for future work are presented.

1.2 Background

Bridges have always been considered as an important and expensive part of North American highway transportation infrastructure. Among all the components of a bridge's superstructure, the bridge deck is the most important component which directly sustains repeated moving wheel loads from passing traffic. That is why the deck is one of the bridge elements most susceptible to fatigue failure *(Sonoda et al. 1982).* Another important factor responsible for the deterioration of bridge decks are environmental effects, such as: freeze-thaw cycles. These problems of aging and deterioration of bridge decks are accelerated by the application of de-icing salt to melt the accumulated ice on bridge decks during winter. Saturated chlorides from the de-icing salt, along with the temperature and thermal cracking, accelerate the corrosion of the reinforcing steel and the corresponding deterioration of the deck concrete. As a result, these types of bridges particularly in cold climate need continuous maintenance. Many of the highway infrastructure network in Canada was constructed during early part of 20^{th} century. Although at that time, bridges were typically designed for a service life of 50 years, most of bridge decks have not been able to sustain the subjected environmental and service conditions. Due to the premature deterioration of the bridge decks, many of the bridges had to be repaired or replace before the end of their expected service life, which cost millions of dollars each year.

A significant reduction or elimination of the internal reinforcing steel would reduce the corrosion of the internal steel reinforcement and the deterioration of the deck concrete. This would also increase the life expectancy of the bridge deck slab. As an innovative solution of this problem the concept of a steel-free concrete bridge deck slab was proposed *(Mufti et al. 1991-a, Mufti et al. 1993)*. The steel-free concrete deck system is considered one of the most important developments in the bridge engineering field in the past 50 years. It is an innovative, economical, corrosion-free structural system to construct new bridges and to replace old reinforced concrete bridge decks. Three highway bridges and one forestry bridge have been constructed in Canada based on this steel-free concrete deck system *(Bakht et al. 1998)*. All of those steel-free bridged decks were constructed between 1995 and 1998. The deck slabs have been instrumented extensively to continuously monitor their performance under the influence of environmental effects and vehicle loads. All the bridges have been performing satisfactorily till now (2010).

1.3 Research objectives

The primary objective of this research program was to investigate the static and fatigue behaviour of circular steel-free concrete bridge deck slabs subjected to concentrated static and fatigue load. In addition, the effect of confinement on circular steel-free concrete decks subjected to freeze-thaw cycles was also studied in this research program. In 2006, a research investigation was carried out by Geethani Mediwake at the University of Manitoba to investigate the effect of concrete confinement on circular steel-free concrete deck models under static loading *(Mediwake 2006).* The experimental program demonstrated that the failure mechanism of circular steel-free concrete deck models is very similar to that of full-scale steel-free bridge deck models, and the load capacity of the circular decks can be predicted using the PUNCH program. In real life situations, bridge decks are subjected to fatigue loading from the wheel loads of passing traffic. This research program aims to extend Mediwake's experimental works and to investigate the effect of confinement on circular steel-free concrete deck models under fatigue load along with static load. Several goals or objectives were established at the onset of this project based on the primary objective of investigating the static and fatigue behaviour of circular steel-free concrete bridge decks. The objectives of this research program are summarized as follows:

- Ascertain the mode of failure of circular steel-free concrete deck slabs under concentric static and fatigue load,
- Study the effect of confinement on circular steel-free concrete deck slabs subjected to freeze-thaw cycles,
- Justify the possibility to incorporate small-scale circular steel-free concrete deck models to study the failure mechanics of steel-free deck slabs.

1.4 Scope of work

This thesis report presents the results of laboratory tests on three steel-free circular concrete deck slabs under both static and fatigue loading. The variables considered were degree of confinement of the slabs, types of loading, and amplitude of fatigue loading. Results obtained from the tests were ultimate load, slab deflections, strain in steel straps and circumferential CFRP wrap, crack widths and crack mapping. The scope of the work involved for this research project encompassed many different aspects of structural engineering. The work included:

- The structural design and construction of three circular steel-free concrete bridge deck models,
- The circumferential wrapping of circular steel-free concrete slabs with CFRP sheet,
- The complete design and installation of instruments for measuring displacement, strain, crack width and crack mapping,
- The design and construction of a base and load frame, including hydraulic pump and actuator, to apply static and fatigue loads,
- The design of a testing scheme,
- The complete analysis of experimental data,

- The use of analytical programs, such as the PUNCH programs, to investigate the goals previously outlined.

The above mentioned aspects will be discussed in the subsequent chapters.

Chapter 2

Literature Review

2.1 Chronological development of concrete bridge deck slab design method

2.1.1 Flexural design method

For many years, reinforced concrete bridge decks were designed throughout the world by the flexural design method. This design method is based on the assumption of failure due to bending of the deck slabs under the vehicle loads. This design technique necessitates the live load transverse moments obtained from the plate bending analysis. Reinforced concrete deck slab designed according to the flexural design method is specified by American Association of Highway and Transportation Officials *(AASHTO-LRFD 1998)*. This deck design method is also specified in Clause 8.18 of Canadian Highway Bridge Design Code *(CSA 2000)*. Reinforced concrete bridge decks designed using this method requires a high amount of steel reinforcement (between 3.2% and 4% of the volume of concrete). The mode of flexural failure and a typical bridge deck slab designed using flexural design method are shown schematically in Figure 1.

This flexural design method has been universal accepted for many years and decks designed by followed this method have been performing satisfactorily from the point of view of strength.

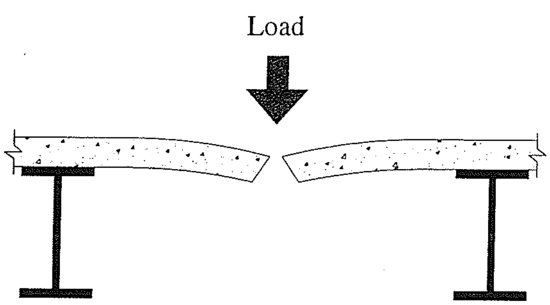

(a)

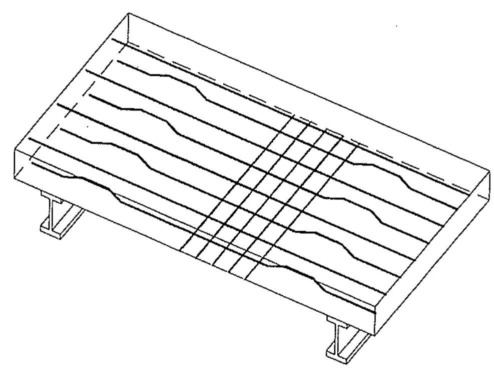

(b)

Figure 1: (a) Flexural failure mode of deck slab under a concentrated load, (b) Typical deck slab designed using flexural design method. Orange lines indicate bottom rebars and blue lines indicate alternate cranked rebars in transverse directions

2.1.2 Empirical design method

An extensive research programs were conducted in Ontario, Canada about three decades ago to investigate the failure mechanism of deck slabs *(Hewitt et al. 1975)*. The research program found that the mode of failure of concrete bridge deck slabs was a punching shear failure mode instead of being pure flexure failure mode. Besides that, the failure loads were much higher than those predicted by flexural theory. The main factor for the punching shear failure mode can be attributed to the presence of internal "arching action" that significantly enhances the overall strength. The "arching action" occurs due to the restraint of the slab provided by the bottom reinforcement and bridge girders in the transverse direction. The Ontario research program concluded that concrete slabs with only nominal steel reinforcement have more than adequate strength to sustain modern commercial heavy vehicles. In order to verify this concept, a prototype test bridge was tested in Ontario in 1975 *(Dorton et al. 1977)*. This research project established the concept that two layers of orthogonally distributed reinforcement of 1.2% of the volume of the concrete would be adequate to provide an acceptable safety margin for both the ultimate and serviceability conditions. In 1979, the Ontario Highway Bridge Design Code *(OHBDC 1979)* incorporated the empirical design method for designing bridge decks. Though the slab designed by the empirical design method requires less reinforcement, the slab is still susceptible to corrosion of the internal steel reinforcement.

The mode of punching shear failure and a typical bridge deck slab designed using empirical design method are shown schematically in Figure 2.

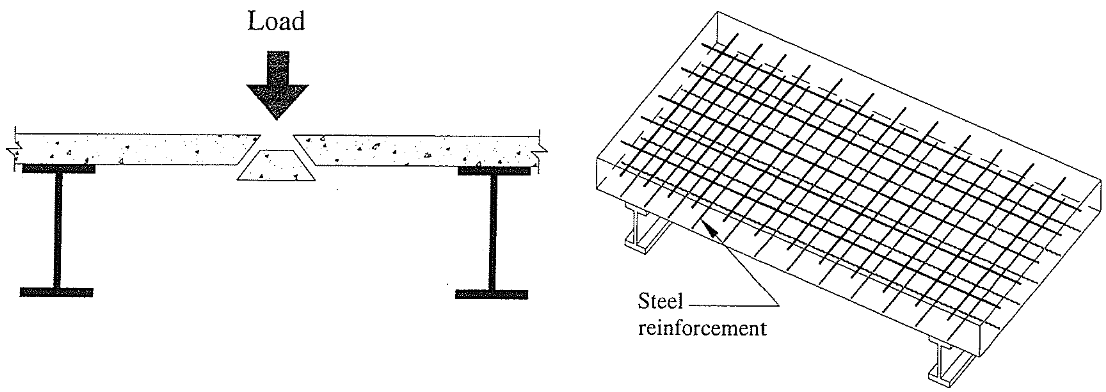

(a) **(b)**

Figure 2: (a) Punching shear failure mode of deck slab under a concentrated load, (b) Typical deck slab designed using the empirical design method. Orange lines indicate bottom rebars and blue lines indicate top rebars

2.1.3 Steel-free bridge deck design method

As an innovative solution to the corrosion problem in the internal reinforcing steel of bridge deck slabs, Mufti et al. proposed the concept of a steel-free concrete bridge deck slab *(Mufti et al. 1991-a)*. A steel-free concrete bridge deck slab is a bridge deck slab which is entirely free of any internal steel reinforcement. It is based on the concept of compressive arching action of the concrete deck slab subjected to concentrated loading. The slab is confined in both the longitudinal and transverse direction to ensure punching failure of the slab. The longitudinal confinement is provided by making the slab composite with longitudinal beams of high flexural rigidity using shear connectors. In the transverse direction, the slab is confined using steel straps welded to the top of the flanges of the longitudinal beams. When the slab is subjected to concentrated load, the slab deforms and the bottom face of the slab experiences tensile stress. Further application of the load initiates radial cracks on the bottom of the slab. If further load is applied, the transverse steel straps provide confinement and carry the tensile stresses. The compressive stresses are carried by the concrete. Thus the slab sustains loads through arching action. The ultimate load of the slab is determined by the degree of lateral restraint provided by the longitudinal beams and transverse straps. The magnitude of the loads causing cracking and failure of the deck slab are several times higher than that of flexural failure. The arching action on a steel-free bridge deck and a typical bridge deck slab designed using steel-free bridge deck design method are shown schematically in Figure 3.

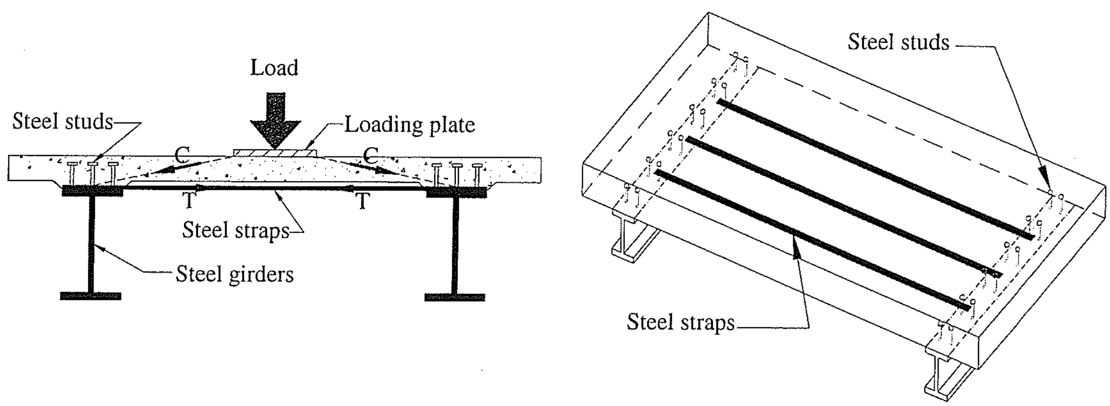

(a) (b)

Figure 3: (a) Arching action in steel-free bridge deck slab, (b) Typical deck slab designed using steel-free bridge deck design method

2.2 Design provision of steel-free bridge deck slabs in the CHBDC

The detailed guidelines for designing of steel-free Fibre-Reinforced Concrete (FRC) deck slab supported on girders are provided in clause 16.7 of the Canadian Highway Bridge Design Code *(CSA 2000)*. The guidelines provided by CHBDC for designing of steel-free FRC deck slab are summarized below:

- The deck slab should be composite with parallel supporting beams in the positive moment regions of the supporting beams.
- The spacing of supporting beams (S) should be less than or equal to 3.0 m.
- The thickness of deck slab (t) should be at least 175 mm and not less than $S/15$.
- The height of the haunch between the deck slab and the top of a supporting beam should be between 25 mm and 125 mm, and the minimum projection of the shear connecting devices in the deck slab (t_s) should be 75 mm. In addition, the minimum cover distance between the top of shear connecting devices and the top surface of the deck should be 75 mm.
- The top flanges of all adjacent supporting beams should be connected by an external transverse confining system, comprising straps that are perpendicular to the supporting beams.

- The spacing of straps (S_l) should not be more than 1.25 m.

- Each strap should have a minimum cross-sectional area (A_s) in mm^2, given by:

$$\frac{F_s S^2 S_l}{Et} 10^9$$

where, F_S = A factor equal to 6 for outer panels and 5 for inner panels,

S = Spacing of the supporting beam (m),

S_l = Spacing of the straps (m),

E = Modulus of elasticity of the material of the strap (MPa),

t = Thickness of the slab (mm).

- Randomly distributed fibre reinforcement is permitted in deck slabs for the control of cracks that develop in concrete during its early life. The fibre volume fraction in FRC shall be such that the post-cracking residual stress index (R_i) of the FRC is at least 0.30, where R_i is given by:

$$R_i = \frac{P_{pcr}}{P_{cr}}$$

Where, P_{pcr} = Post-cracking load of FRC test beam,

P_{cr} = Cracking load of concrete.

The guidelines provided by Canadian Highway Bridge Design Code are demonstrated in Figure 4.

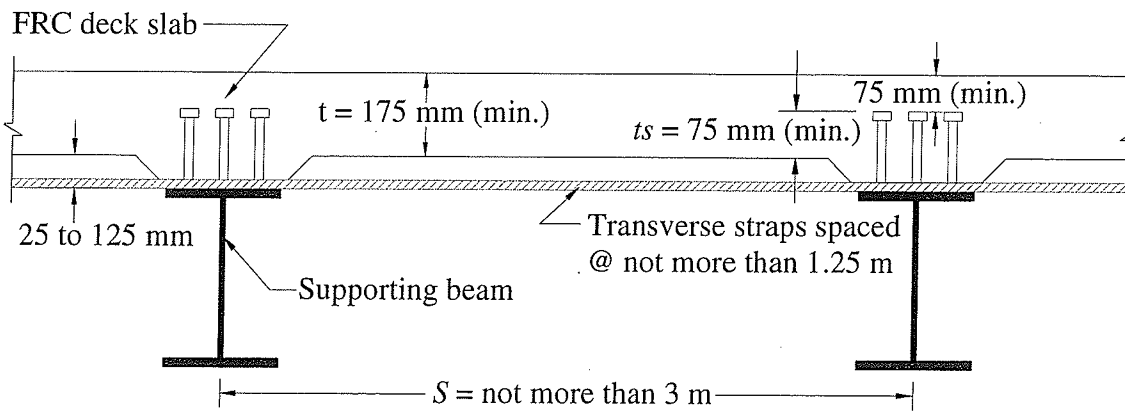

Figure 4: Summary of guidelines provided by CHBDC for designing of steel-free FRC deck slab supported on girders *(After CSA 2000)*

2.3 Effect of freeze-thaw cycles

2.3.1 Freeze-thaw effects on concrete

There are several hypotheses available regarding the effect of freeze-thaw cycles on concrete. Two of the most acceptable hypotheses are known as hydraulic pressure theory and osmotic theory.

The first hypothesis available, known as hydraulic pressure theory, was proposed by Powers in 1945 *(Powers 1945)*. According to this hypothesis, at freezing temperature, the pore water in the concrete start to freezes. Thus the volume of pore water increases by approximately 9% due to change of state from water to ice. This increased volume of ice forces the remaining water to move into the pores and generates internal hydraulic pressure. If the internal pressure is sufficiently high and exceeds the tensile strength of binding matrix, it initiate crack in the concrete. When the concrete are thawed back, the concrete become weaker than it was in its original condition. On repeating freezing and thawing, the concrete get weaker and finally disintegrate

In 1953, *Powers et al.* presented another hypothesis regarding the frost effect on concrete, known as osmotic theory (*Powers et al. 1953*). According to this theory, when the internal temperature of the concrete reaches the freezing point, the pore fluids in capillary cavities start to freeze. After the initially freezing of the pore fluids, the concentration of remaining unfrozen fluid raises. Due to the concentration difference of solution, the internal pressure develops within the concrete. This internal pressure creates unstable condition within the concrete and lead to produce cracking and finally crashing of concrete.

Proper air entrainment in concrete is considered as a potential solution of cracking due to freeze-thaw cycles *(NeVille 1995)*. This entrainment air, which is different from the accidentally entrained air, is incorporated into the concrete using suitable air-entraining agent. As the air is entrained into the concrete, discrete cavities are formed in the concrete paste. These cavities do not form continuous channel to pass the water, and thus the permeability of the concrete do not increase. The pressure, generated due to the freeze-thaw cycles, pumps the air out of the cavities and forces the water into the cavities. Thus, during freezing, escaping of the expanding water into the adjacent air-filled cavities prevents concrete form damage. It is suggested that, air entrainment of between 5% and

8% of the volume of concrete can protect concrete from damage due to freeze-thaw effect *(NeVille 1995)*. It is also recommended that the potential freeze-thaw damage can be reduced by following different ways *(NeVille 1995, Popovics 1992)*:

- limiting the water-cement ratio to 0.45,
- drying the aggregates before using into concrete mix,
- using smallest acceptable maximum aggregate size,
- providing impermeable coating on the coarse aggregate,
- maintaining minimum cement content of 335 kg/mm^3 of concrete,
- curing of concrete above 10°C for at least seven days,
- drying the concrete for minimum of 30 days.

2.3.2 Freeze-thaw effects on FRP sheets

Though fibre-reinforced polymer (FRP) sheets have been using in aviation industry for many years, they have been used as strengthening material of civil engineering structures now-a-days. These sheets are light in weight, high in strength and durability, and are free of corrosion. The constituent materials of FRPs are the high-resistance fibers and polymer resin matrix. The two major freeze-thaw effects on FRP sheets as identified by researchers are the thermal incompatibility and embrittlement (*Green 2007*).

The thermal incompatibility occurs due to the difference in the thermal expansion of the constituent materials of FRP sheets (fibers and polymer resin matrix). The coefficient of thermal expansion of FRP fibres varies from $-2\times10^{-6}/°C$ to $12\times10^{-6}/°C$ *(ISIS 2001)*. Whereas, that of polymer resin matrix range from $45\times10^{-6}/°C$ to $65\times10^{-6}/°C$ *(Mufti et al. 1991-b)*. When the FRP sheets are subjected to thaw effect, due to the differnce in coefficient of thermal expansion, different amount of expansion occur in the two constituent materials of FRP sheets. As a result of this unequal expansion, internal residual stresses develop in the interface of fibre and polymer resin matrix. This internal stresses initiate micro cracking at the fibre-matrix interface. The repeated freeze-thaw cycles lead to the formation of more cracks, increase in crack width, propagation of cracks through the resin matrix, and finally weaken the bonding between FRP and concert (*Green 2007*).

The second major freeze-thaw effect on FRP sheets is polymer embrittlement. The strength, stiffness and brittleness of polymer increase with decreasing the temperature. The increment of stiffness of polymer lead to reduction in the effectiveness of the matrix to transfer stresses between fibres, or between the FRP sheet and substrate concrete (*Green 2007*).

2.4 Effect of fatigue load on bridge deck slab

2.4.1 Fatigue performance of steel-free deck slab

Memon (2002) conducted a research to study the fatigue behaviour of a full-scale concrete bridge deck slab. The length and thickness of the slab were 9000 mm and

175 mm respectively. The slab was rested over two steel girders spaced at 2000 mm center-to-center. The composite action between the slab and steel girders were ensured using shear connectors. The slab had a cantilever overhang of 500 mm length beyond the center of each girders. The monolithically casted slab was divided into three segments (A, B and C). Segment A was reinforced with two meshes of steel reinforcement. Segment B and C were reinforced with a crack control grid of CFRP and GFRP bars. Segment B and C were confined externally using 25.5 mm × 38.1 mm transverse steel straps spaced at 1000 mm interval. The three segments were tested under a cyclic load which peaked at 60 tonne.

The experimental results indicated that all the segments of the slab failed in punching shear failure mode. The segments A, B and C failed after 23162, 198863 and 420682 load cycles respectively. Segment C, which was transversely confined using external steel straps and was reinforced using GFRP bars, showed best fatigue resistance. From the results of the fatigue tests, it was concluded that the fatigue resistance of steel-free deck slabs depend on the types of confinement. Moreover, either the deflection of slab, strain in transverse straps or crack width can be considered as an indicator of fatigue damage in steel-free concrete deck slabs.

2.4.2 Fatigue performance of cantilever overhang

Klowak (2007) conducted another research to study the fatigue behaviour of cantilever overhang of a full-scale concrete bridge deck slab. The length and thickness of the slab were 9000 mm and 200 mm respectively. The slab was rested over two steel girders spaced at 2500 mm center-to-center. The composite action between the slab and steel girders were ensured using shear connectors. The slab had a cantilever overhang of 1250 mm length beyond the center of each girders. The monolithically casted cantilever overhang was divided into three segments (D, E and F). The internal panel of the slab was confined externally using 50 mm × 25 mm transverse steel straps spaced at 1200 mm interval. All the segments were reinforced with #10 GFRP bottom bars spaced at 200 mm center-to-center. The top of the slab was longitudinally reinforced using #10 GFRP bars at 600 mm center-to-center. Segment D and F contained 2-#19 top transverse GFRP bars and 1-20 M top transverse steel bars spaced at 200 mm center-to-center. The central cantilever section (E) had 2-#13 top transverse CFRP bars spaced at 200 mm center-to-center. The three segments were tested under cyclic load.

The experimental results indicated that all the segments of cantilever overhang failed in punching shear failure mode. At first, the longitudinal cracks developed over the girders. The width of the longitudinal crack did not increase throughout the fatigue life of cantilever overhang. The second cracks observed below the concentrated loading plate were the full-depth transverse cracks. The last cracks observed at the top of cantilever overhang, in a semi-circular pattern around the loading plate, were the circumferential cracks. Both the transverse and circumferential cracks widened as the cantilever approached failure. From the results of the fatigue tests, it was concluded that arching-action presents in the cantilever overhang which lead to punching shear failure.

2.5 Fatigue life evaluation models for steel-free concrete deck slabs

In real life situation, a bridge deck slab experiences a large numbers of moving load (from moving wheel of passing vehicles) of different amplitude. On the other hand, in laboratory, the slabs are tested under small numbers of fatigue load of constant amplitude. This mathematical fatigue life models can be used to obtain the number of fatigue load cycles of fixed amplitude, that are required to cause the damage in a deck slab, which (damage) is equivalent to the cumulative damage caused by a given number of another load cycles of known amplitude. Several researches *(Matsui et al. 2001, Mufti et al. 2002, Memon 2005, El-Ragaby et al. 2007)* proposed different fatigue life evaluation models for steel-free bridge deck slabs. These empirical models were proposed based on the laboratory test results. Some of those models are discussed in the following sections.

2.5.1 Model proposed by Matsui et al.

In 2001, based on the fatigue tests on steel-free and reinforced concrete deck slabs under the Wheel Running Machine, *Matsui et al. (2001)* proposed a fatigue life model as below.

$$\log(\frac{P}{P_u}) = -0.07835\log(N) + \log(1.52)$$

where P is applied cyclic load, P_u is static fatigue load and N is number of load cycles. For static failure ($N = 1$), this equation gives the value of P/P_u equal to 1.52. *Matsui et al. (2001)* mentioned that this mathematical model is valid for N greater than 10,000, and is applicable to both reinforced and steel-free concrete bridge deck slabs.

2.5.2 Model proposed by Mufti et al.

In 2002, based on the compression fatigue test on concrete cylindrical specimens, *Mufti et al. (2002)* proposed another fatigue life model as below.

$$\frac{P}{P_u} = 1.0 - \frac{\log(N)}{30}$$

where P is applied cyclic load, P_u is static fatigue load and N is number of load cycles. For static failure ($N = 1$), this equation yields correct result of P/P_u (equal to 1.0). This model is applicable to all concrete deck slabs along with the steel-free bridge deck slabs.

2.5.3 Model proposed by Memon

In 2005, based on the fatigue test results of full-scale steel-free concrete deck models, *Momon (2002)* proposed the following equation to predict the number of load cycles to fatigue failure.

$$N = 10 \times \sqrt[6]{\frac{1}{(P/P_u)} - 1}$$

where P is applied cyclic load, P_u is static fatigue load and N is number of load cycles. This fatigue model demonstrates that the value of P/P_u is equal to 1.0 for static failure ($N = 1$). Moreover, for P = 0, the relationship yields infinite.

2.5.4 Model proposed by El-Ragaby et al.

In 2007, based on the compression fatigue test on concrete bridge deck slabs reinforced with glass fiber-reinforced polymer (GFRP) composite bars, *El-Ragaby et. al (2007)* proposed a fatigue life model as below.

$$\frac{P}{P_u} = 0.0034(\log N)^2 - 0.11873(\log N) + 1.0752$$

where P is applied cyclic load, P_u is static fatigue load and N is number of load cycles. For static failure ($N = 1$), this equation yields the value of P/P_u equal to 1.075.

2.5.5 S-N curves

The graphical representation of the above mentioned fatigue life evaluation models are called 'S-N curves' and are shown in Figure 5. For N greater than 10,000, all of these models show nearly same results. The S-N curves also suggest that, for P/P_u equal or less than 0.2, the fatigue life of the steel-free bridge deck slab is infinite. This indicates that, if a steel-free deck slab is subjected to the fatigue load having amplitude less than or equal to 20%, it will take infinite number of load cycles to fail.

According to AASHTO *(AASHTO 2002)*, the minimum number of fatigue load cycles require to fail a bridge deck slab should be 2,000,000. For N = 2,000,000, the value of P/P_u yield by the models proposed by Matsui et al., Mufti et al., Memon and El-Ragaby et al. are 0.49, 0.52, 0.48 and 0.46 respectively.

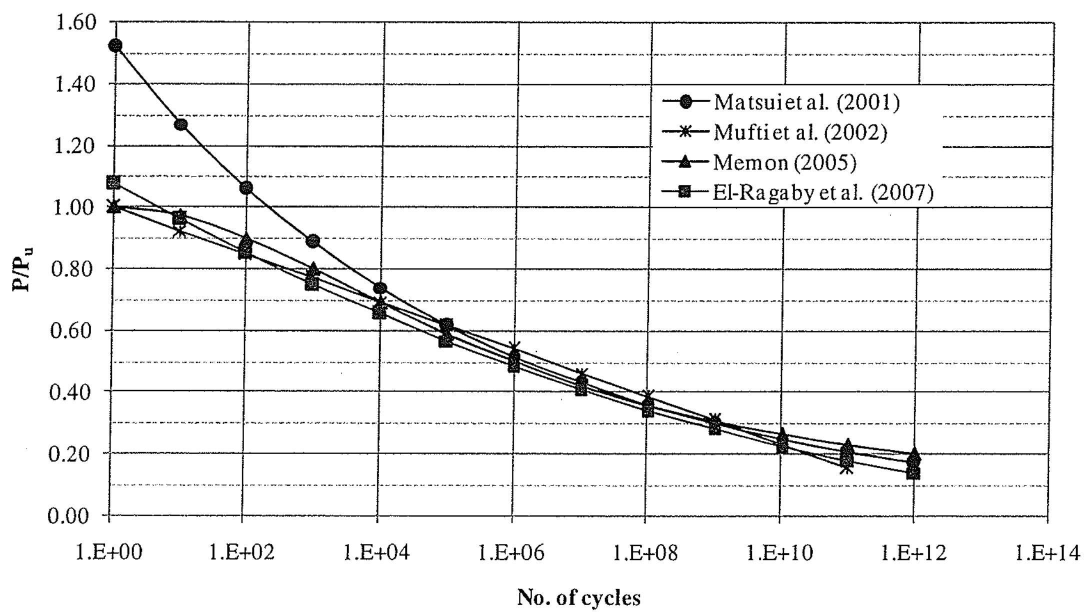

Figure 5: Comparison of S-N curves of different fatigue life evaluation models

2.6 Related research

In 2006, Geethani Mediwake conducted a research at The University of Manitoba to study the effects of confinement from lateral restraints in circular steel-free concrete deck models under static loading *(Mediwake 2006)*. The experimental program consisted of static loading tests on nine circular steel-free concrete deck models. The experimental models were designed and confined according to the guidelines provided in section 16.7 of the Canadian Highway Bridge Design Code *(CSA 2000)*. Confinement was provided in three ways: using a reinforced concrete ring beam, using external radial steel straps, and using external carbon fiber reinforced polymer (CFRP) wraps in the circumferential direction. Some specimens without any confinement were also tested for the purpose of comparison of the test results with that of other slabs with confinement. The external diameter of the circular deck models was chosen to be 1,810 mm. The depth of the slabs was 175 mm, which is the minimum thickness recommended by the CHBDC for steel-free slabs.

According to the geometric properties and the methods of confinement, the deck models were divided into two groups. The first group consisted of five specimens, which were with or without external steel straps. Each of the circular deck slabs was seated on a ring beam which provided confinement of the concrete slabs as well as acted as a supporting beam for the concrete deck. The width and height of the ring beam was 225 mm and 375 mm, respectively. The ring beam was reinforced using three 15M steel bars on both top and bottom, and with 15M stirrups spaced at 155 mm centre-to-centre. The ring beam stirrups were extended into the circular deck to provide composite action between the ring beam and the concrete deck. Two of the specimens (designated as G1-6SC and G1-6S) were confined using six radial steel straps and another two specimens (designated as G1-8SC and G1-8S) were confined using eight radial steel straps. One specimen (designated as G1-0S) was cast without any steel straps or CFRP wrap for the purpose of comparison of the test results with that of other slabs with confinement. The area cross sectional area of each steel strap was 20 mm× 40 mm. For the specimens with radial steel straps, the composite action between straps and concrete was ensured using two 19 mm diameter Nelson steel studs provided at the top and bottom on the end of each straps. The specimens were designed with a haunch of 75 mm height over each ring beam so that the radial steel straps passed through the haunch of the deck slab above the ring beam. Typical specimen dimensions and details of reinforcement of samples of Group 1 are illustrated in Figure 6.

The second group consisted of four specimens, which were designed without any ring beam. Confinement was provided by external steel straps and/or external CFRP wraps. Two of the specimens (designated as G2-6SC and G2-6S) were confined using six radial steel straps and one specimen (designated as G2-4SC) was confined using four radial steel straps. One specimen (designated as G2-0S) was cast without any steel strap or CFRP wrap for the purpose of comparison of the test results with that of other slabs with confinement. The width and height of the base of the circular slab were 275 mm and 50 mm, respectively. The total thickness of the haunch and transition was 50 mm. The composite action between the straps and the concrete was ensured using three 19 mm diameter Nelson steel studs provided at the top end of each strap. Typical specimen dimensions and details of samples of Group 2 are illustrated in Figure 7.

All the specimens were tested under monotonic load until failure. The experimental results suggested that confinement played an important role in punching shear failure and was the key to the development of arching forces within the concrete. This arching force contributed to the load carrying capacity of circular decks. In the absence of ring beam restraint, use of radial straps alone did not seem to influence triaxiality significantly to confirm punching failure, but straps combined with CFRP did result in inducing a punching failure. The mode of failure of the circular slabs sufficiently confined with steel straps and a ring beam or CFRP wraps, was punching shear failure. The other deck models without any confinement failed in flexure. The ring beam provided a greater amount of confinement compared to the straps. External steel straps did not significantly contribute to the ultimate failure load but did increase the stiffness of the specimens.

The computer program called PUNCH was use to analyse the slab. The analytical results obtained using the computer program matched well with that of the experimental results of the circular slab designated as G2-6SC (having six radial steel straps and circumferential CFRP wrap) of second group.

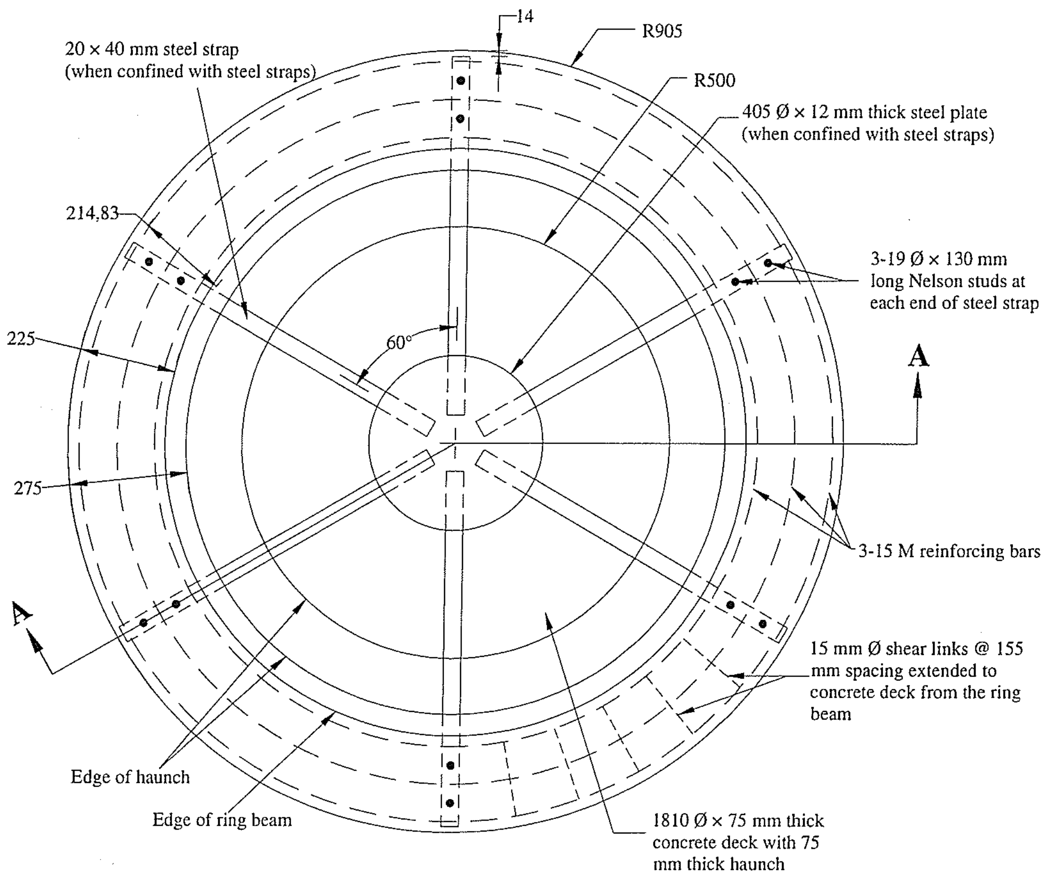

Bottom View

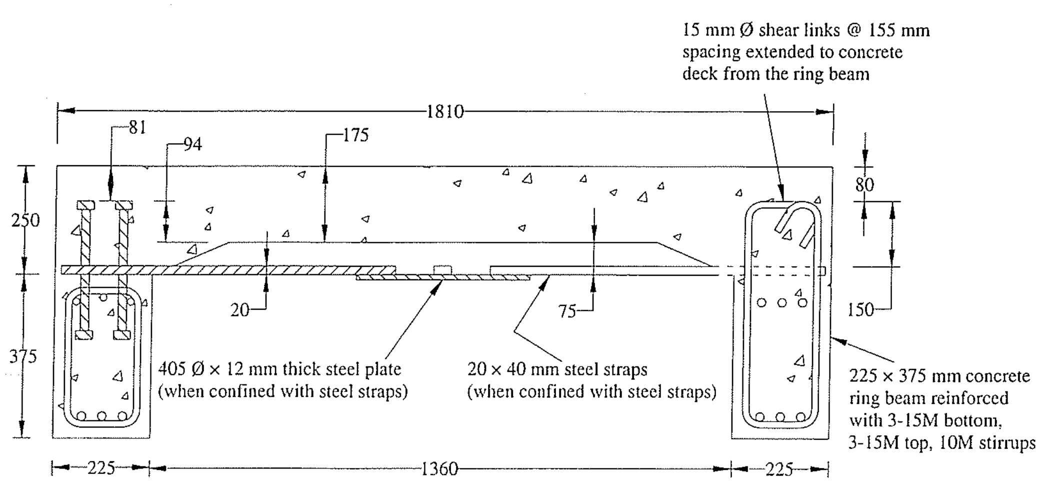

Section A-A

Figure 6: Typical specimen detail of Group 1 specimens *(After Mediwake 2006)*

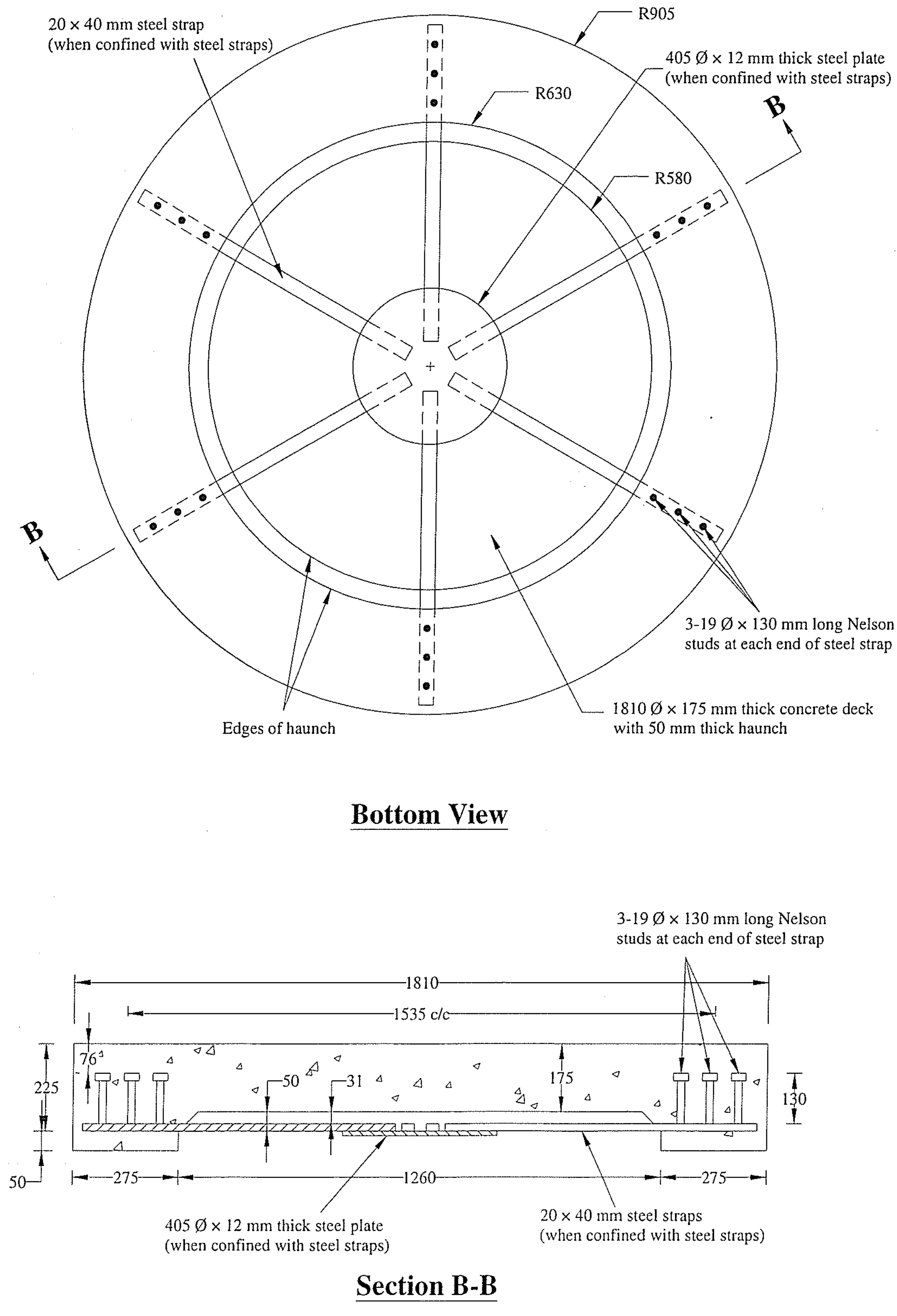

Figure 7: Typical specimen detail of Group 2 specimens *(After Mediwake 2006)*

Chapter 3

Experimental Program

3.1 Detail of specimens

In total three identical circular steel-free concrete deck models were built for this research program. As discussed in section 2.5 the analytical results obtained using the computer program (PUNCH program) matched well with that of the experimental results of the circular slab designated as G2-6SC (having six radial steel straps and circumferential CFRP wrap) of second group. A similar slab of G2-6SC *(Mediwake 2006)* will be used for this research program. The slabs were designed following the guidelines provided by Clause 16.7 of Canadian Highway Bridge Design Code *(CSA 2000)*. The guidelines provided by Canadian Highway Bridge Design Code (CHBDC) are summarized in section 2.2. Typical detail of the circular steel-free concrete deck slabs is demonstrated in Figure 8. The design and details of the specimens is discussed in the following sections.

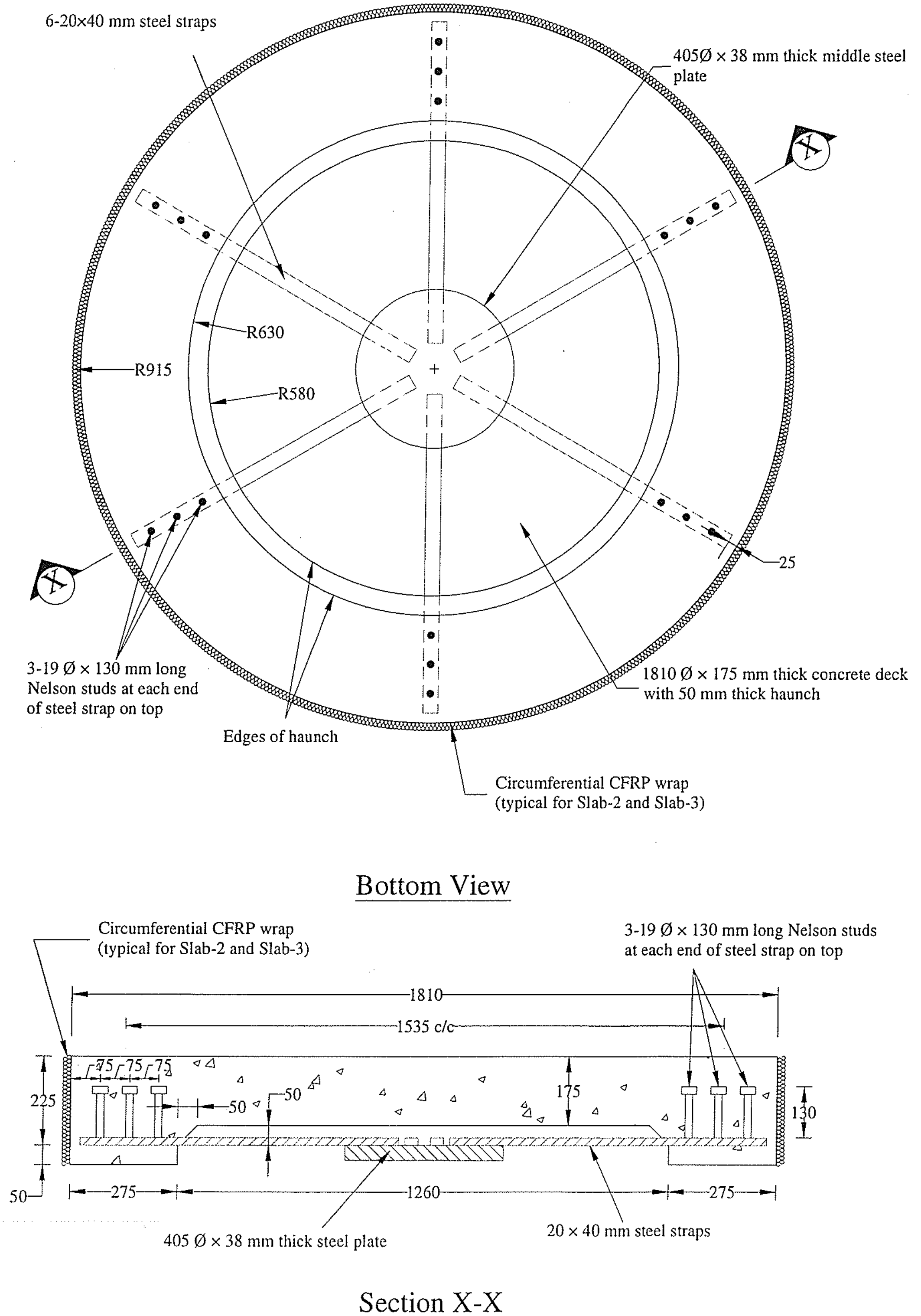

Figure 8: Typical detail of circular steel-free concrete deck slabs

3.1.1 Detail of radial steel straps

The number and cross sectional area of the steel-straps was selected based on the experimental and theoretical results of previous research work done by Geethani Mediwake *(Mediwake 2006)*. As discussed in section 2.5, the analytical results obtained using the computer program (PUNCH program) matched well with that of the experimental results of the circular slab designated as G2-6SC (having six radial steel straps and circumferential CFRP wrap) of second group. For this research program, the design of the steel straps was chosen to be similar to that of the slab designated as G2-6SC of Geethani Mediwake *(Mediwake 2006)* research workl. Detail of the steel straps is shown in Figure 9. Six external radial steel straps were used to transversely confine each of the circular steel-free concrete deck slabs. The cross sectional area of each steel strap was 20 mm × 40 mm. The calculations related to the design of radial steel straps are presented in Appendix A. The steel straps were welded together with a central steel circular plate of 405 mm diameter and 38 mm thickness. It is worth noting that the thickness of the circular plate of previous research work *(Mediwake 2006)* was 12 mm. The thickness of the central steel circular plate was increased to check if it would affect the degree of confinement and the mode of failure of the circular steel-free deck slab. The composite action between the steel straps and concrete was ensured using three 19 mm diameter Nelson steel studs provided at the end of each steel strap on top.

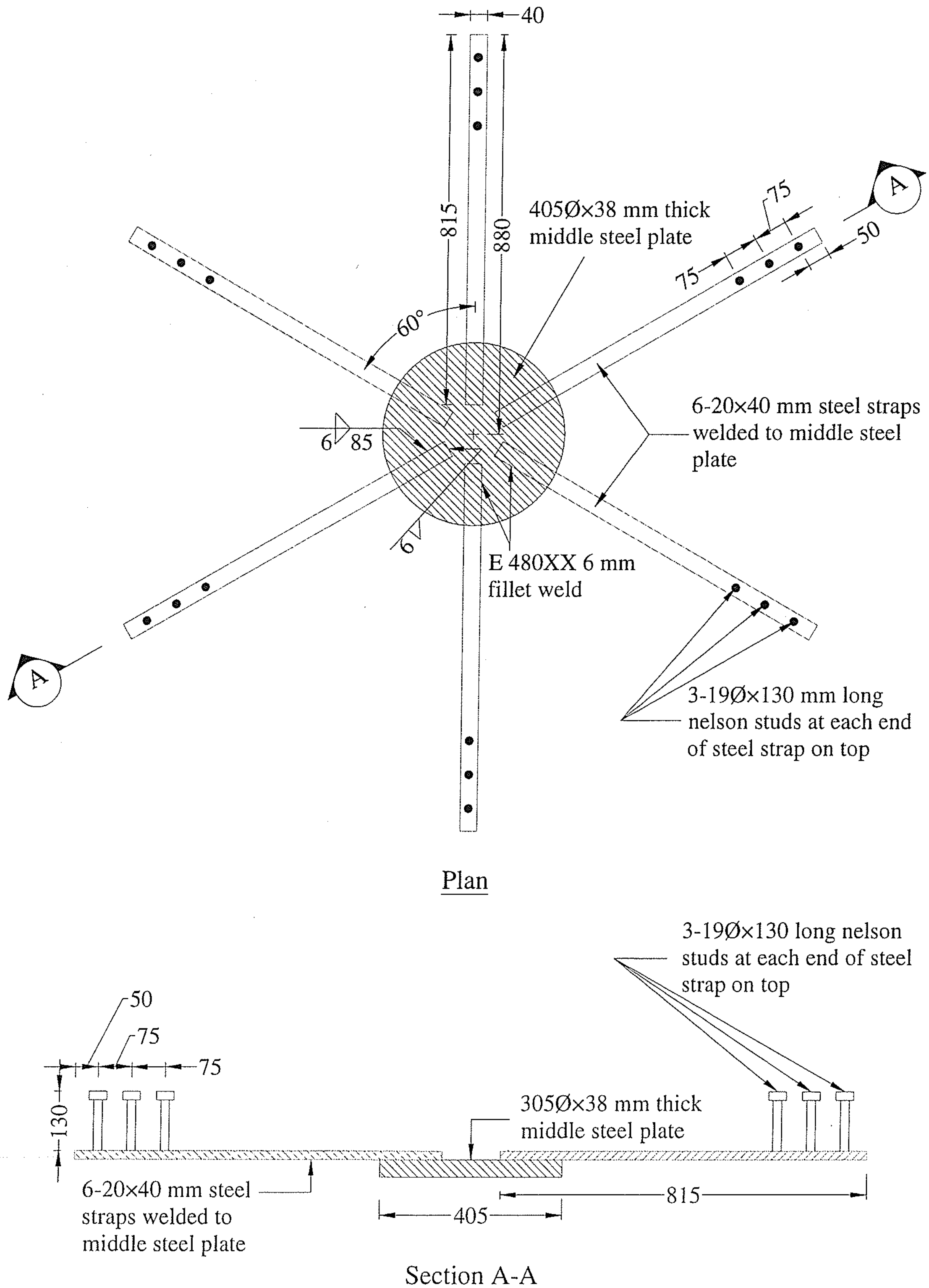

Figure 9: Detail of radial steel straps

3.1.2 Detail of concrete slab

The external diameter of the circular steel-free concrete deck models was selected as 1810 mm so that the deck models would fit into the laboratory's environmental chamber. The thickness of the decks was selected to be 175 mm, which is the minimum thickness recommended by CHBDC for steel-free deck slabs. A circular base having width and height of 275 mm and 50 mm respectively was built as an integral part of the slab. The specimens were designed with a haunch of 50 mm of depth over each circular base. The steel straps passed through the haunch of the deck slab, above the circular base. Four lifting hooks were provided at the mid height of the four corners of the circular base to provide lifting points for movement of the circular decks. Polypropylene fibers, supplied by FORTA Corporation, and of 38 mm length were mixed with the concrete (0.3% by weight) to control shrinkage and thermal cracking.

3.1.3 Detail of circumferential CFRP wrap

The second and third test specimens (Slab-2 and Slab-3) were confined by circumferential wrapping of unidirectional high strength carbon fiber reinforced polymer (CFRP) sheets. The first sample (Slab-1) was not confined by any circumferential CFRP wrap. The CFRP wrapping for Slab-2 and Slab-3 was designed according to the guidelines provided by the ISIS Canada Design Manual-4 *(ISIS 2001)*. The ultimate confining pressure due to FRP strengthening was determined using the following equation provided by ISIS Canada Design Manual-4:

$$f_{lfrp} = \frac{2N_b \phi_{frp} f_{frpu} t_{frp}}{D_g}$$

where f_{lfrp} = Ultimate confinement pressure due to FRP strengthening (MPa)

N_b = Number of layers of FRP sheets

Φ_{frp} = Resistance factor for FRP

f_{frpu} = Tensile strength in FRP sheet (MPa)

t_{frp} = Thickness of one layer of FRP sheet (mm)

D_g = External diameter of the specimen (mm)

According to the *Thériault et al. (2000)*, the minimum confinement pressure (f_{lfrp}) from FRP confining wrap should be 4 MPa. Following the guidelines provided by ISIS Canada Design Manual-4 *(ISIS 2001)*, the number of layers of CFRP sheets required to circumferentially confine the circular decks was selected to be four. The calculations related to the design of radial steel straps are presented in Appendix A. The properties of the Wobo®MBrace system, that was used to circumferentially confine the circular steel-free deck slabs, are presented in Appendix B. The width of the CFRP layers was selected to be 275 mm which was the same as the height of the edge of the slab. The procedure of circumferential wrapping of CFRP sheets are described in section 3.4.

3.2 Casting of slabs

All the specimens for this research program were cast and tested in the W.R. McQuade Structural Laboratory at the University of Manitoba. A set of circular wooden formwork was manufactured as shown in Figure 10. A three dimensional array of 12 electric strain gauges, arranged as a cube, was placed at the centre of the slab. The strain cube was glued to the formwork to prevent movement and rotation. Detail description of the three dimensional array of strain gauges is presented in section 3.7.6. Ready mixed concrete of grade 35 MPa was ordered from ready-mixed concrete supplier 'Lafarge'. The volume of concrete required for each deck model was approximately one cubic meter. Slump test was conducted just after arrival of the concrete to the laboratory to determine the workability of the supplied concrete following the guidelines provided by ASTM C 143/C 143M-03 standard specification *(ASTM 2003)*. After that, 0.3% (by volume of concrete) polypropylene fibers were mixed with the concrete to control shrinkage and thermal cracking. As mixing of polypropylene fibers reduces the workability of concrete, superplasticisers were mixed with the concrete to increase the workability. Superplasticisers were mixed with the concrete until the desired slump (190 mm or greater) was achieved. After achieving the required slump, the inverted slump cone test was conducted to check the workability of the concrete for compliance with ASTM C 995-01 standard specifications *(ASTM 2001)*. Photographs of typical slump tests and inverted slump cone tests are shown in Figure 11.

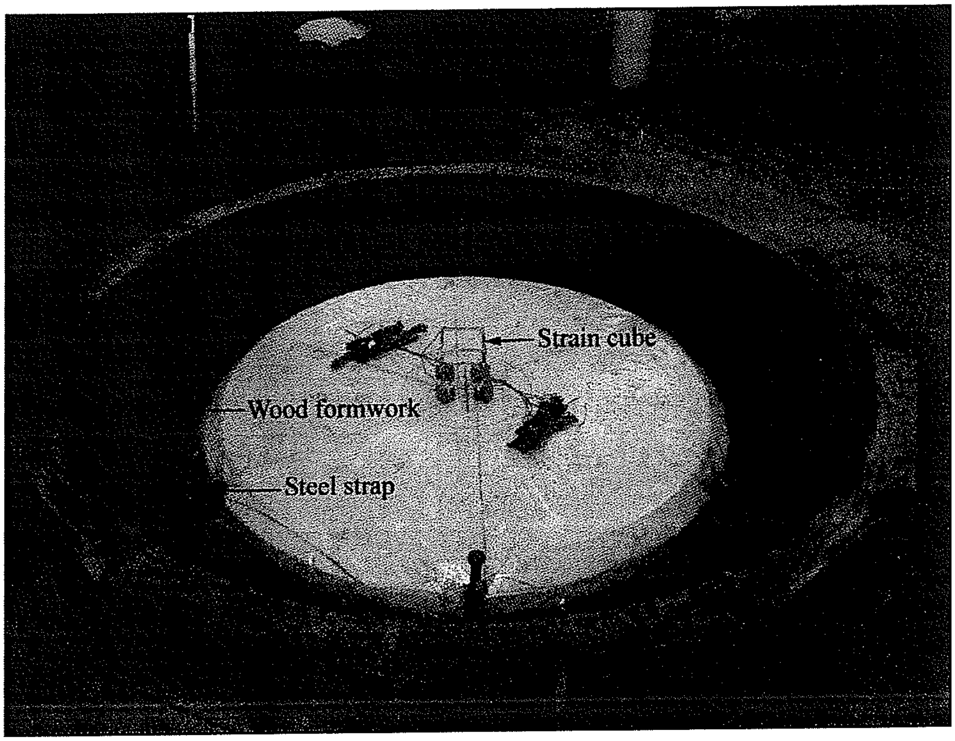

Figure 10: Formwork used to cast the circular steel-free deck slabs

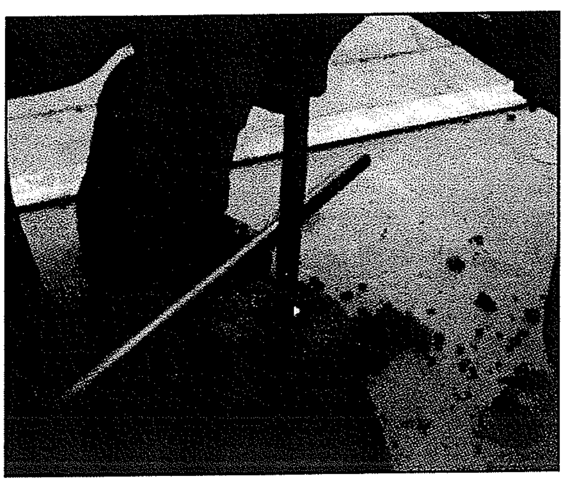

(a) Slump cone test

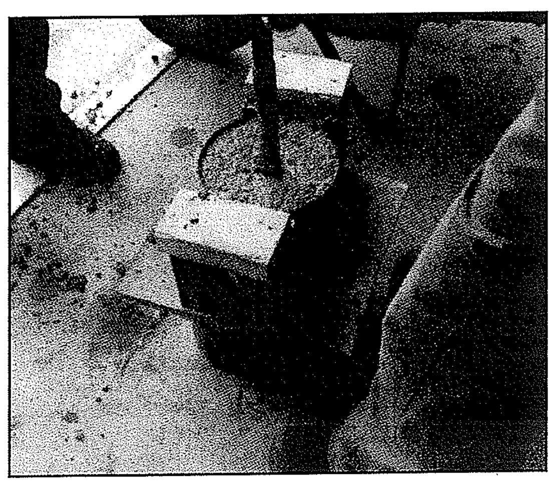

(b) Inverted slump cone (flow) test

Figure 11: Slump cone test and inverted slump cone (flow) test

The time required to flow the fiber-reinforced concrete through the inverted slump cone apparatus were recorded. In total 18 concrete cylinders for each deck slab were cast for future compression and tension tests. At last the concrete was placed on the formwork as shown in Figure 12.

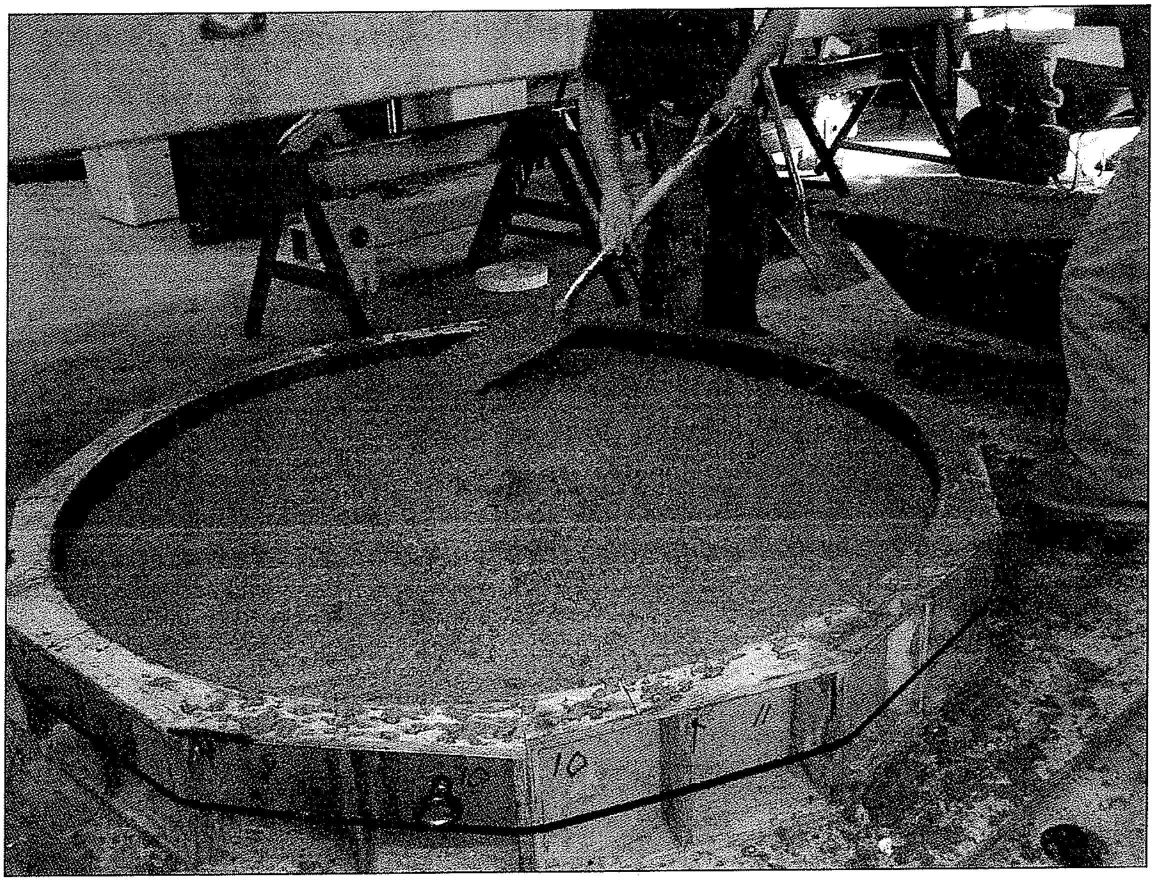

Figure 12: Casting of circular steel-free concrete deck slab

Concrete cylinder compressive strength tests were conducted following the guidelines provided by ASTM C 39/C 39M-05e standard specification *(ASTM 2005)* and splitting tensile strength tests were conducted following the guidelines provided by ASTM C496/C 496M-04 standard specification *(ASTM 2004)*.

The specific concrete parameters are outlined in Table 1.

Table 1: Specified concrete parameters

Slab designation	**Slab-1**	**Slab-2**	**Slab-3**
Cement type	Normal (Type 10)	Normal (Type 10)	Normal (Type 10)
Maximum aggregate size (mm)	16 mm	16 mm	16 mm
Specific air content (% by volume)	5-8	5-8	5-8
Polypropylene fibers (% by volume)	0.3	0.3	0.3
Slump test result (mm)	195	210	200
Flow test result (Seconds)	34.56	28.18	35.00
Target 28-day concrete compressive strength (MPa)	35	35	35
28-day concrete cylinder compressive strength (MPa)	40.00	46.28	32.90
28-day concrete cylinder tensile strength (MPa)	3.43	3.93	3.35

The concrete cylinder data from the tests are outlined in Appendix C.

3.3 Casting of circular supporting ring beam

A circular reinforced concrete beam of 1810 mm external diameter, 1260 mm internal diameter and 275 mm height was used to provide support during testing of Slab-2 and Slab-3. The beam was reinforced with two 10M top bars and three 20M bottom bars. 10M stirrups were provided at an interval of 200 mm centre-to-centre. The detail of the ring beam is shown in Figure 13 and the casting of the ring beam along with the finished ring beam is shown in Figure 14. The concrete cylinder data from testing for the circular beam are outlined in Appendix C.

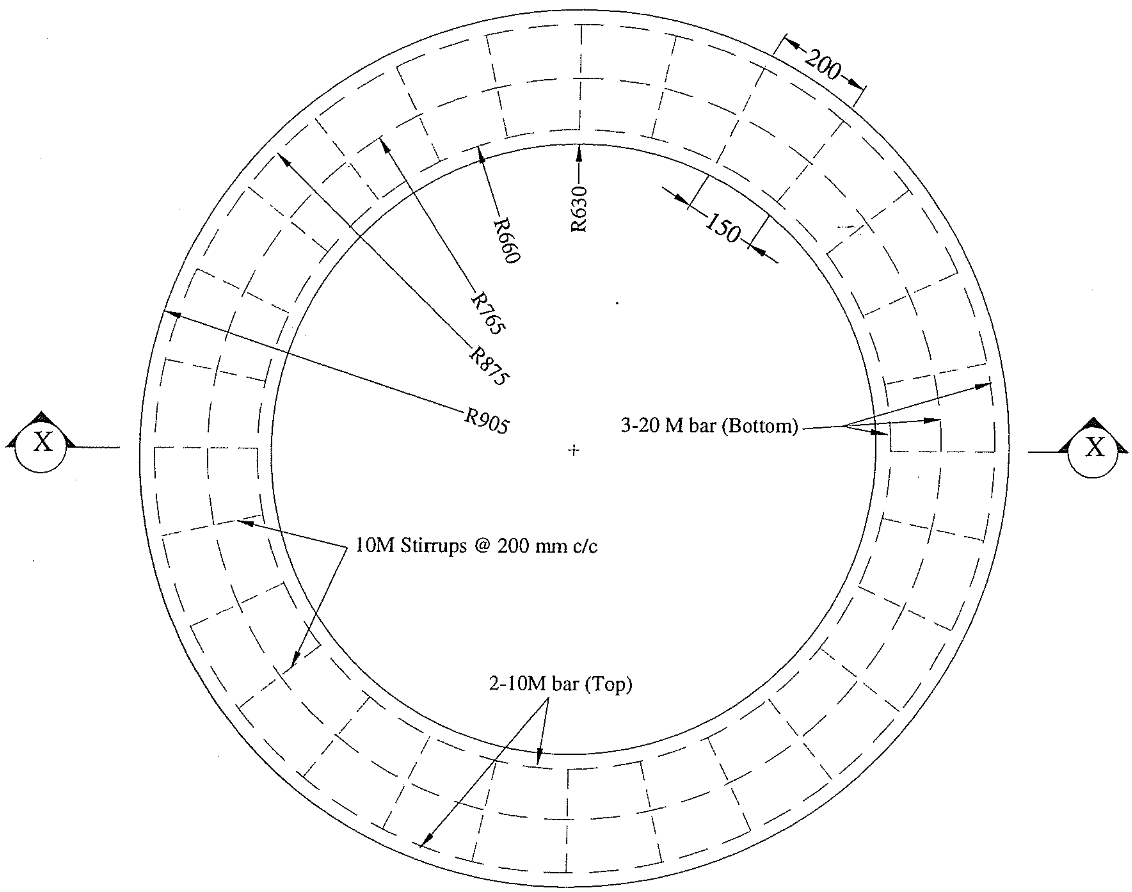

Bottom view

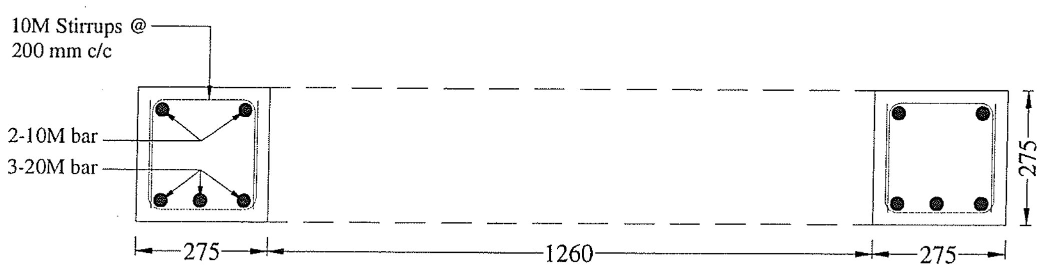

Section X-X

Figure 13: Detail of circular supporting reinforced beam

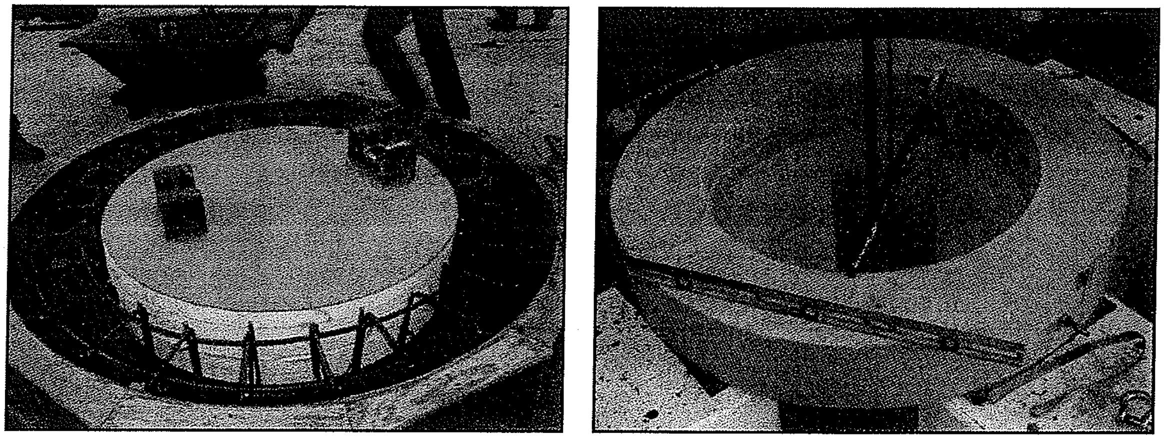

(a) (b)

Figure 14: (a) Casting of supporting circular reinforced concrete beam, (b) finished supporting circular reinforced concrete beam

3.4 Circumferential wrapping of CFRP sheet

Slab-2 and Slab-3 were confined by circumferentially wrapping them with unidirectional high strength carbon fiber reinforced polymer (CFRP) sheets. The procedure used to wrap the circular slabs with CFRP sheets is called the CFRP strengthening system or the Wabo®MBrace system *(Wobo MBrace 2008)*. Wabo®MBrace system consisted of four components: primer, putty, saturant and CF 160. Different steps of CFRP wrapping procedure are demonstrated in Figure 15. At first the surface of the concrete was smoothed using a grinder. Wabo®MBrace primer was the first component of the CFRP strengthening system that was applied by brush to the concrete surface. It was a low viscosity, 100% solid, and polyamine cured epoxy. As the first applied component of the Wabo®MBrace system, it was used to penetrate the pore structure of cementious substrates and to provide a high bond base coat for the Wabo®MBrace system.

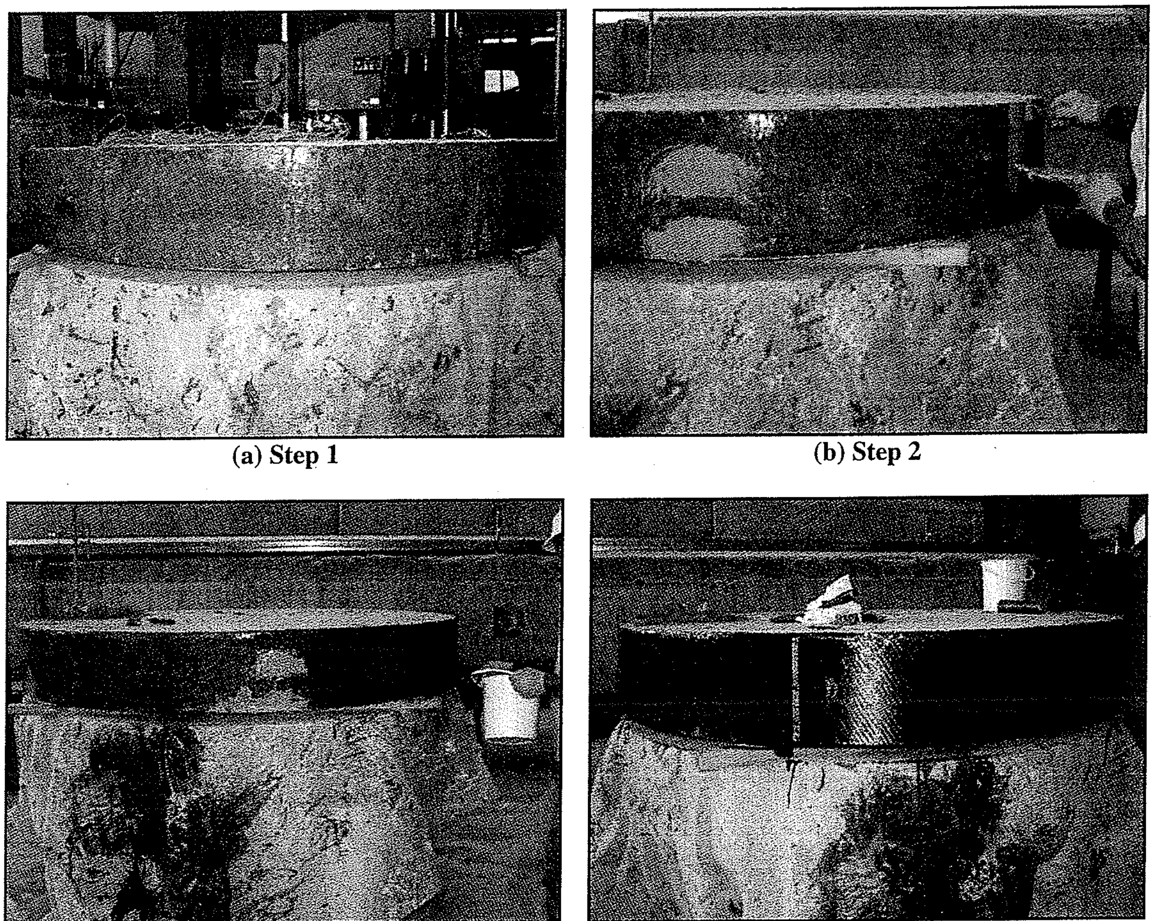

(a) Step 1 (b) Step 2

(c) Step 3 (d) Step 4

Figure 15: Different steps of CFRP wrapping procedure. (a) Step 1: Application of Wabo®MBrace primer, (b) Step 2: Application of Wabo®MBrace putty, (c) Step 3: Application of Wabo®MBrace saturant coat, Step 4: Coating the circular base with MBrace® CF 160

The next coating of the Wabo®MBrace composite strengthening system was the Wabo®MBrace putty, which was a 100% solid non-sag epoxy paste. It was applied with a spring-steel trowel to level small surface defects and to provide a smooth surface to which the Wabo®MBrace system would be applied.

The Wabo®MBrace saturant was applied to the substrates after the primer and putty coats have achieved full cured. Two coats of Wabo®MBrace saturant were applied for each layer of Wabo®MBrace CF 160 fiber fabric applied (one base coat and one top coat) such that the fiber fabric was completely encapsulated by the saturant. Wabo®MBrace saturant is a 100% solid, low viscosity epoxy material used to encapsulate Wabo®MBrace carbon fiber fabrics. When reinforced with Wabo®MBrace fiber fabrics, the Wabo®MBrace saturant cured to provide a high performance FRP laminate.

At last, four layers of MBrace® CF 160 sheets were coated using a rolling brush. It was a dry fabric constructed of unidirectional, very high strength, aerospace grade carbon fibers.

Detail properties of different components of Wabo®MBrace system are presented in Appendix B. Important material properties of Wabo®MBrace system are summarized in Table 2.

Table 2: Material properties of Wabo®MBrace system

Ultimate tensile strength of MBrace primer	17.2 MPa
Ultimate tensile strength of MBrace putty	15.2 MPa
Ultimate tensile strength of MBrace saturant	55.2 MPa
Ultimate tensile strength of MBrace® CF 160	3800 MPa
Thickness of one layer of MBrace® CF 160	0.33 mm/ply

3.5 Freeze and thaw cycles

Freeze-thaw durability of steel-free concrete slabs is probably one of the most important characteristics that ought to be investigated to understand the behaviour of concrete slabs exposed to harsh cold weather. Slab-2 and Slab-3 were exposed to a series of rapid freeze and thaw cycles in a large, temperature controlled environmental chamber. The freeze and thaw exposure conditions used in this test program followed the guidelines specified in the ASTM C 666/C 666M–03 *(ASTM 2003-a)*.

The environmental chamber was programmed to complete a freeze and thaw cycle in 16 hours. The freeze and thaw cycle ramped up the air temperature in the environmental chamber from -25°C to +15°C followed by a hold at +15°C for about 4 hours and a ramped down to -25°C followed by a hold at -25°C for about 8 hours. After that the temperature of the environmental chamber was increased to +15°C, and thus a freeze-thaw cycle was completed. The circular slabs were exposed to 100 freeze and thaw cycles. A plot showing the changes in temperature at the environmental chamber for a short period of time during freeze-thaw cycle is presented in Figure 16.

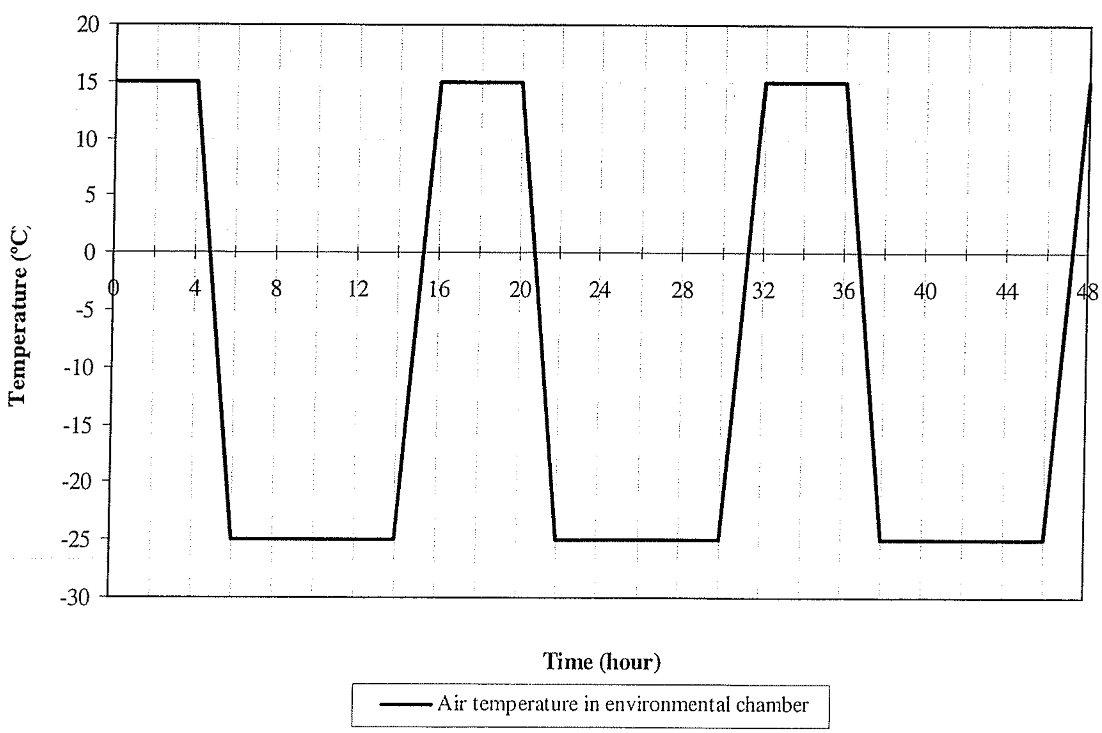

Figure 16: Freeze and thaw cycles profile for circular steel-free concrete deck slabs

3.6 Test setup

Two different types of test setup were used for this research project. The first test setup was prepared to do the static test of the first circular steel-free concrete deck (Slab-1). The second test setup was prepared to conduct fatigue tests of the second and third circular steel-free concrete deck models (Slab-2 and Slab-3). The detail of the test setups are described in the following sections.

3.6.1 Test setup for static load test

This test setup was used to test the first circular steel-free concrete deck model (Slab-1). The circular slab was supported over four concrete blocks measuring 750 mm in length by 750 mm in width and by 1000 mm in depth. A piece of plywood was placed in between the circular slab and each of the concrete blocks as a bearing pad to provide an even surface for the deck slab. The WWF900×262 steel loading beams were supported by four W310×202 steel columns. The columns were cross braced with several C380×50 and HSS102×102×4.8 sections. The W310×202 steel columns were tensioned to the structural floor using high strength dywidag bars. A325 structural bolts were used in all the bolted connections.

A hydraulic actuator was used to apply static load on the circular slab. A steel loading plate of 520 mm diameter was placed concentric to the circular slab over a neoprene pad. The schematic detail of the static test setup is shown in Figure 17. A photograph of the test setup for the static load test is shown in Figure 18.

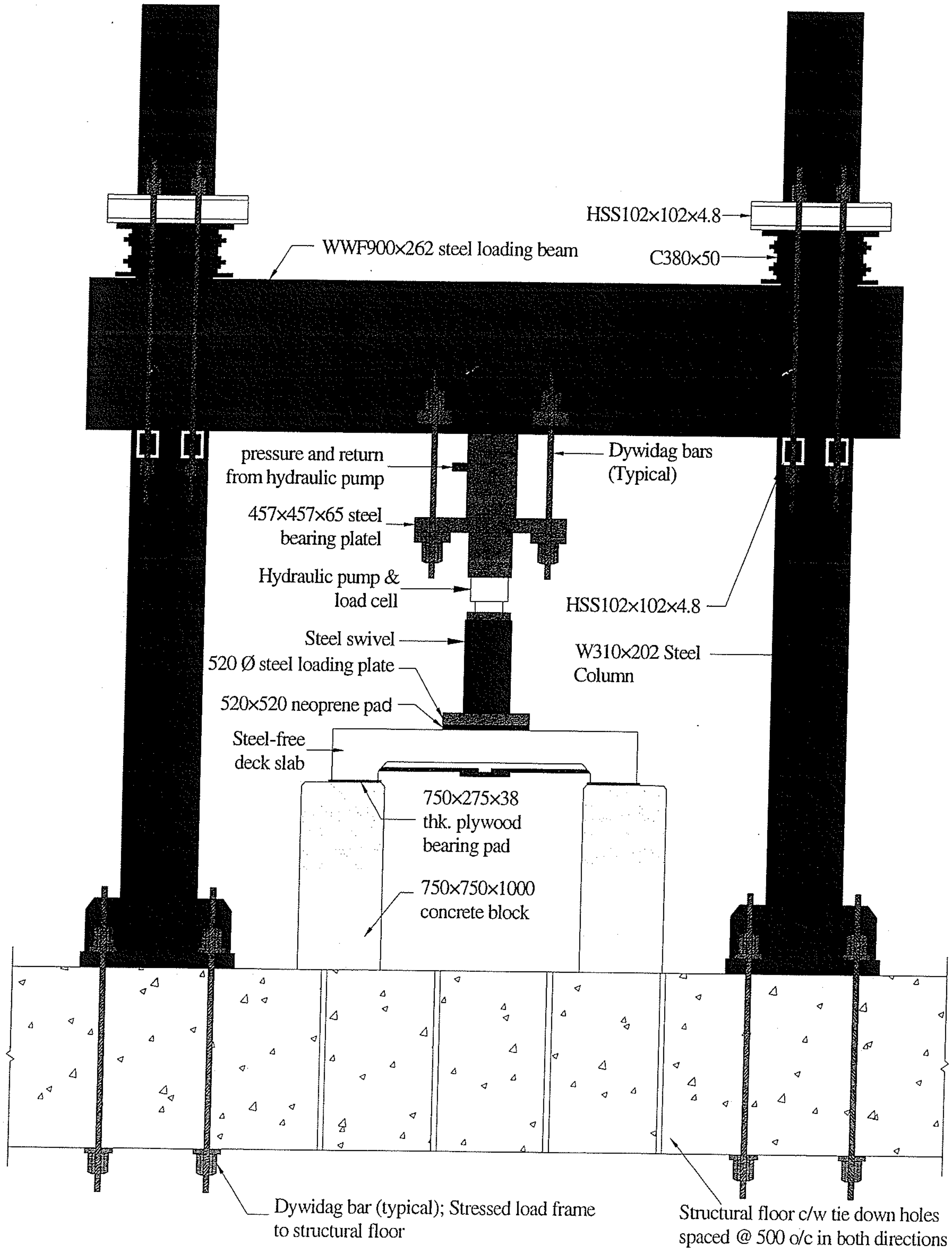

Figure 17: Cross sectional view of test setup for static test of Slab-1

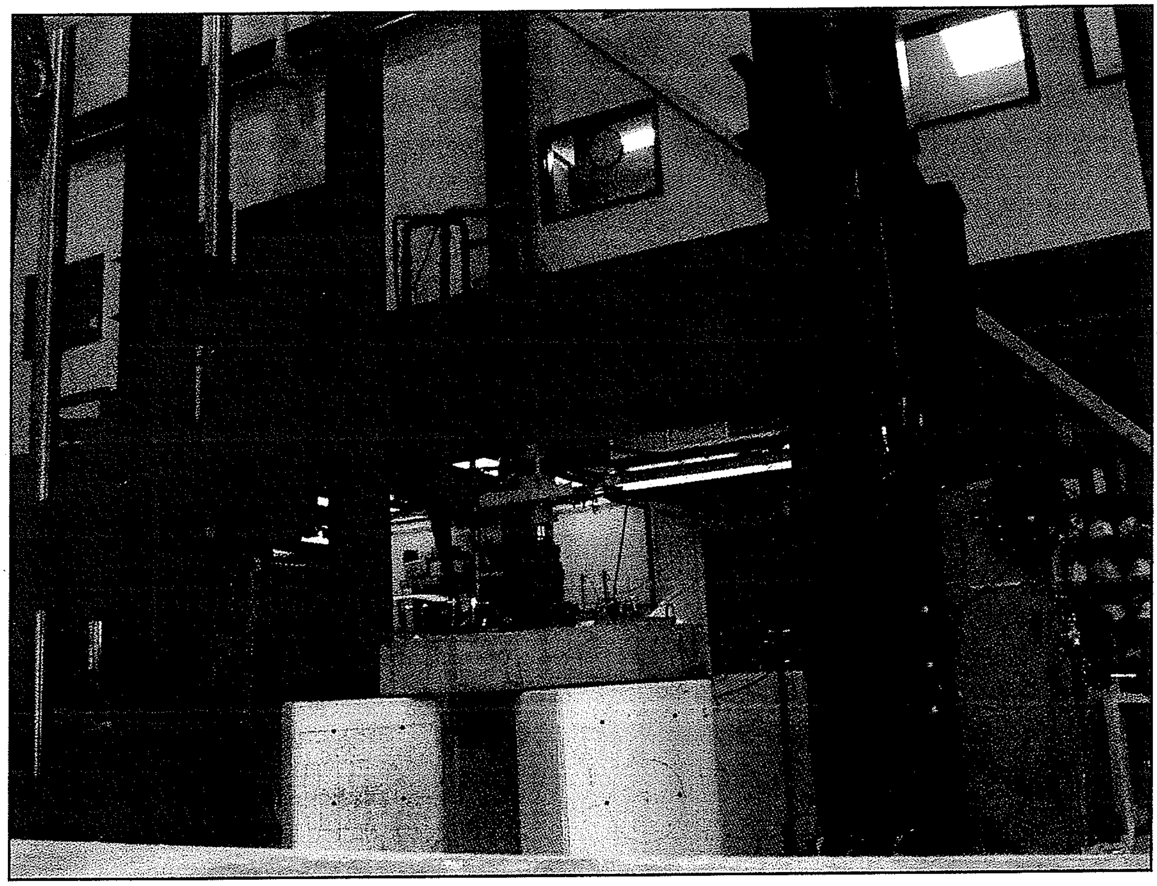

Figure 18: Photograph of test setup for static test of Slab-1

3.6.2 Test setup for fatigue load tests

This test setup was build to test the second and third circular steel-free concrete deck models (Slab-2 and Slab-3) under fatigue loading. A circular concrete beam of 275 mm width, 275 mm depth and 1810 mm of external diameter was placed over four concrete blocks measuring 750 mm in length by 750 mm in width and by 1000 mm in depth. The circular slab was placed over the circular beam. A piece of plywood was placed in between the circular beam and each of the concrete blocks as a bearing pad to provide an even surface for the deck slabs. A layer of non-shrink, cementations grout

(Sika Grout®212) was used in between the circular beam and the circular slab to provide a regular flat support.

Two WWF900x231 steel loading beams were supported by two W1200x333 steel columns. The columns were crossed braced using two HSS254x254x9.5 sections. The W1200x333 steel columns were tensioned to the structural floor using high strength dywidag bars. A325 structural bolts were used in all the bolted connections.

A hydraulic actuator with maximum capacity of 1,000 kN was used to apply the fatigue load on circular slabs. A steel loading plate of 520 mm diameter was placed concentric to the circular slab over a neoprene pad. Steel chains were used to keep the hydraulic actuator stable and levelled. Schematic detail of typical fatigue test setup is shown in Figure 19. A photograph of the test setup for fatigue load tests is shown in Figure 20.

3.7 Detail of instrumentations

Various types of instruments were installed on the circular slabs to record the experimental data such as: the magnitude of applied load, vertical deflection of the slab, strains in steel straps, crack width, strain in circumferential CFRP wrap and strain in concrete. Instrumentations for both static and fatigue tests were identical, except the first slab (Slab-1), where no strain gauges were installed to record the strain in circumferential CFRP wrap as the slab was not wrapped with any circumferential CFRP sheet. The detail descriptions of instruments are outlined in the following sections.

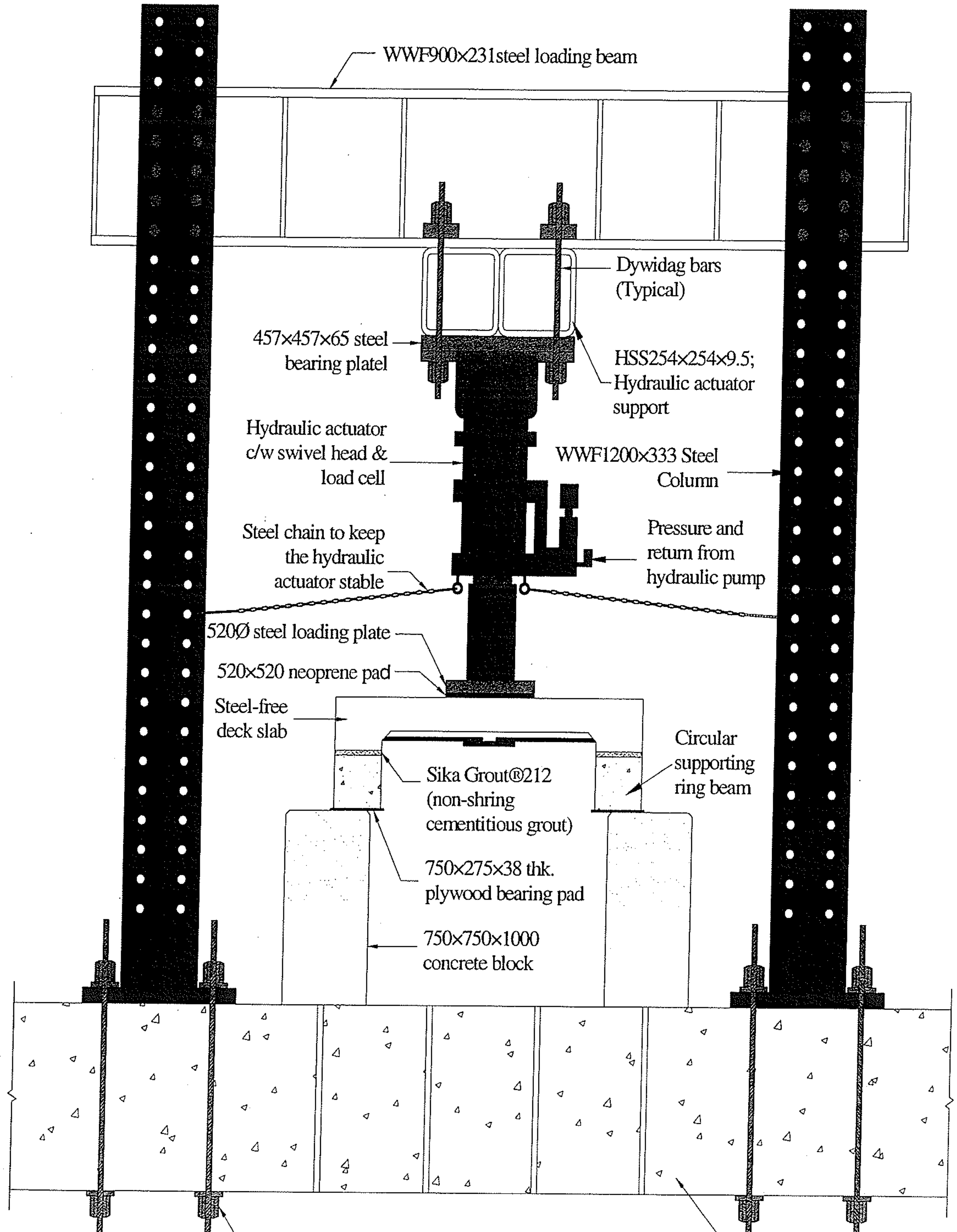

Figure 19: Cross sectional view of test setup for fatigue test of Slab-2 and Slab-3

Figure 20: Photograph of test setup for fatigue tests of Slab-2 and Slab-3

3.7.1 Load measurement

The concentric static load was applied to the first circular steel-free concrete slab (Slab-1) using a hydraulic pump. An external load cell connected to a data acquisition system (DAQ) was installed to record the applied static load.

For Slab-2 and Slab-3, a hydraulic actuator with maximum capacity of 1,000 kN was used to apply the fatigue load on circular slabs. A data acquisition system was connected to the load cell attached to the hydraulic actuator in order to record and display the magnitude of applied load during fatigue tests.

3.7.2 Deflections measurement

The vertical deflections of the circular slabs were recorded with respect to the top surface of the corresponding slab using four linear variable displacement transducers (LVDTs). The LVDTs were installed along the north-south radial line at top of the slab. The inner and outer LVDTs were installed at a distance of 280 mm and 420 mm respectively from the centre of the circular slab. Typical locations of the installed LVDTs are shown in Figure 21. All LVDTs were supported by clamps attached to a steel uni-strut. The uni-struts were placed over two pieces of steel angle placed over the slab. All the LVDTs were connected to the DAQ through electric wires to record the vertical deflection measurements of the slabs during static and fatigue loading tests.

3.7.3 Strains measurement in steel straps

A 25 mm long electric strain gauge was installed at the bottom, mid length of each steel strap to record the strain in steel straps during static and fatigue loading tests of circular steel-free concrete slabs. Typical locations of installed strain gauges are shown in Figure 22. All the strain gauges were connected to the DAQ through electric wires.

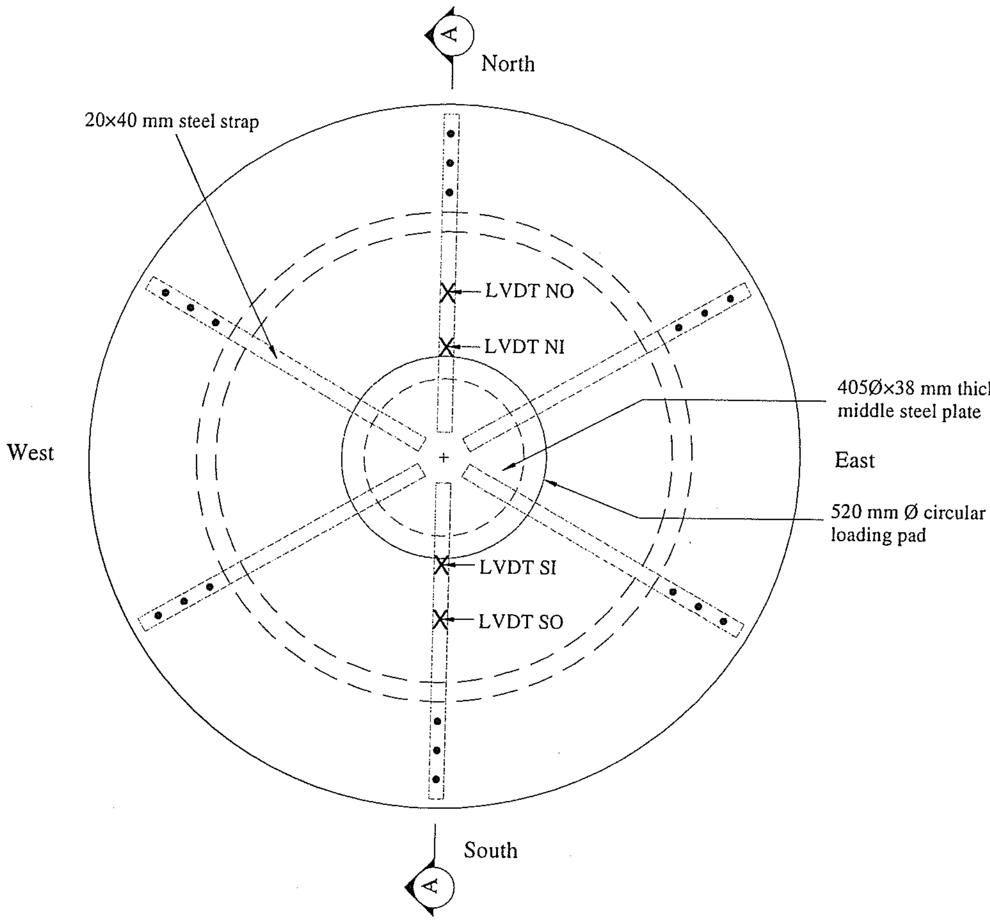

Top view

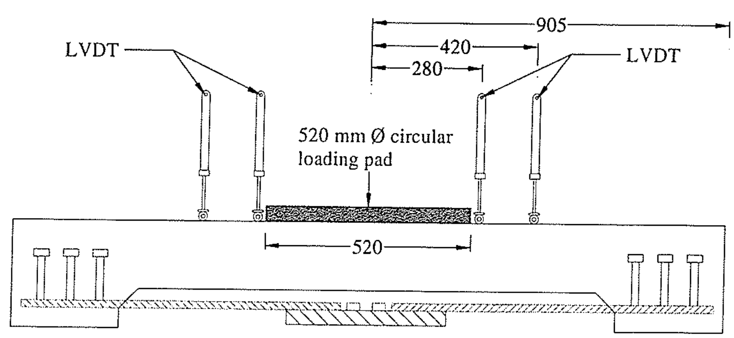

Section A-A

Figure 21: Four LVDTs (marked as "X") were installed along the north-south radial line at top of each circular slab

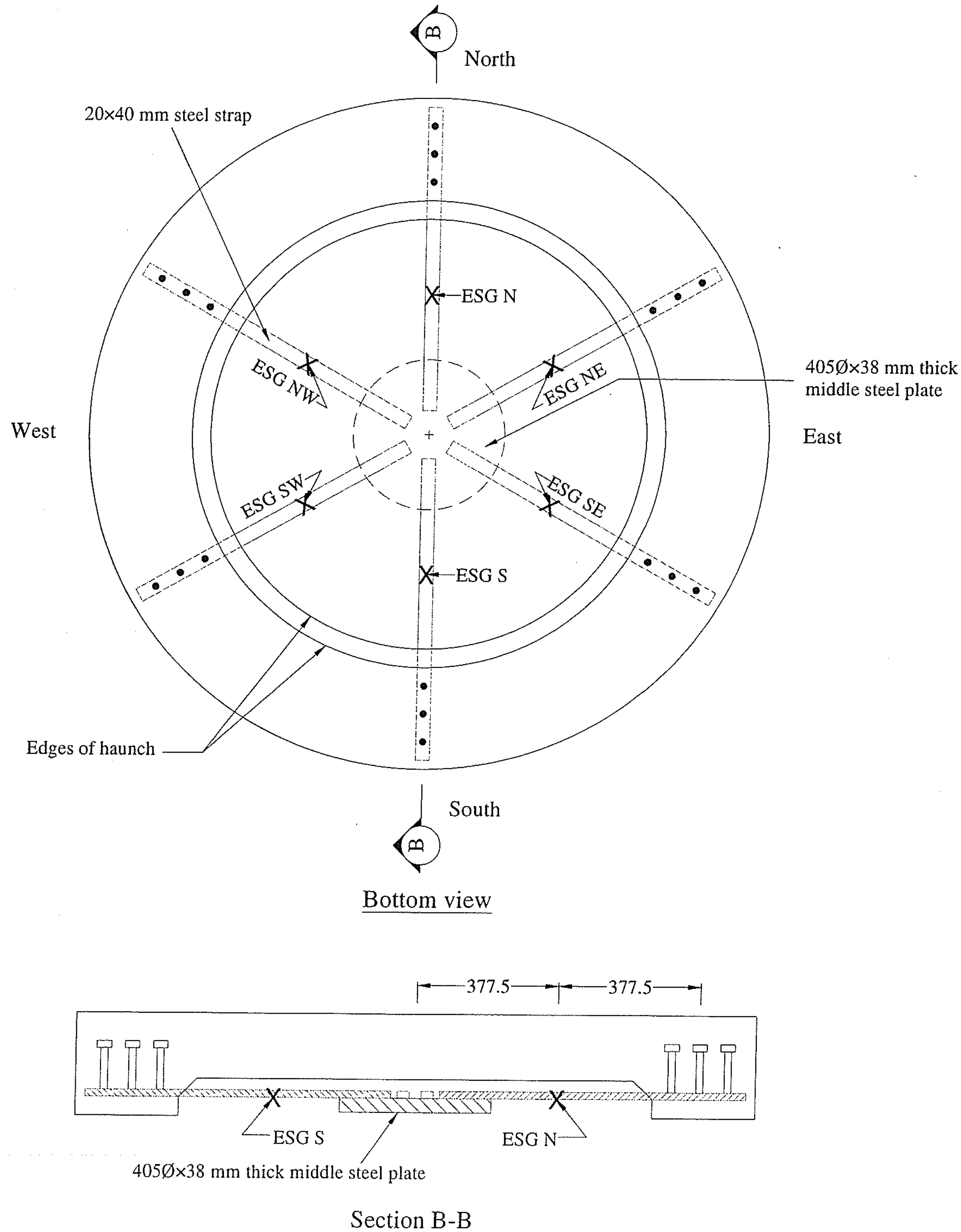

Figure 22: An electronic strain gauge (marked as "X") was installed at mid length of each steel strap

3.7.4 Crack widths measurement

In total four pi gauges with gauge length of 200 mm were installed on the underside each of the circular slabs to record the measurements of crack width during static and fatigue tests. Two pi gauges (Pi-1 and Pi-3) were installed along the north-south radial line of the slab to span the radial cracks along the north-south radial direction. Two other pi gauges (Pi-2 and Pi-4) were installed to measure the radial crack widths along the east and west directions. All the pi gauges were connected to the DAQ through electrical wires to record the magnitudes of crack width under static and fatigue loading. The typical locations of the installed pi gauges are shown in Figure 23.

3.7.5 Strains measurement in CFRP wrap

In total four 25 mm long electric strain gauges were installed in the four corners (North, South, East, and West) of the outer surface of the CFRP wrap of Slab-2 and Slab-3 to record measurements of strain in the CFRP wraps during tests. The strain gauges were installed at the mid height of the base of each circular slab as shown in Figure 24. All the strain gauges were connected to the DAQ through electrical wires to record the measurements of strain in the CFRP wrap under static and fatigue loading.

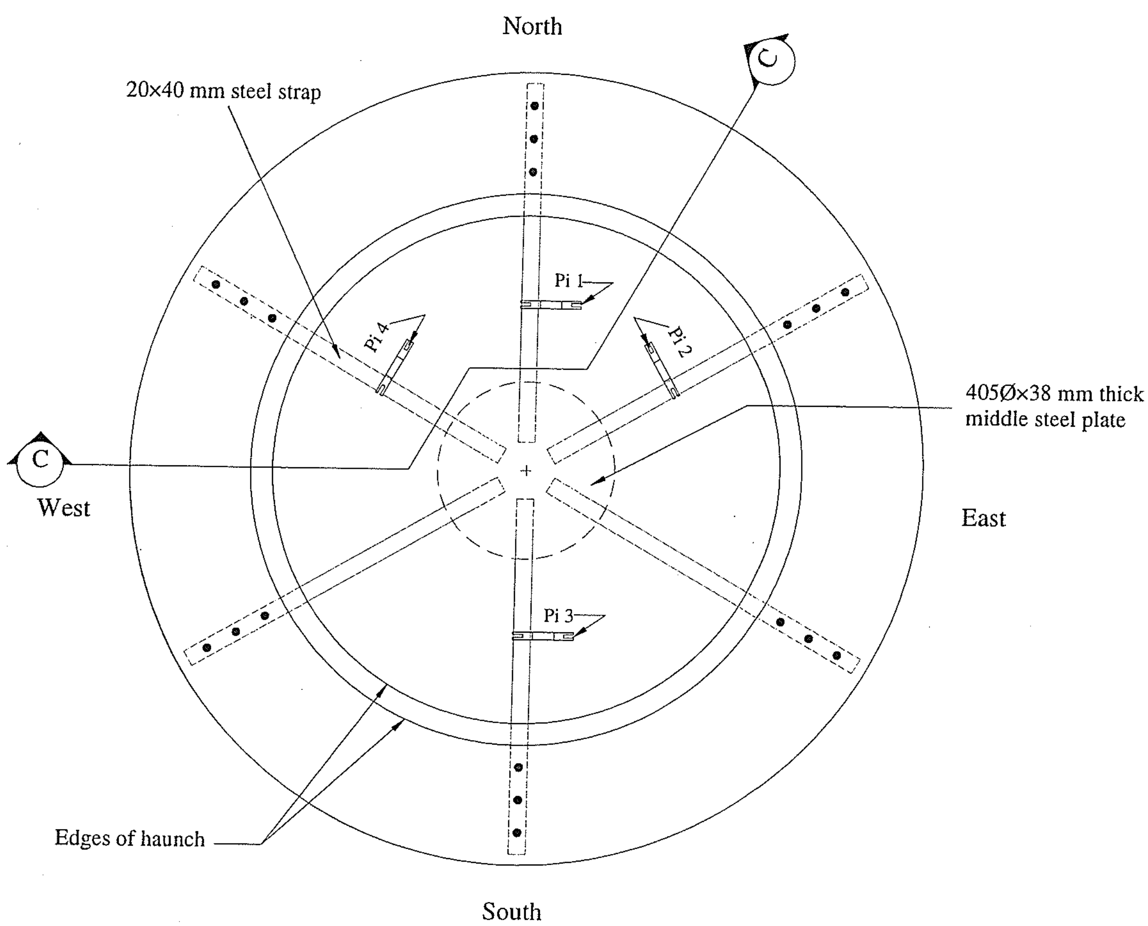

Bottom view

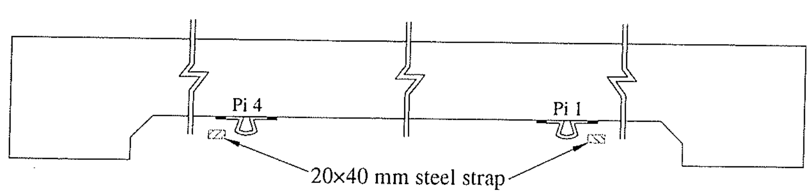

Section C-C

Figure 23: Four Pi gauges were installed under the slab to record the crack width

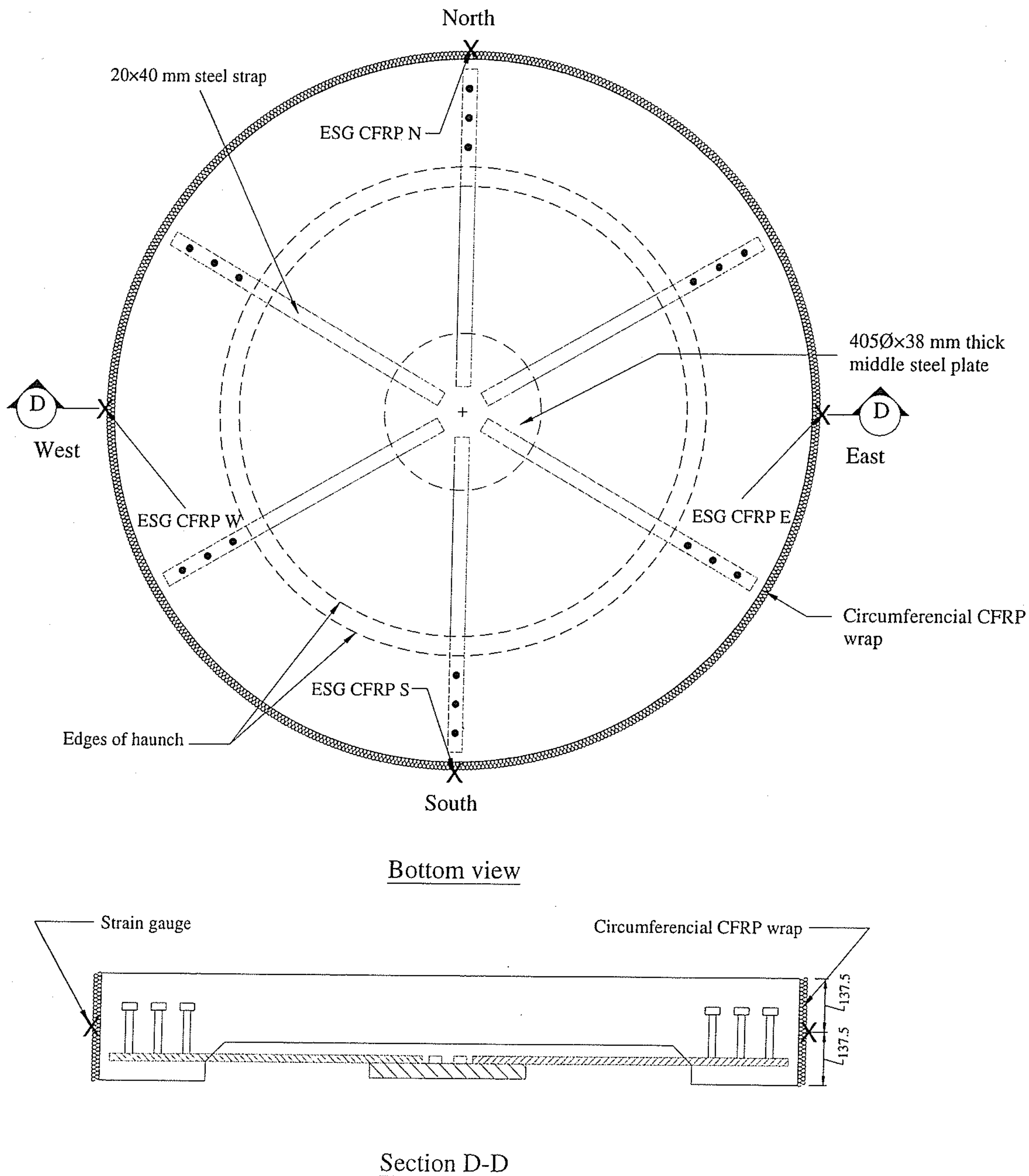

Figure 24: Four electronic strain gauges (marked as "X") were installed at mid height in four corners of circular support for fatigue tests

3.7.6 Strains measurement in concrete slab

A three dimensional array of twelve 25 mm long electric strain gauges were installed at the centre of each circular slab to record the three dimensional state of strains in the concrete slab under static and fatigue loading. A cube of 105 mm side length was made of 5 mm diameter GFRP bars as shown in Figure 25. The edges of the GFRP bars were glued together to form a cube. A 25 mm electronic strain gauge was installed on the mid length of each of the GFRP bars. One strain cube was placed over the formwork of each circular slab before casting. Detail procedure of placement of the strain cube is described in section 3.2. All the strain gauges were connected to the DAQ through electronic wires to record the measurements of strain in the concrete slabs during static and fatigue tests. The typical locations of the strain cube in the circular slab are schematically shown in Figure 26. Figure 27 shows typical photographs of the three dimensional array of strain gauges and location of the strain cube in circular formwork.

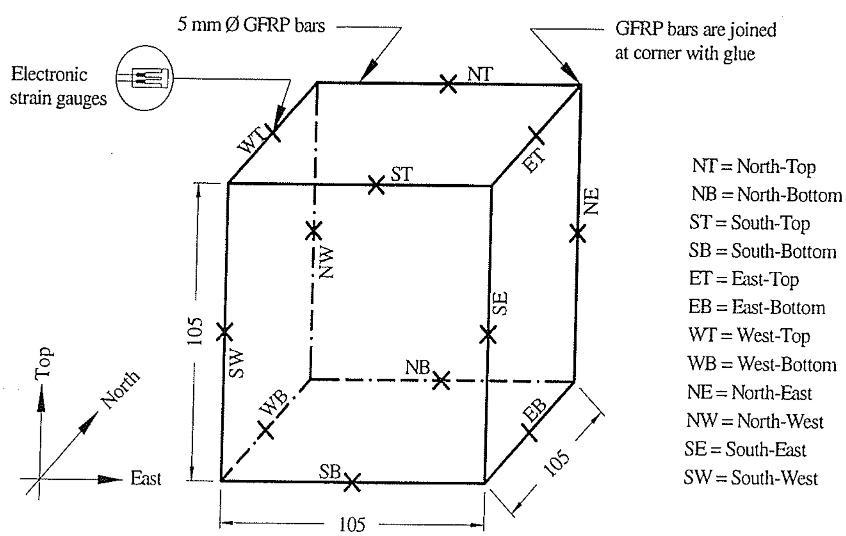

Figure 25: Three dimensional arrays of strain gauges (marked as "X")

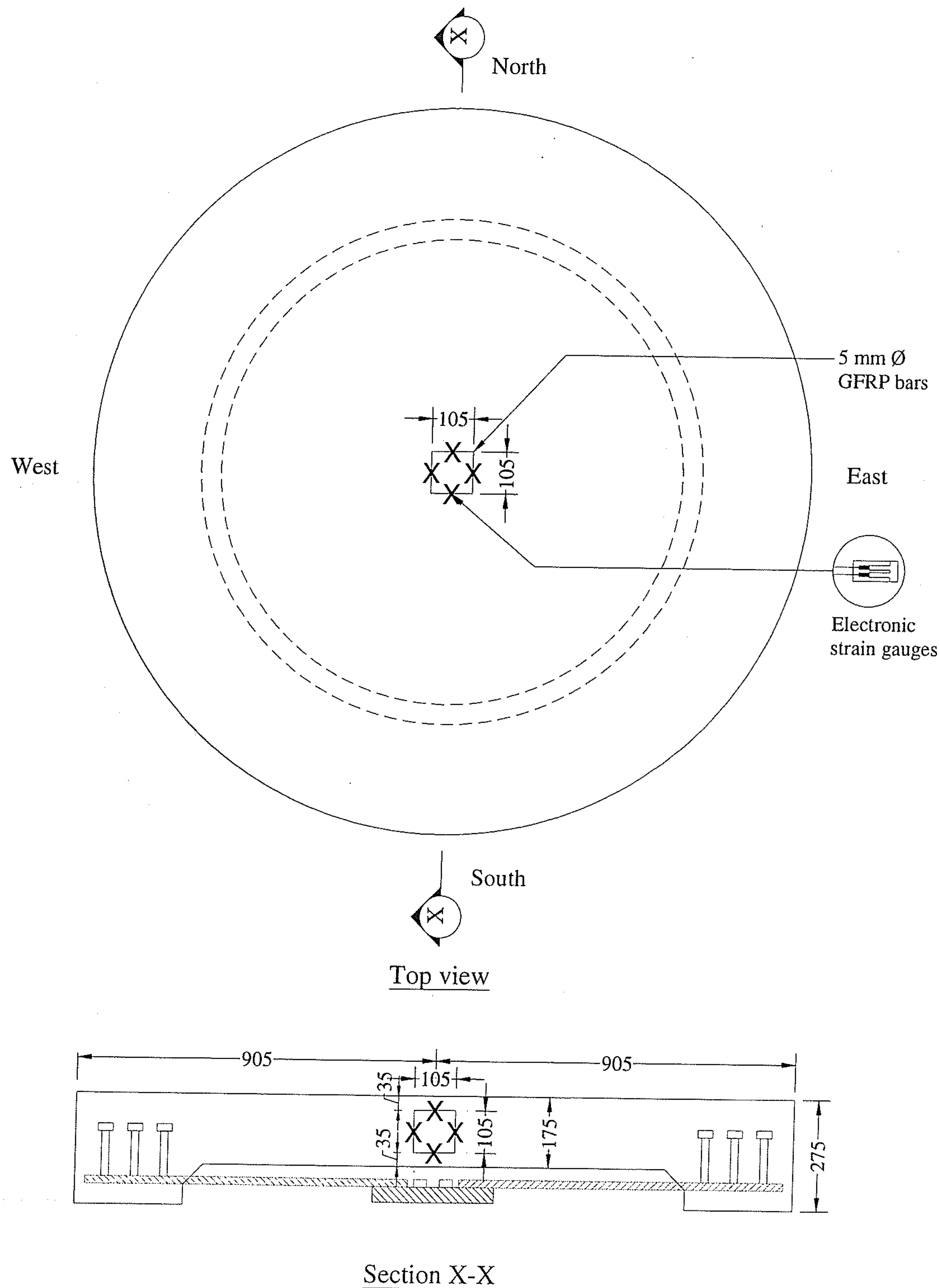

Figure 26: Location of strain gauges (marked as "X") in steel-free concrete slab

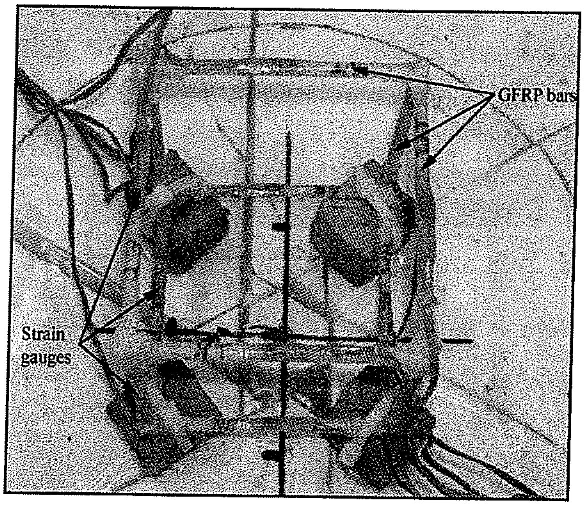

(a)

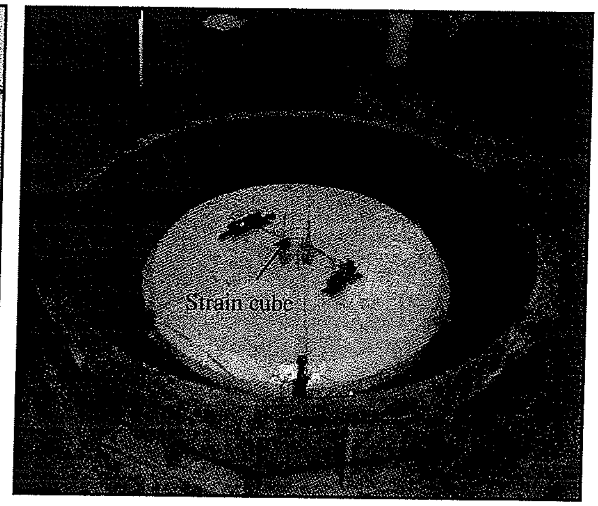

(b)

Figure 27: (a) Photograph of three dimensional arrays of strain gauges, (b) Photograph of the location of strain gauges installed at the centre of circular slab

3.8 Test procedure

3.8.1 Test procedure of Slab-1

The first circular steel-free concrete slab (Slab-1) was tested under static load until failure. The load was monotonically increased in 25 kN increments. After each 25 kN step, the test was held steady for some time to inspect the slab and to mark the cracks under the slab. The first radial crack was visible at the bottom of the slab at around 100 kN along the north-south direction. As it appeared that some of the instruments were not functioning properly, loading was removed twice after reaching 115 kN and 175 kN to inspect the instruments and to fix the problems. Loading was started again after fixing the problems and was continued until the failure of the slab. The number of radial cracks increased with the increment of load. The slab failed at 460 kN in flexural failure mode. The load was removed after failure of the slab and final inspection of the slab was performed, which included assessment of damage, crack mapping and taking photographs.

3.8.2 Test procedure of Slab-2

The second circular steel-free concrete slab (Slab-2) was tested under compression fatigue load followed by a static load until failure. The initial magnitude of the applied fatigue cyclic load for Slab-2 was selected based on a previous static ultimate load test of a similar circular steel-free concrete slab conducted at the University of Manitoba *(Mediwake 2006)*. The ultimate load obtained from the static test conducted previously was 742 kN. The initial magnitude of the applied cyclic load for Slab-2 was selected to be 60% of the previous static ultimate load, which was 445 kN.

During the first loading cycle, the load was monotonically increased in 25 kN increments up to 445 KN. After each 25 kN step, the test was held steady for some time to inspect the slab and to mark the cracks under the slab. The first radial crack was visible at the bottom of the slab at around 200 kN along the south direction. The numbers of radial crack were increasing with the increasing of load. Load was removed after reaching 445 kN, and thus the first loading cycle was completed. After the first loading cycle, four pi gauges were mounted to span the appropriate cracks and all other instruments were inspected to confirm that they were functioning properly. After completion of the first loading cycle, a sine wave loading was programmed to apply the cyclic loading with maximum and minimum amplitude of 445 kN and 5 kN respectively. It was found that the DAQ was not able to count the number of load cycles accurately with a frequency higher than 0.4 Hz for a maximum load of 445 kN. That is why the frequency of the loading cycle was set to 0.4 Hz. The magnitudes of the slab deflection, crack width, strain in the steel straps, strain in the CFRP wrap and strain in the concrete were recorded through a DAQ.

The fatigue cycles with maximum load of 445 kN were continued up to 400,000 loading cycles. As after 400,000 loading cycles no significant increase in the deflection, crack width, strain in steel straps and strain in CFRP wrap were observed; the fatigue cycling was stopped and it was decided to increase the maximum load.

The load was again monotonically increased in 25 kN increments and was held constant for some times after each 25 kN step to inspect the slab and to mark the cracks. The circumferential crack was first visible at the top of the slab at around 500 kN. At 550 kN, significant numbers of radial cracks at the bottom of the slab were observed and the circumferential crack was widening. Cracks formed around each steel strap at the locations of joints between steel straps and concrete. From the practical observation of the radial and circumferential crack pattern, it was decided to remove the load after 550 kN. Thus the 400,001st loading cycle was completed.

Based on the observations as mentioned above, the maximum load for next fatigue cycles was selected to be 550 kN with an amplitude of 0.25 Hz. Deflection of the slab, strain in the steel straps, strain in the CFRP wrap and rotation of base of the slab were increasing with the increment of loading cycles. The behaviour of the slab was observed until 550,000 cycles.

Since the slab did not fail after 550,000 loading cycles, the maximum load was increased to 600 kN and the frequency was set to 0.2 Hz. The loading cycles were continued up to 616,026 cycles. The CFRP wrap was found ruptured at different location in between 550,000 and 616,026 loading cycles. The grout under the slab base was damaged seriously.

Due to the excessive damage of the grout and rupture of the CFRP wrap after 616,026 numbers of loading cycles, it was decided to halt the fatigue test prior to failure and to test the slab under static load until failure.

The load was increased monotonically at 25 kN intervals and was held constant for some time to inspect the slab. The slab failed at 920 kN in punching shear failure mode. After failure, the load was removed from the slab and final inspection of the slab was performed, which included assessment of damage, crack mapping and taking photographs.

3.8.3 Test procedure of Slab-3

The second circular steel-free concrete slab (Slab-2) was tested under compression fatigue load until failure. The magnitude of applied fatigue cyclic load for Slab-3 was selected to be 750 kN. During the first loading cycle, the load was monotonically increased in 25 kN increments. After each 25 kN step, the test was held steady for some time to inspect the slab and to mark the cracks under the slab. The first radial cracks were visible at the bottom of the slab at around 200 kN along the north, north-west and south-east directions. The numbers of radial crack increased with the increment of the load. It was observed that, radial cracks spanned through all four pi gauges. All other instruments were inspected to confirm that they were functioning properly and it was found that the LVDT in the north inner side (LVDT NI) was not functioning properly. That is why the test was stopped after 600 kN and the problem with the LVDT was fixed. Then the loading was started again. The circumferential crack was first visible at the top of the slab at around 700 kN. Load was removed after reaching 750 kN, and thus the second loading cycle was completed.

After completion of the second load cycle, a sine wave loading was programmed to apply the fatigue load with maximum and minimum amplitude of 750 kN and 10 kN respectively. It was found that the DAQ was not able to count the number of load cycles accurately with a frequency higher than 0.2 Hz for a maximum load of 750 kN. That is why the frequency of the loading cycles was set to 0.2 Hz. The magnitudes of deflection of the slab, crack width, strain in the steel straps, strain in the CFRP wrap and strain in the concrete were recorded through the DAQ. The slab failed after 18,204 loading cycles in the punching failure mode. Final inspection of the slab was performed after failure of the slab, which included assessment of damage, crack mapping and taking photographs.

Chapter 4

Experimental Results

The experimental test results of three circular steel-free concrete deck slabs are presented in this chapter. The test results of each slab dealing with deflection, strain in the steel straps, crack width and crack pattern, strain in the CFRP wrap (for Slab-2 and Slab-3), and state of strain in the concrete.

4.1 Test results of Slab-1

4.1.1 Deflection

Vertical deflection of Slab-1 was measured along the north-south radial direction of the slab. The recorded load versus deflection of the circular slab subjected to static loading is illustrated in Figure 28. The mode of failure of the slab was flexure rather than punching. The load-deflection curve suggested that the inner portion of the deck deflected more than the outer portion of the deck. The maximum vertical deflection of the circular slab was 4.6 mm just prior to failure at a static load of 460 kN under the South-Inner LVDT (LVDT SI) location.

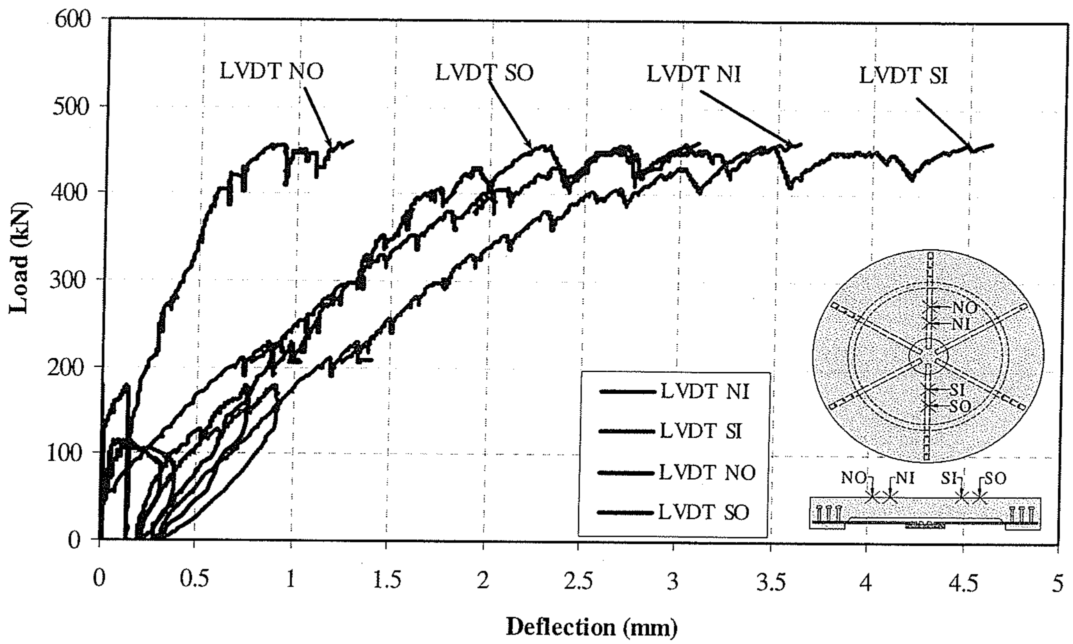

Figure 28: Load vs. deflection behaviour at all LVDT locations of Slab-1

4.1.2 Strains in steel straps

Strains in each steel strap were measured using electronic strain gauges installed at the mid length of each radial steel strap. The recorded load versus strain in steel straps of the circular steel-free concrete slab subjected to static loading is illustrated in Figure 29. The graph indicates that straps along the north and south directions experienced less strain than that of other directions. The reason behind this is that the slab failed in flexure along the north-south direction which led to higher strain experienced by the steel straps in north-east, north-west, south-east and south-west directions. The maximum and minimum strain recorded at the failure load of 460 kN were 1694 με on the steel strap along the south-east direction and 891 με on the steel strap along the north direction.

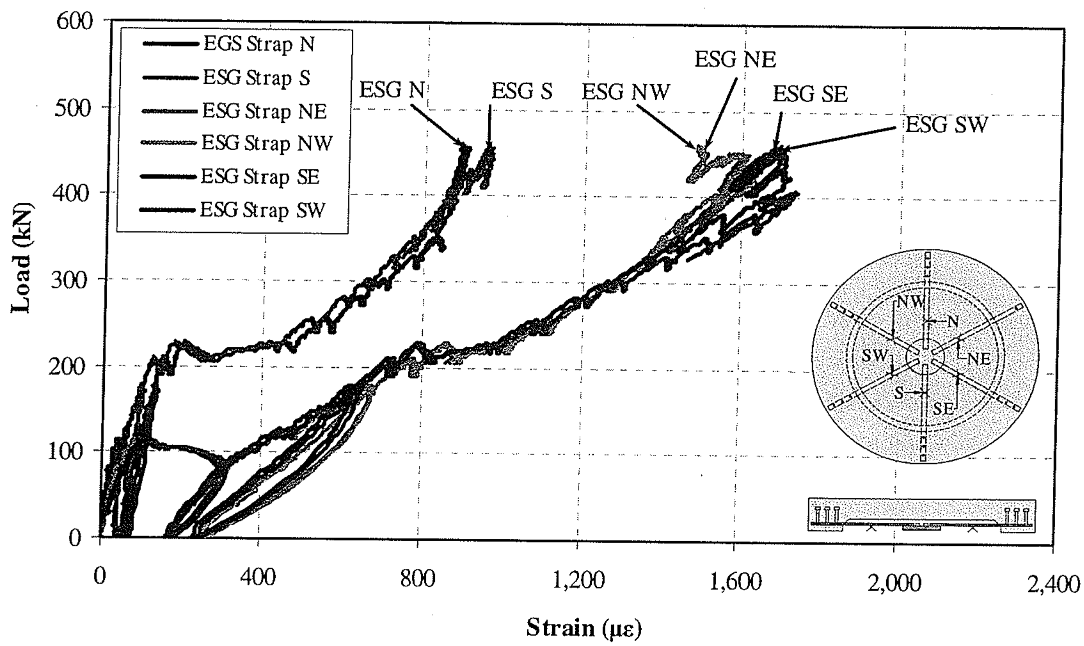

Figure 29: Load vs. strain in steel strap at all ESG locations of Slab-1

4.1.3 Crack width and crack mapping

Four pi gauges were installed under the deck to record the width of radial cracks. Initial cracks started on the support of the deck at a load of approximately 100 kN. The number and width of the cracks increased and the specimen continued to deflect more with increase in load. The first radial crack formed at the locations of pi gauges Pi-1 and Pi-3, which were installed on the north and south sides, respectively, under the circular slab.

The slab failed in flexure along the north-south direction. The widest crack width recorded at the failure load of 460 kN was 2.63 mm under the location of pi gauge Pi-3. The recorded load versus crack width behaviour of the circular slab subjected to static loading is illustrated in Figure 30.

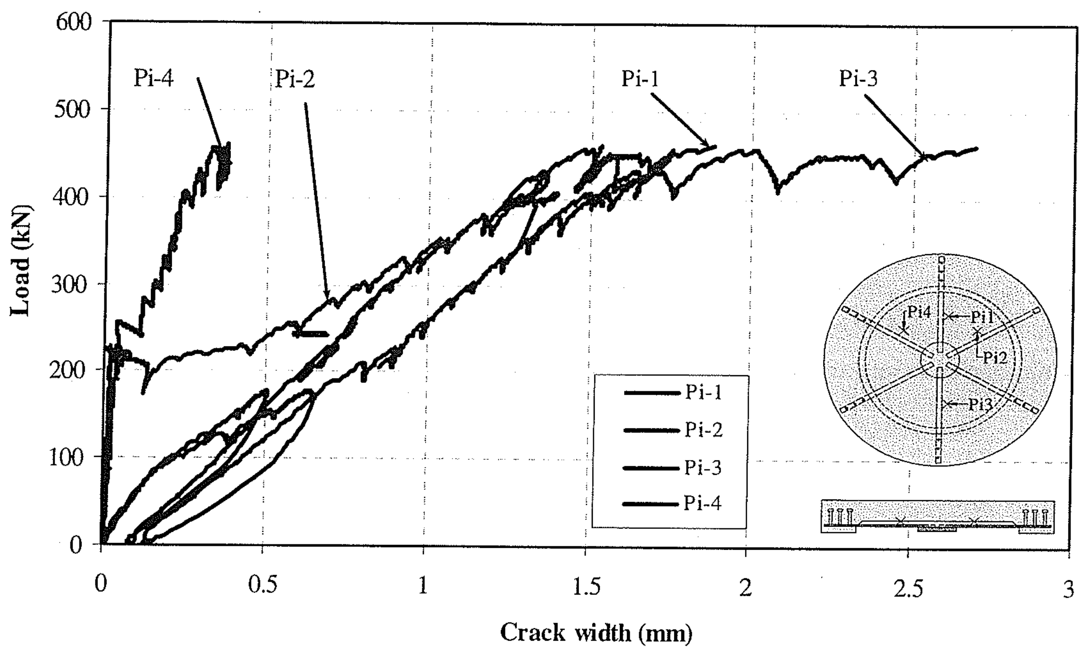

Figure 30: Load vs. crack width at all Pi gauge locations of Slab-1

Schematic drawings of crack propagation at top and bottom of Slab-1 at different loading stages are shown in Figure 31. Photographs of the crack patterns of Slab-1after failure are shown in Figure 32.

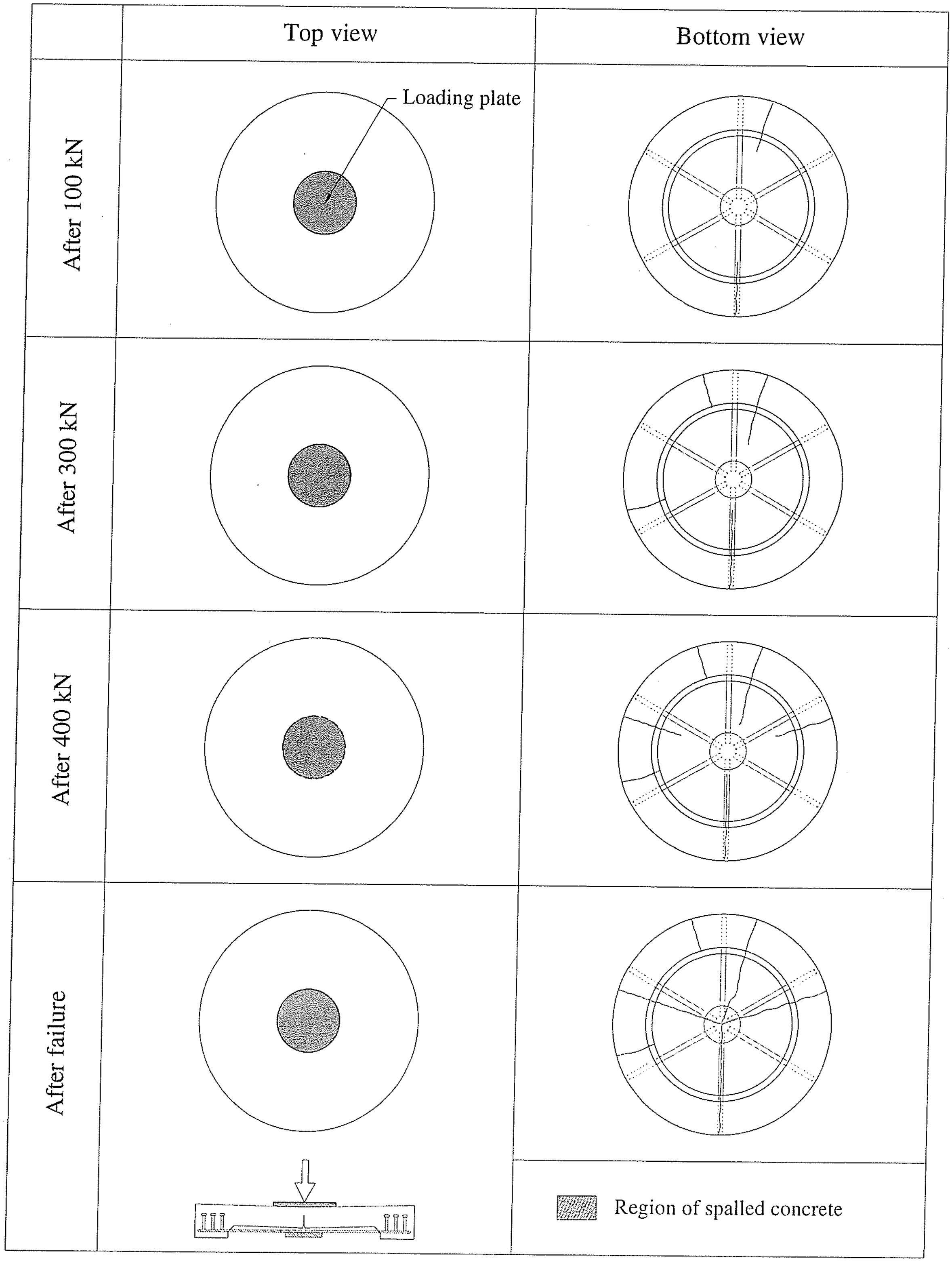

Figure 31: Crack patterns of Slab-1 at different stages of loading

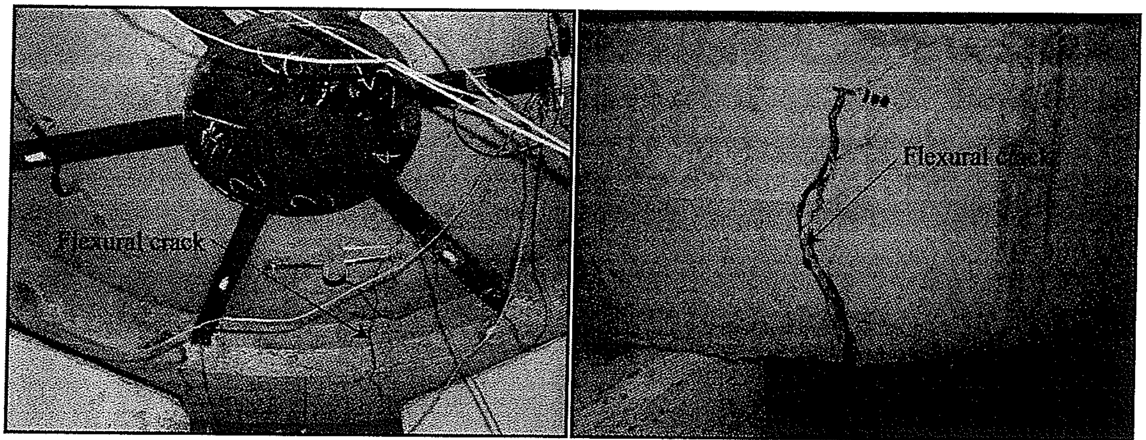

Bottom view **Side view**

Figure 32: Crack pattern of Slab-1 after failure

4.1.4 Strains in concrete

The three dimensional state of strains in the concrete slab was recorded during static loading test using a three dimensional array of twelve strain gauges installed at the centre of the circular slab. The recorded strains in the concrete slab at the failure load of 460 kN are shown in Figure 33. Red lines in this figure indicate strain gauges experienced tension, whereas the blue lines indicate strain gauges experienced compression. The values of the strains are shown within parenthesis. The recorded strains indicate that the top surface of the slab experienced compression and the bottom surface experienced tension during failure.

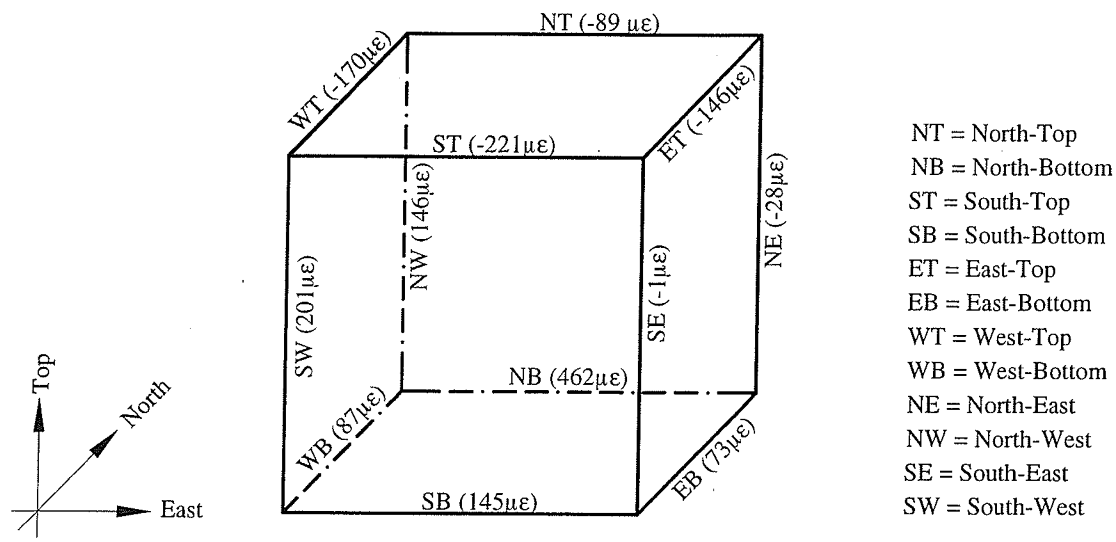

Figure 33: Strain in concrete slab at failure load of 460 kN

4.2 Test results of Slab-2

4.2.1 Deflection

The progressive increase in both residual deflection and elastic deflection along with the loss of flexural stiffness, with increasing of peak load and number of loading cycles, are shown in the load verses deflection curves at the 'South-inner LVDT' and 'South-outer LVDT' locations (Figure 34 and Figure 35). The initial magnitude of the applied cyclic load was selected to be 445 kN. The load verses deflection curves indicated that the load-deflection behaviour was monotonic under the cyclic load of 445 kN at the inner and outer LVDT locations of the slab. The number of load cycles verses deflection profile (Figure 36 and Table 3) dictated that the deflection was almost stable up to 400,000 cycles, which was around 2.3 mm for internal LVDTs and around 1 mm for external

LVDTs. After increasing the cyclic load to 550 kN, the slab deflected steadily until 550,000 loading cycles. The amount of energy lost with each of the cycles represented by the area between loaded and unloaded curves for each cycle was almost equal. The deflections of the slab after 550,000 loading cycles at the inner and outer LVDTs locations were recorded as around 7 mm and 3.7 mm respectively. After increasing the load to 600 kN at 550,001 loading cycles, the slab deflected steadily and the amount of energy lost with each of the cycles was almost equal. After 616,026 loading cycles, the deflections at the location of the inner and outer LVDTs were around 10 mm and 6 mm respectively. The slab finally failed at 920 kN of statically applied load in punch mode of failure. The deflections of the slab during failure at the location of inner and outer LVDTs were around 16.5 mm and 10 mm respectively. The deflection profile along the north-south centre-line of the slab subjected to fatigue and static loading is shown in Figure 37.

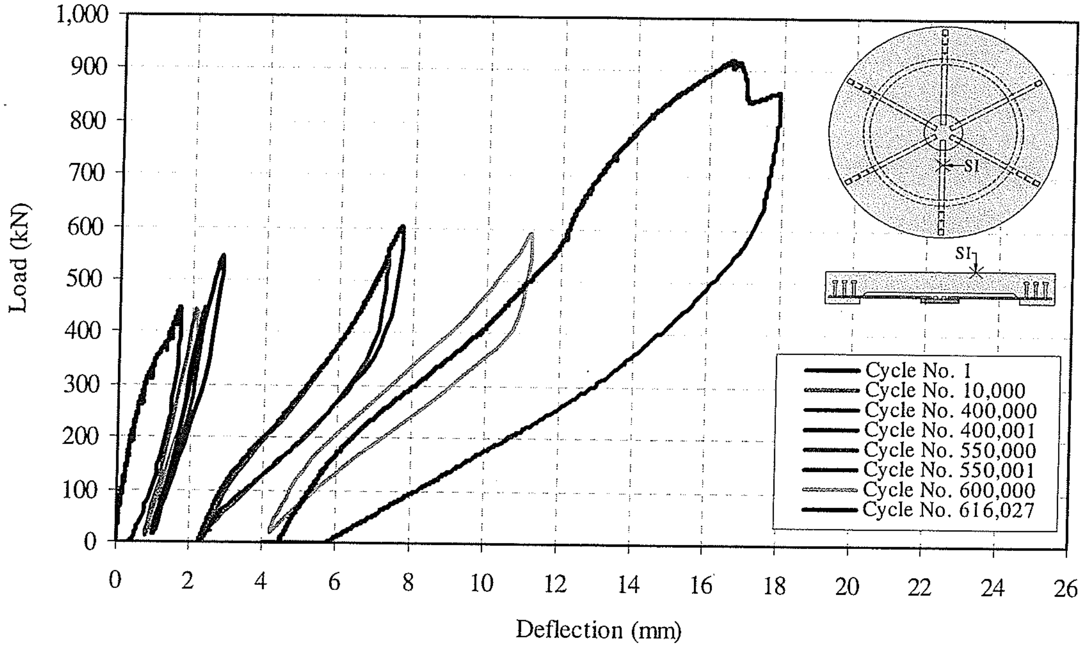

Figure 34: Load vs. deflection behaviour at LVDT SI location of Slab-2

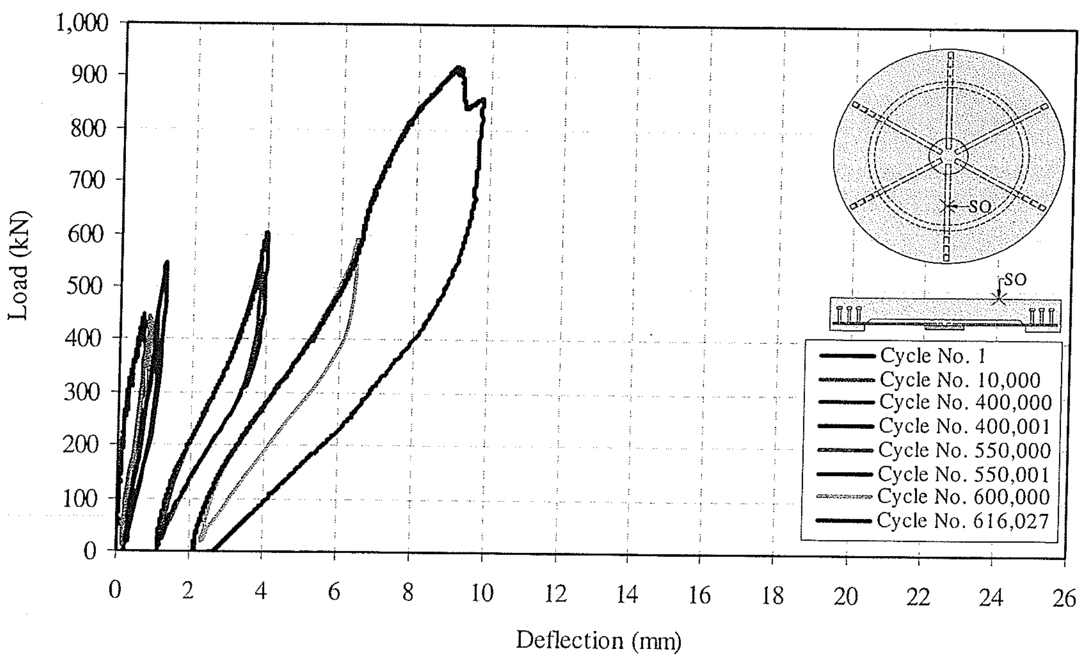

Figure 35: Load vs. deflection behaviour at LVDT SO location of Slab-2

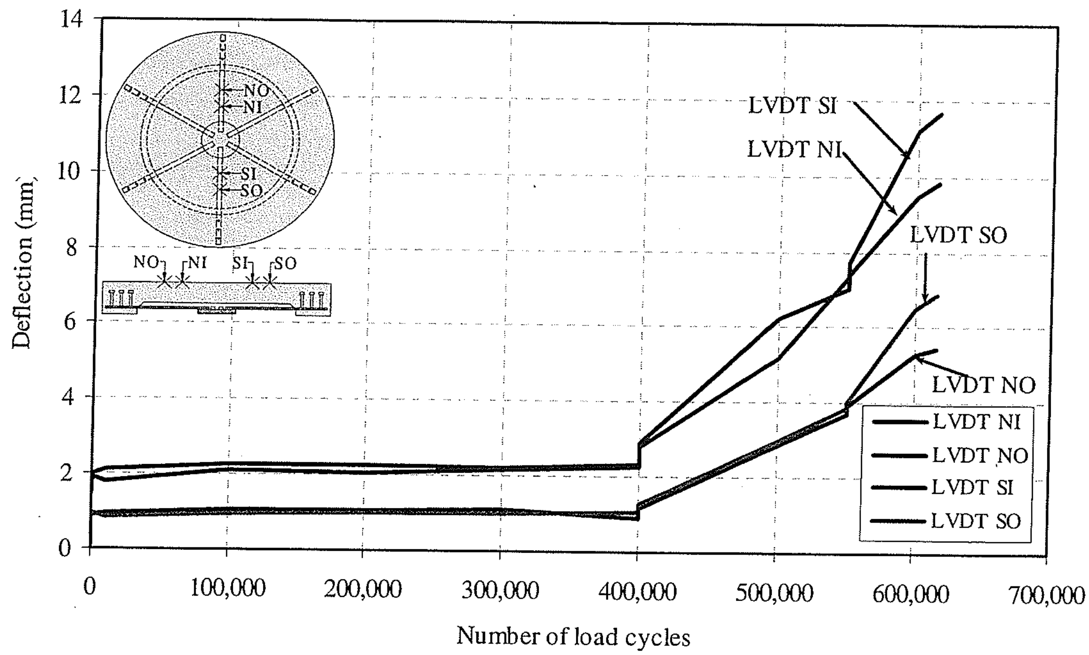

Figure 36: Deflection vs. number of load cycles behaviour of Slab-2

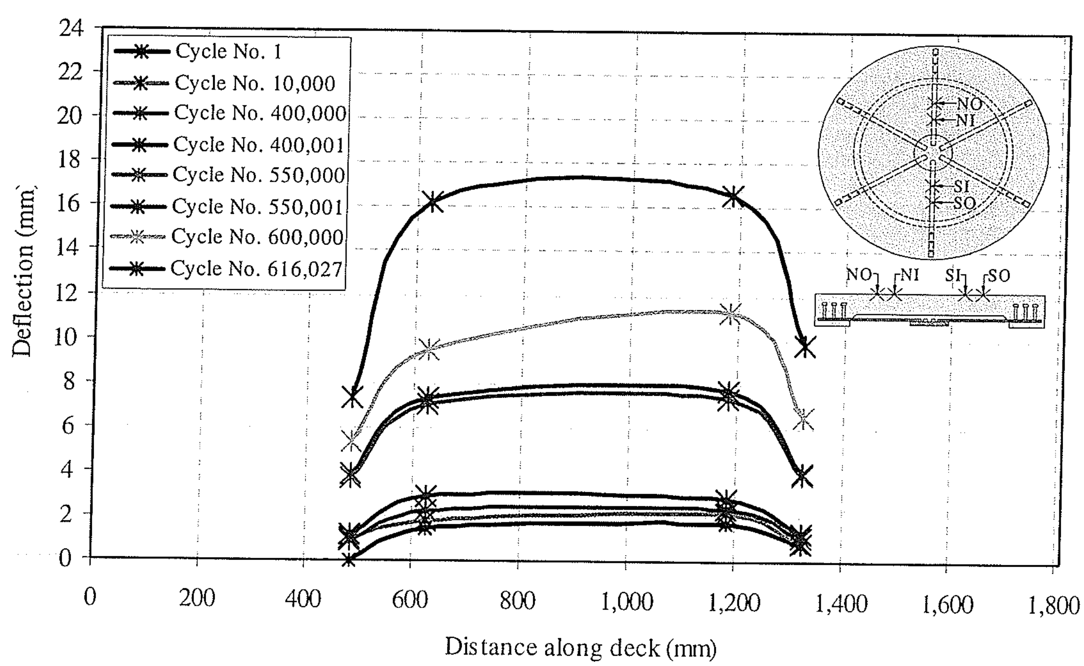

Figure 37: Deflection profile of Slab-2 along north-south centre line of the slab

Table 3: Deflection profile of Slab-2 along north-south centreline of the slab

Amplitude of load (kN)	Distance along deck (mm) / Number of load cycles	485	625	1185	1325
445	1	0.04	1.47	1.69	0.70
	10	0.79	1.67	1.85	0.85
	100	0.85	1.78	2.00	0.88
	1,000	0.89	1.88	2.00	0.94
	10,000	0.97	1.81	2.14	0.86
	100,000	1.08	2.11	2.28	0.94
	400,000	0.92	2.25	2.31	1.06
550	400,001	1.18	2.89	2.79	1.24
	550,000	3.71	7.02	7.32	3.86
600	550,001	3.90	7.38	7.69	4.03
	600,000	5.30	9.47	11.21	6.48
	616,026	5.44	9.82	11.67	6.89
920 (Static)	616,027	7.37	16.25	16.58	9.78

Note: All deflections are in millimetres

4.2.2 Strains in steel straps

The recorded strains in six steel straps are shown in load verses strain curves (Figure 38, Figure 39, Figure 40, Figure 41, Figure 42 and Figure 43). The number of load cycles verses strain profile (Figure 44 and Table 4) suggested that the strain in the steel straps increased steadily up to cycle number 400,000 under a 445 kN load. After 400,000 cycles, the maximum load was increased to 550 kN. The increase in of the strain in the steel straps was due to the increase of the cyclic load from 445 kN to 550 kN. After 400,001 cycles the strain in the steel straps began to decrease gradually which continued up to cycle number 550,000. It was observed that radial cracks propagated through all of the Nelson studs at the end of each radial steel straps. Due to those radial cracks, the anchorage between the steel straps and concrete were deteriorating with the increasing of number of fatigue load cycles. For this reason the stresses experienced by the radial steel straps were decreasing with the progression of the fatigue test, which lead to the downward trend of strain in the steel straps. After 550,000 cycles, when the load was increased from 550 kN to 600 kN, the strain in the steel straps increased again due to the increment of the load from 550 kN to 600 kN. After that the strain in steel straps started to decrease again and the down ward trend of the strain in the straps continued up to 616,026 cycles. The stain in all steel straps again increased during the failure of the slab under static test. The maximum strain of 1089.55 $\mu\varepsilon$ was observed in the steel strap spanning in the south-west direction.

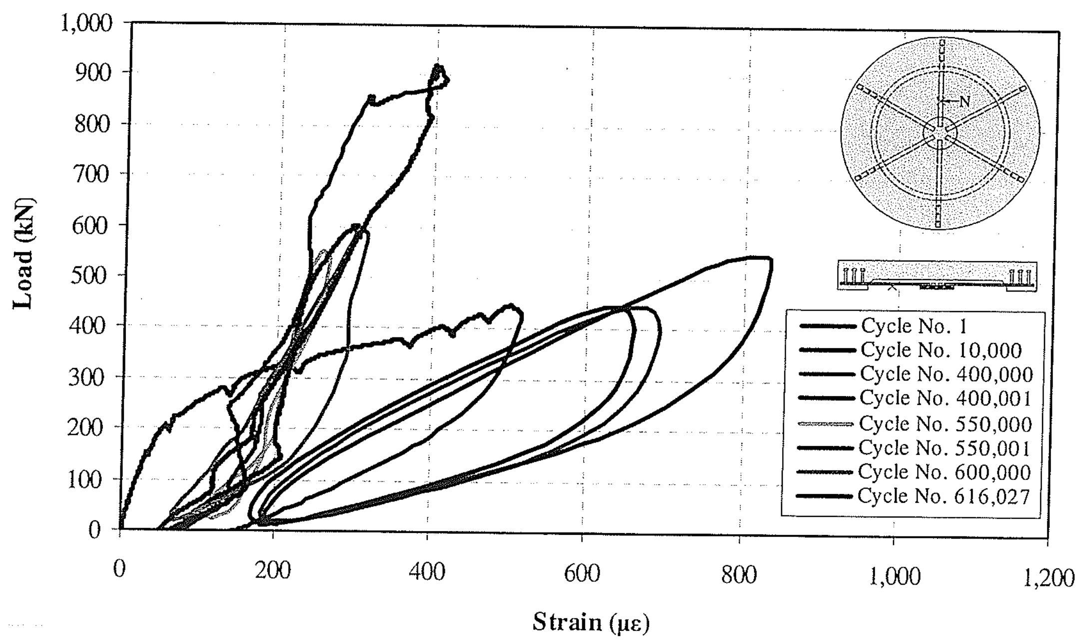

Figure 38: Load vs. strain behaviour in steel strap at ESG N location of Slab-2

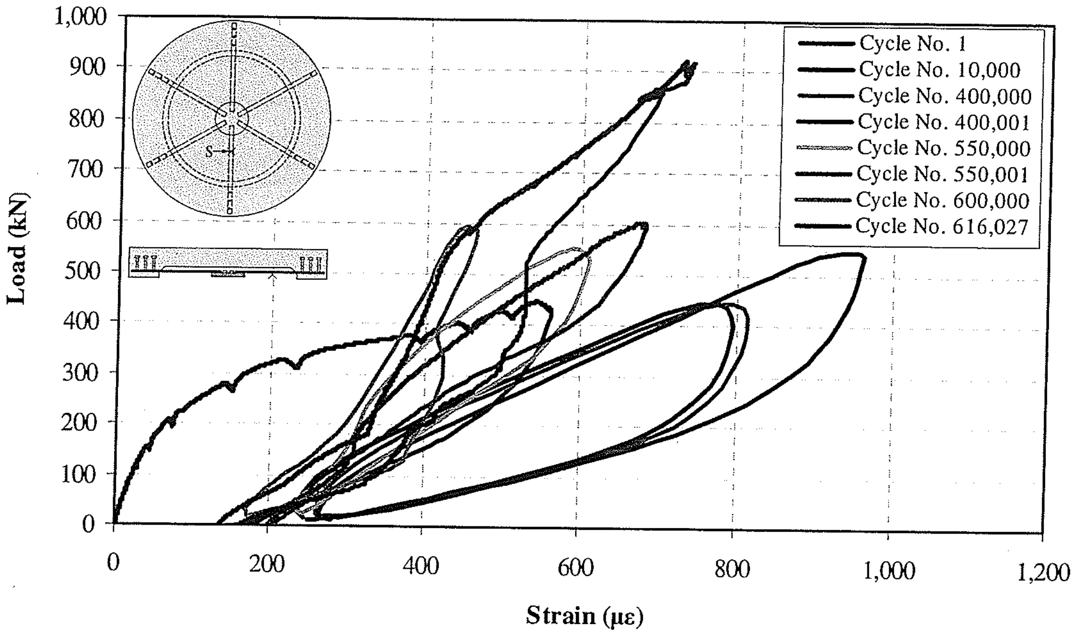

Figure 39: Load vs. strain behaviour in steel strap at ESG S location of Slab-2

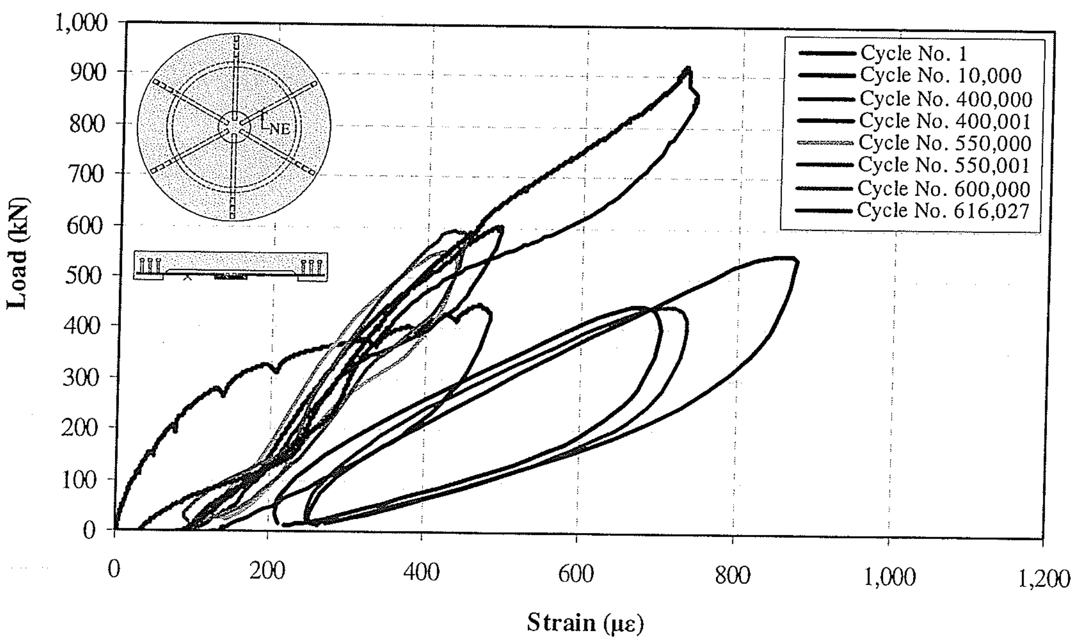

Figure 40: Load vs. strain behaviour in steel strap at ESG NE location of Slab-2

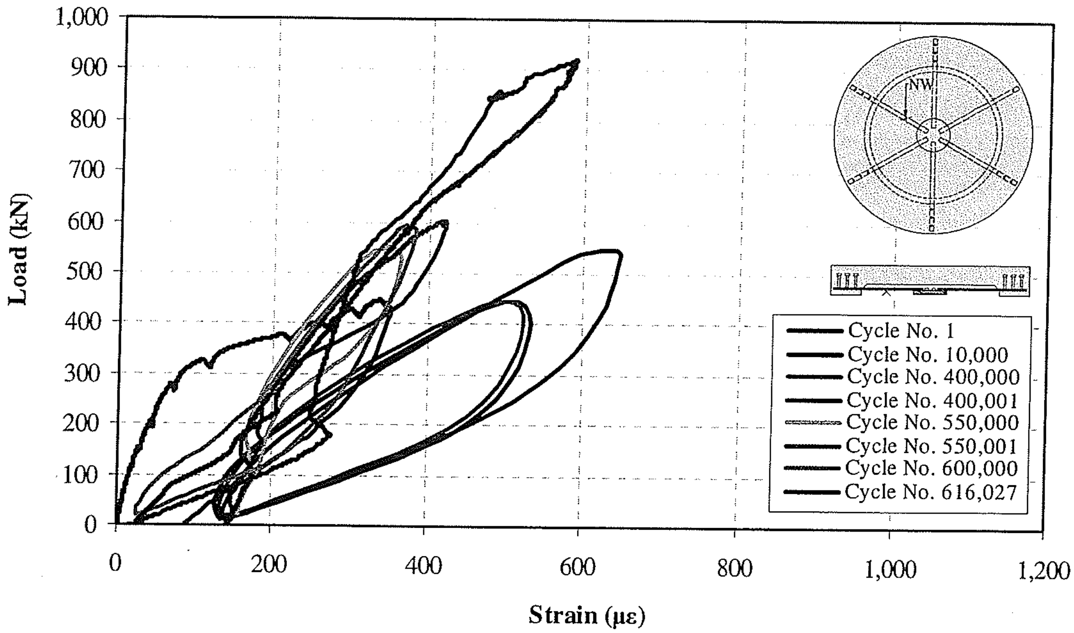

Figure 41: Load vs. strain behaviour in steel strap at ESG NW location of Slab-2

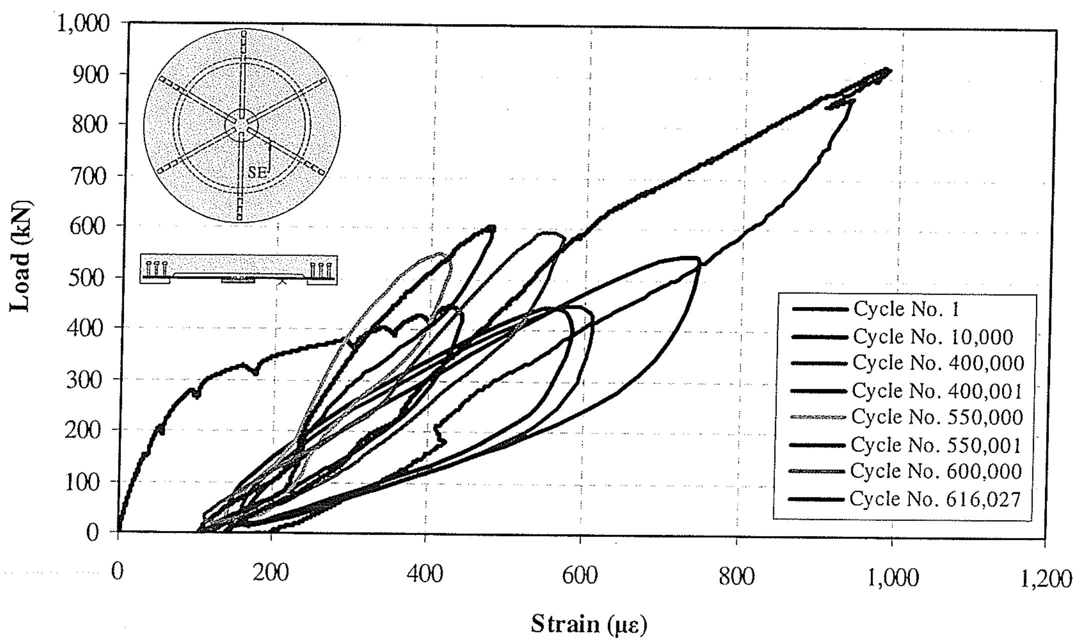

Figure 42: Load vs. strain behaviour in steel strap at ESG SE location of Slab-2

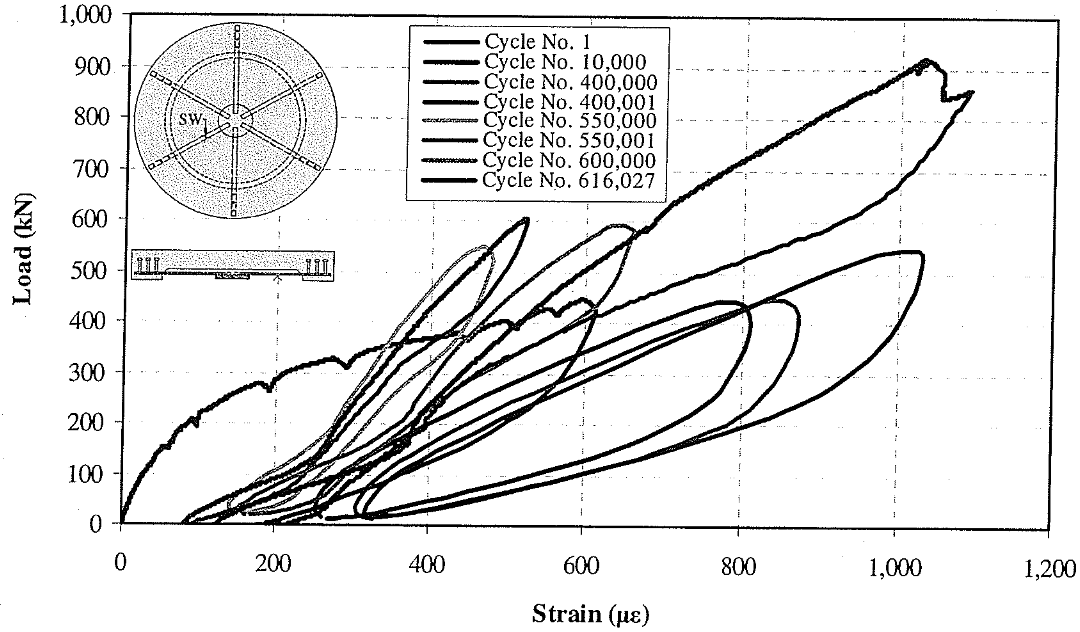

Figure 43: Load vs. strain behaviour in steel strap at ESG SW location of Slab-2

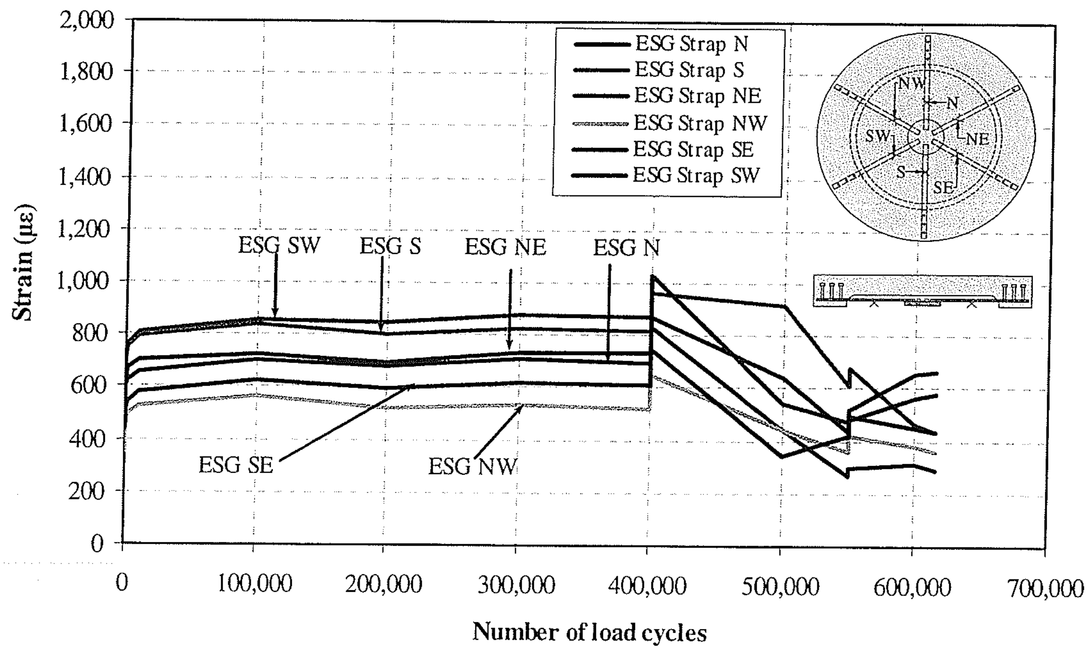

Figure 44: Strain in steel straps vs. number of load cycles behaviour of Slab-2

Table 4: Strain in steel straps vs. number of load cycles behaviour of Slab-2

Amplitude of load (kN)	Number of load cycles	Strain in steel straps (με)					
		ESG strap N	ESG strap S	ESG strap NE	ESG strap NW	ESG strap SE	ESG strap SW
445	1	515.19	561.37	482.26	351.20	440.67	612.75
	10	574.89	654.03	567.51	415.46	494.58	694.23
	100	606.13	705.18	615.26	444.06	503.53	728.81
	1,000	623.82	757.83	671.78	499.06	540.01	766.68
	10,000	658.75	794.38	698.62	530.50	580.08	808.07
	100,000	700.04	838.26	726.78	562.98	627.42	853.84
	400,000	692.78	814.07	734.90	522.04	610.14	873.36
550	400,001	834.22	959.38	872.37	645.62	744.53	1030.90
	550,000	265.77	607.34	436.02	361.91	422.68	476.33
600	550,001	301.05	681.67	494.49	420.51	477.56	522.83
	600,000	313.65	463.82	448.53	380.63	568.68	658.75
	616,026	291.47	436.19	436.37	360.66	581.74	660.89
920 (Static)	616,027	411.47	738.24	742.93	585.52	984.21	1089.55

4.2.3 Crack width and crack mapping

In total four pi gauges were installed on the underside of the slab to measure the width of radial cracks. The increase of crack widths with the increase of loading and number of load cycles is shown in Figure 45, Figure 46, Figure 47 and Figure 48. As the cracks did not propagate through the initial location of the pi gauges, no data for the crack widths were available for the first loading cycle. During the first loading cycle, the first radial crack was visible at around 200 kN on the bottom of the slab along the south direction. The number of radial cracks increased with increasing load. The load was removed after reaching 445 kN, and thus the first loading cycle was completed. After the first loading cycle, four pi gauges were mounted to span the appropriate cracks. The number of cycles verses crack width profile (Figure 49 and Table 5) shows that the crack widths in all directions were almost stable up to 400,000 loading cycles. After 400,000 cycles, the fatigue cycling was stopped and it was decided to increase the magnitude of the maximum load for the load cycles. The load was monotonically increased by 25 kN increments. The circumferential crack was first visible at the top of the slab at around 500 kN. At 550 kN, a significant number of radial cracks were observed at the bottom of the slab and the circumferential crack widened. A significant increase in the number and width of the radial cracks was observed in all directions under the slab from 440,001 to 550,000 load cycles. The widest radial crack was observed at the north-east direction under pi gauge Pi-2. Again a significant increase in the crack widths was observed after the increase of the cyclic load from 550 kN to 600 kN at 550,000 loading cycles. The pi gauge Pi-1 detached from the slab between cycle number 550,001 and 616,026, and for that reason the data from pi gauge Pi-1 was not available between cycle 550,001 to 616,026. After 616,026 loading cycles the detached pi gauge Pi-1 was mounted again. The deck failed after shear cracks formed at the bottom of the deck at a static load of 920 kN. The widest radial crack observed during failure of the slab was under pi gauge Pi-2 and the width of that crack was 8.11 mm.

Schematic drawings of crack propagation at top and bottom of Slab-1 at different loading stages are shown in Figure 50. Photographs of the crack patterns of Slab-1after failure are shown in Figure 51.

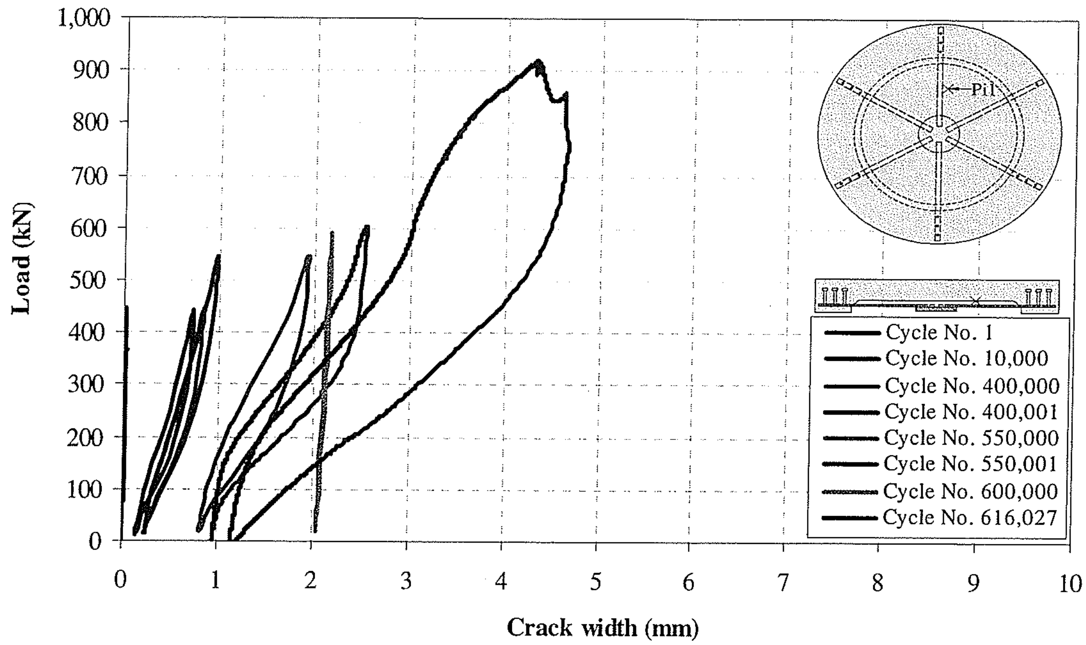

Figure 45: Load vs. crack width behaviour at Pi-1 location of Slab-2

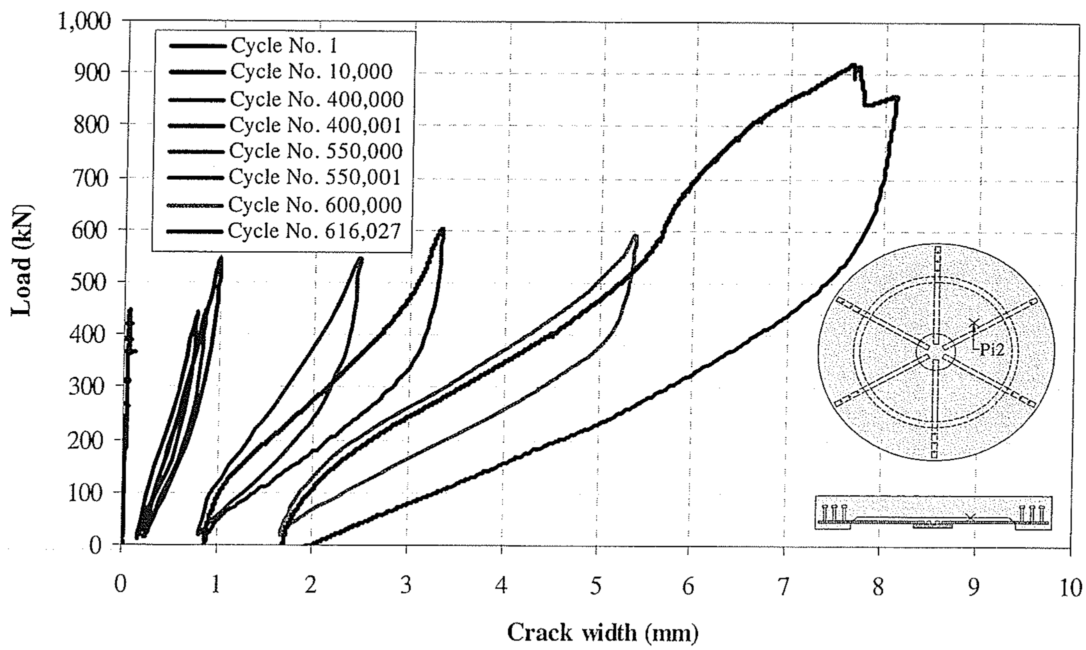

Figure 46: Load vs. crack width behaviour at Pi-2 location of Slab-2

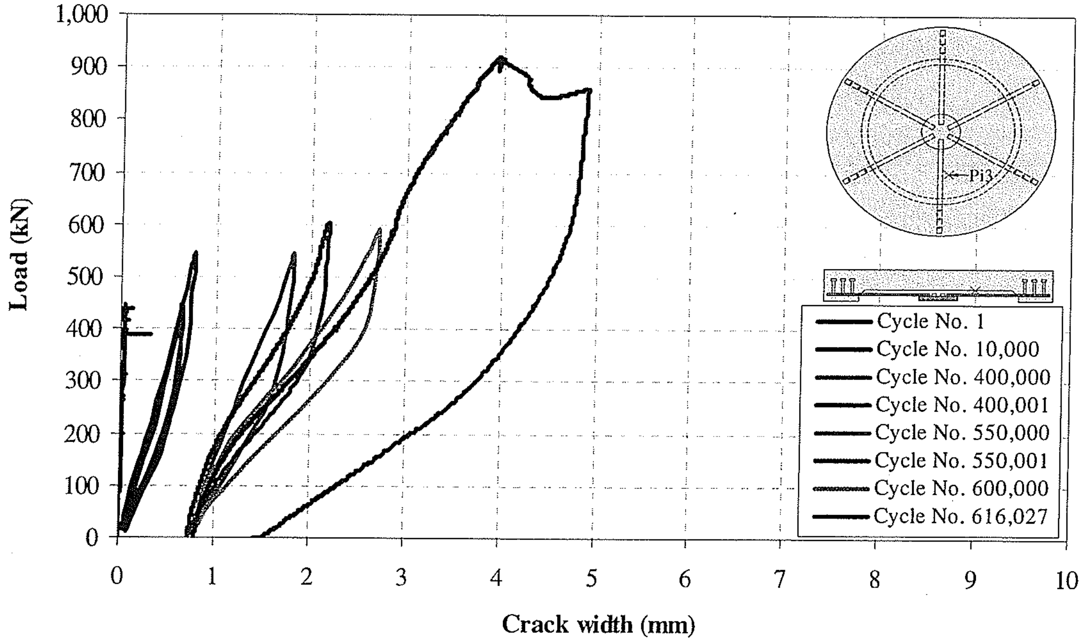

Figure 47: Load vs. crack width behaviour at Pi-3 location of Slab-2

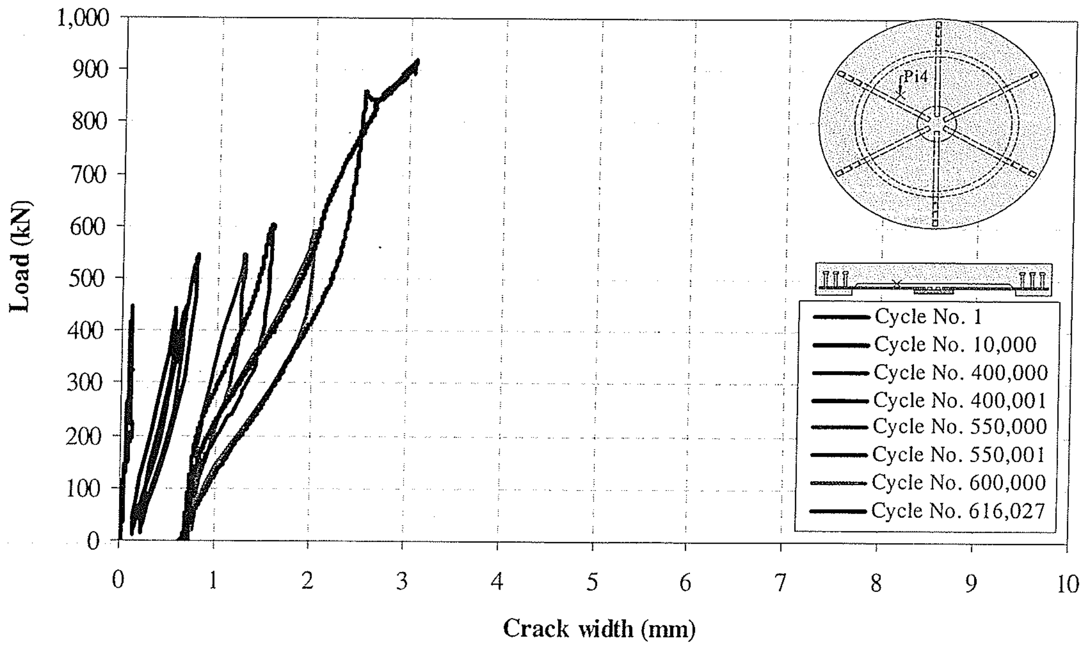

Figure 48: Load vs. crack width behaviour at Pi-4 location of Slab-2

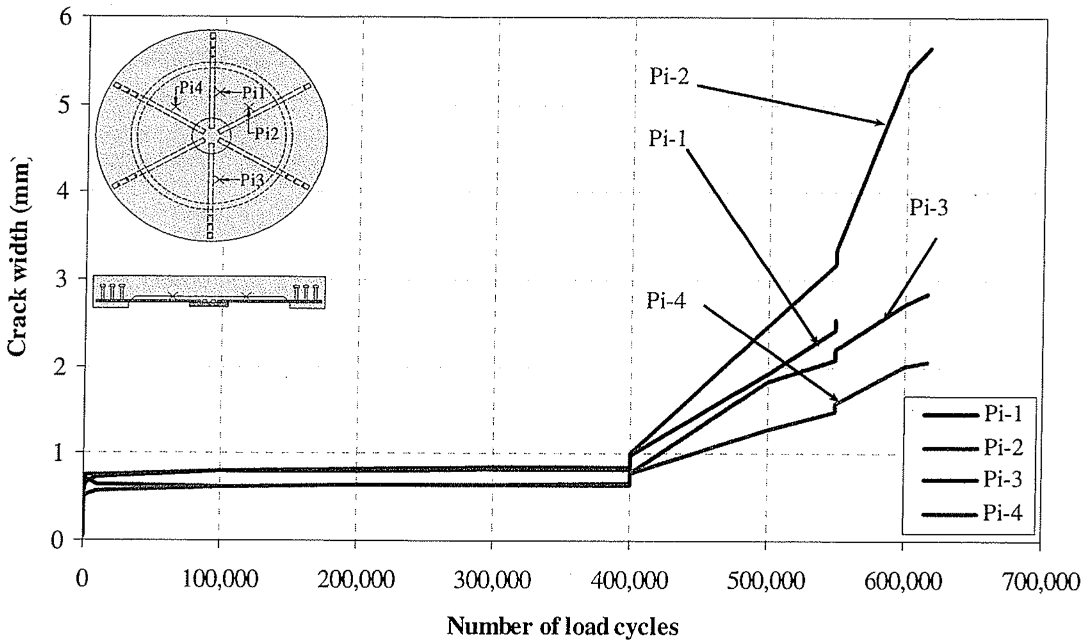

Figure 49: Crack width vs. number of load cycles behaviour of Slab-2

Table 5: Crack width vs. number of load cycles behaviour of Slab-2

Amplitude of load (kN)	Number of load cycles	Crack width (mm)			
		Pi-1	Pi-2	Pi-3	Pi-4
445	1	0.04	0.12	0.32	0.12
	10	0.49	0.66	0.61	0.43
	100	0.56	0.68	0.65	0.48
	1,000	0.65	0.76	0.71	0.54
	10,000	0.74	0.76	0.64	0.57
	100,000	0.80	0.80	0.61	0.61
	400,000	0.83	0.86	0.63	0.66
550	400,001	0.98	1.00	0.78	0.79
	550,000	2.43	3.19	2.08	1.49
600	550,001	2.55	3.34	2.19	1.58
	600,000	-	5.39	2.72	2.02
	616,026	-	5.65	2.83	2.07
920 (Static)	616,027	4.65	8.11	4.90	3.07

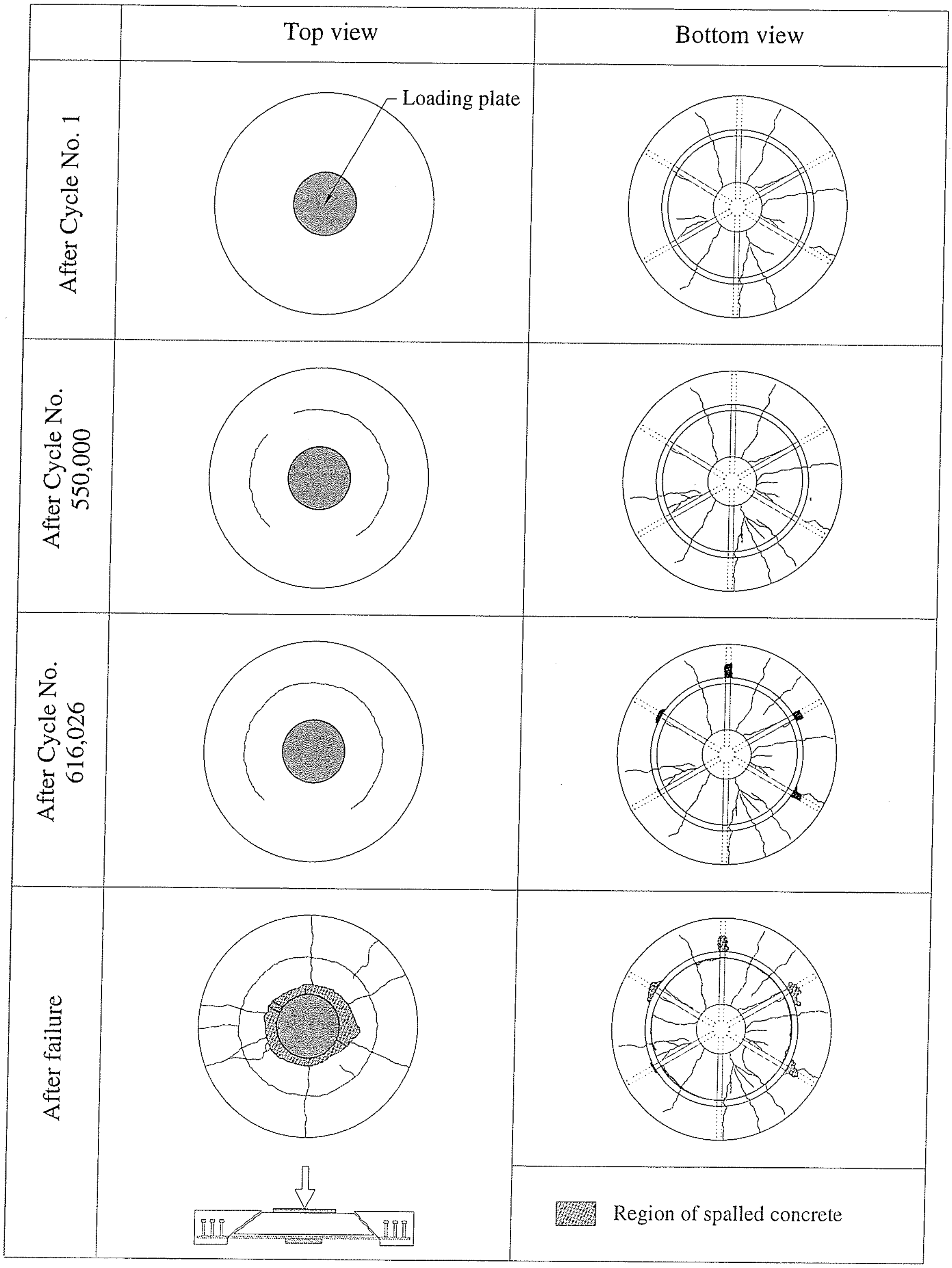

Figure 50: Crack patterns of Slab-2 at different stages of loading cycles

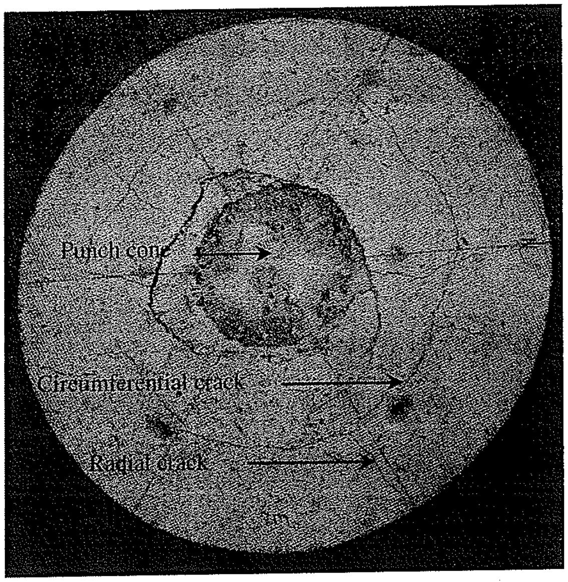

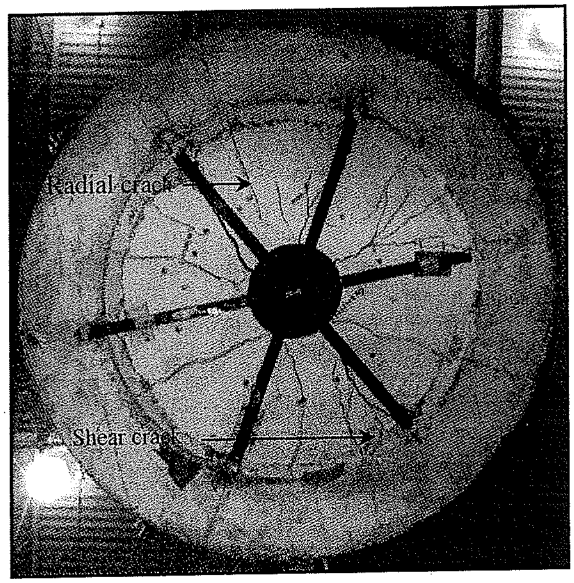

Top view **Bottom view**

Figure 51: Crack patterns of Slab-2 after failure

4.2.4 Strains in circumferential CFRP wrap

The progressive increase in strain in the circumferential CFRP wrap with the increase of peak load and number of loading cycles are shown in the load verses strain in CFRP wrap curves (Figure 52, Figure 53, Figure 54 and Figure 55). As shown in strain in CFRP wrap vs. number of load cycles (Figure 56 and Table 6), the strains in all locations of the CFRP wrap were almost steady until 400,000 loading cycles under 445 kN load. The CFRP wrap experienced higher strains in the north and south directions than the east and west directions. The increase in the strains in the CFRP wrap in the north and south directions are apparent due to the increase of the cyclic load from 445 kN to 550 kN. The strain in the CFRP wrap increased steadily in all directions until 550,000 loading cycles. There was a little jump in the strain in the CFRP wrap in all directions due to the increase of the load from 550 kN to 600 kN. The strain gauges in the CFRP wrap in the north and south directions were damaged due to the falling of broken grout over the wires of the strain gauges. That is why the data from strain gauges 'EGS CFRP N' and 'EGS CFRP S' were not available in between cycle number 550,001 to 616,026. The damaged strain gauges were replaced with new strain gauges after 616,026 loading cycles. Finally, the slab failed at 920 kN of statically applied load in the punched failure mode when the strain in the CFRP wrap at the north, south and east directions were around 4,200 με and the west direction was 3,231 με.

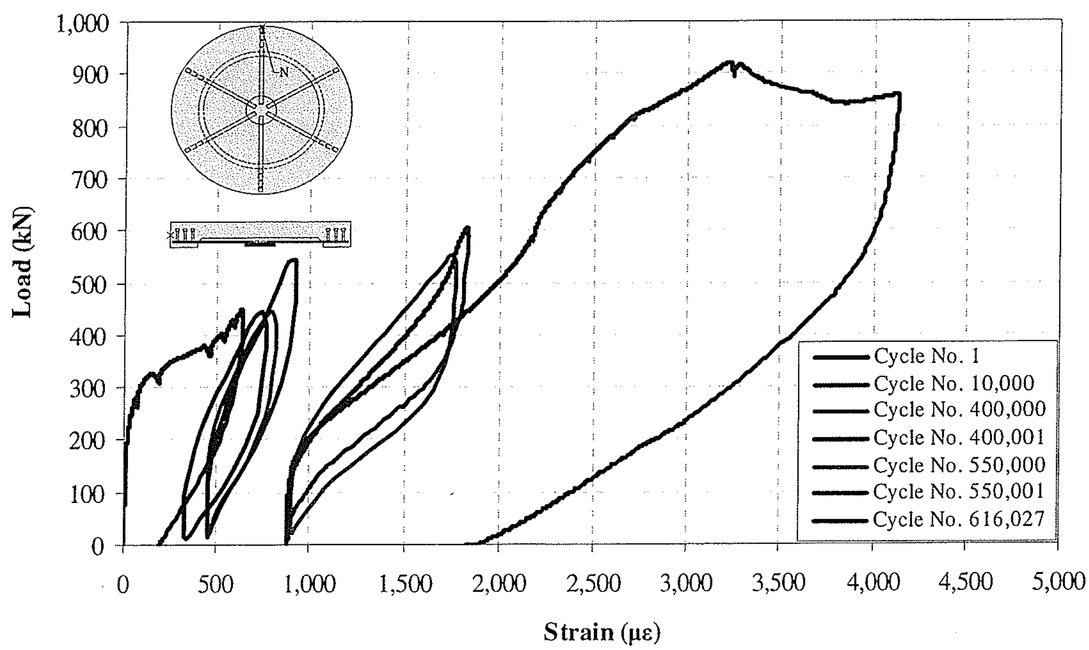

Figure 52: Load vs. strain behaviour in CFRP wrap at EGS CFRP N location of Slab-2

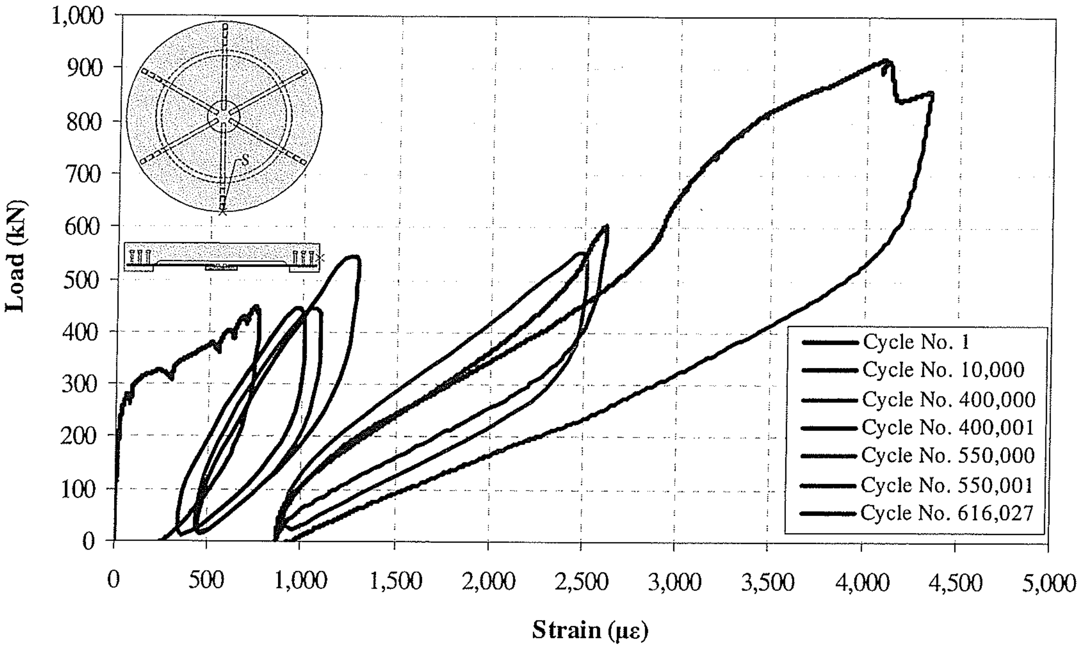

Figure 53: Load vs. strain behaviour in CFRP wrap at EGS CFRP S location of Slab-2

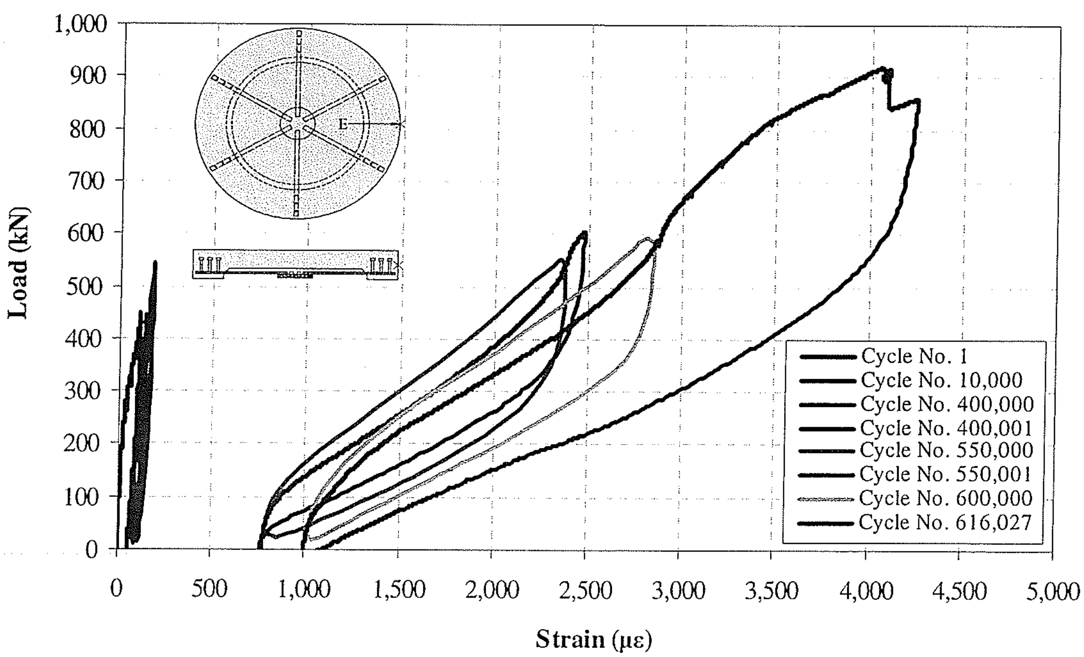

Figure 54: Load vs. strain behaviour in CFRP wrap at EGS CFRP E location of Slab-2

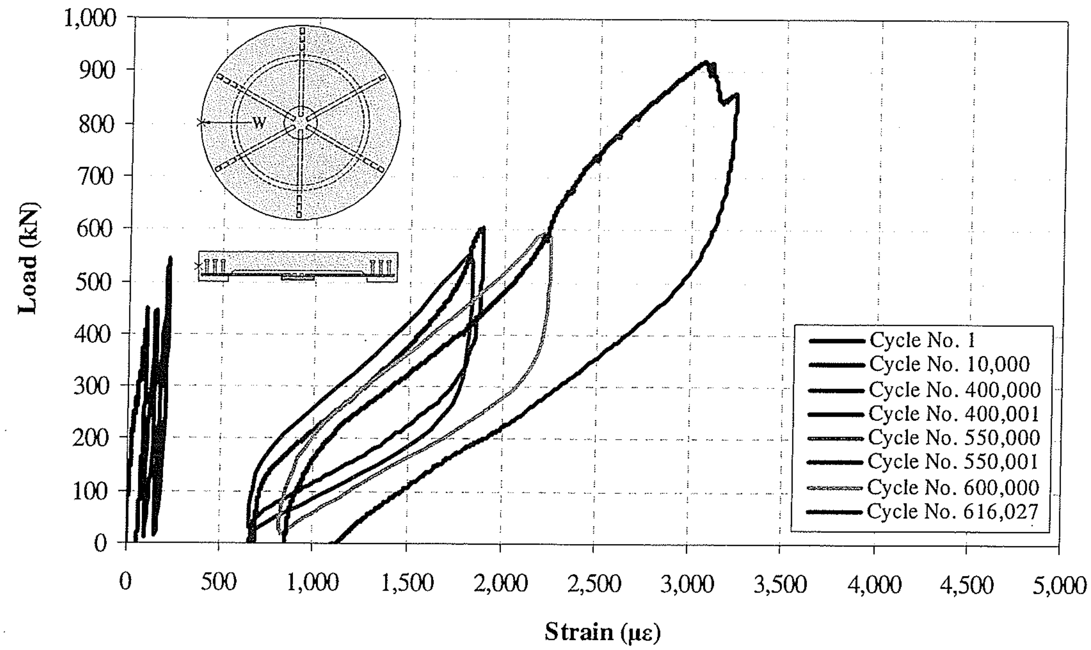

Figure 55: Load vs. strain behaviour in CFRP wrap at EGS CFRP W location of Slab-2

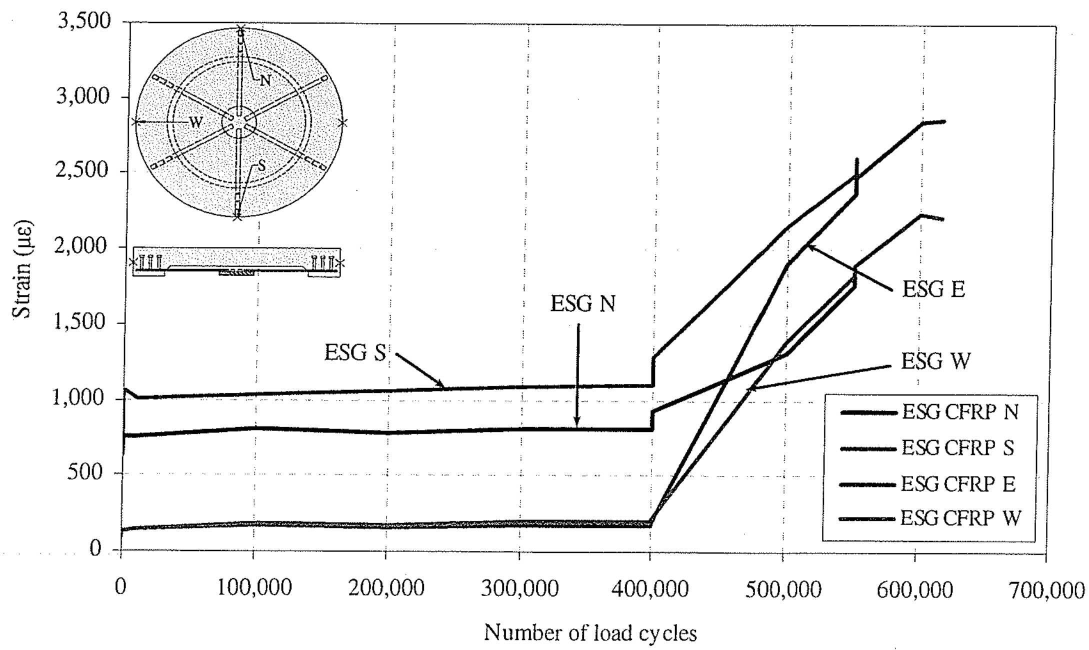

Figure 56: Strain in CFRP wrap vs. number of load cycles behaviour of Slab-2

Table 6: Strain in CFRP wrap vs. number of load cycles behaviour of Slab-2

Amplitude of load (kN)	Number of load cycles	Strain in CFRP wrap (με)			
		ESG CFRP N	ESG CFRP S	ESG CFRP E	ESG CFRP W
445	1	638.64	763.71	111.32	99.29
	10	686.59	957.76	123.62	113.42
	100	730.67	1021.26	127.60	118.07
	1,000	749.47	1065.62	136.58	130.92
	10,000	759.66	1008.54	143.66	145.64
	100,000	810.27	1039.46	167.50	182.43
	400,000	812.17	1096.30	168.71	201.43
550	400,001	926.77	1291.22	180.73	214.94
	550,000	1769.74	2509.87	2377.79	1835.39
600	550,001	1832.03	2617.45	2478.90	1890.67
	600,000	-	-	2849.86	2246.17
	616,026	-	-	2868.31	2213.63
920 (Static)	616,027	4131.11	4341.92	4247.30	3231.14

4.2.5 Strains in concrete

A three dimensional array of twelve 25 mm electronic strain gauges were installed at middle of the slab to record the three dimensional state of strains in concrete of the slab. Unfortunately after around 200,000 loading cycles all the strain data recorded by the strain gauges appeared abnormal, which indicate that none of the strain gauges were functioning properly after around 200,000 loading cycles and were damaged under fatigue load due to the friction between concrete and strain gauges.

4.3 Test results of Slab-3

4.3.1 Deflection

The progressive increase of both residual deflection and elastic deflection along with the loss of flexural stiffness; with the increase in number of loading cycles are shown in load verses deflection curves at 'LVDT SI' and 'LVDT SO' locations (Figure 57 and Figure 58). The amount of energy lost with each of the cycles, represented by the area between the loaded and unloaded curves for each cycle, increased gradually with the increase in the number of loading cycles. The energy lost at failure was significant. The number of cycle verses deflection profile (Figure 59 and Table 7) demonstrates that the deflection in both the inner LVDT and outer LVDT locations increased gradually until 16,000 loading cycles. After 18,000 loading cycles the rate of change in the deflections began to increase. The slab finally failed after 18,204 loading cycles in the punched failure mode. The deflections of the slab during failure at the location of the inner and outer LVDTs were around 22.33 mm and 7.13 mm respectively. The deflection profile along the north-south centre-line of the slab subjected to fatigue loading is shown in Figure 60.

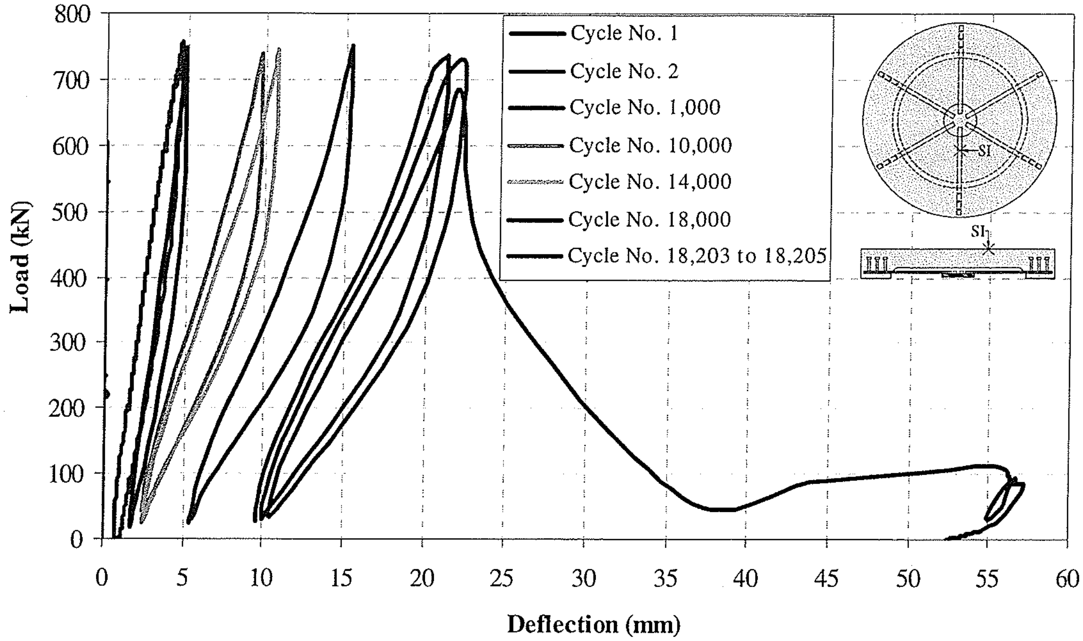

Figure 57: Load vs. deflection behaviour at LVDT SI location of Slab-3

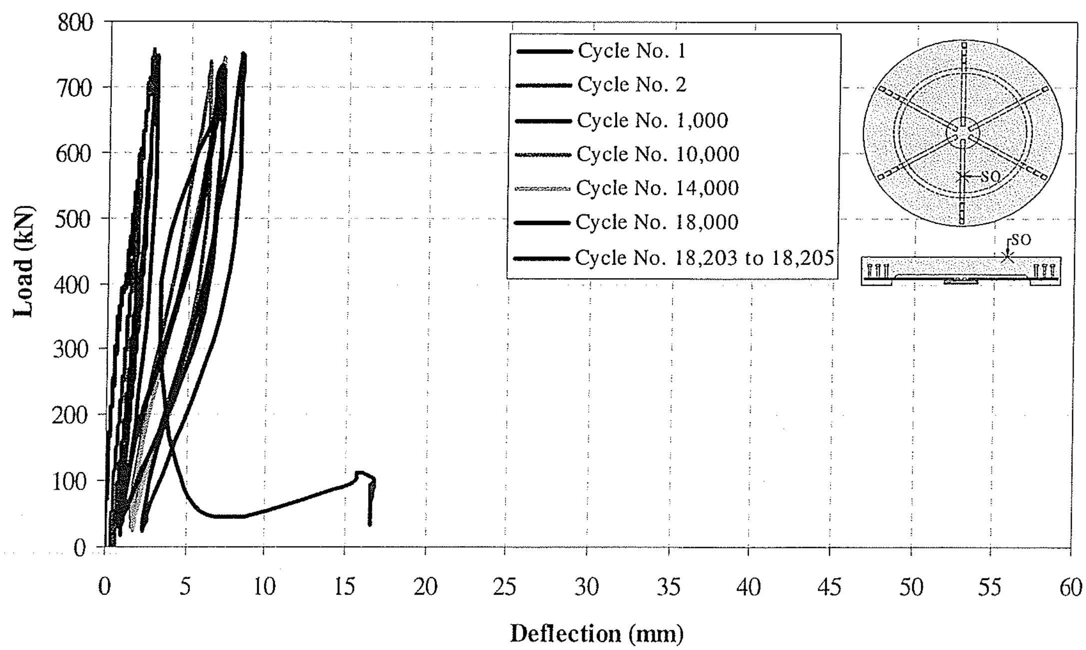

Figure 58: Load vs. deflection behaviour at LVDT SO location of Slab-3

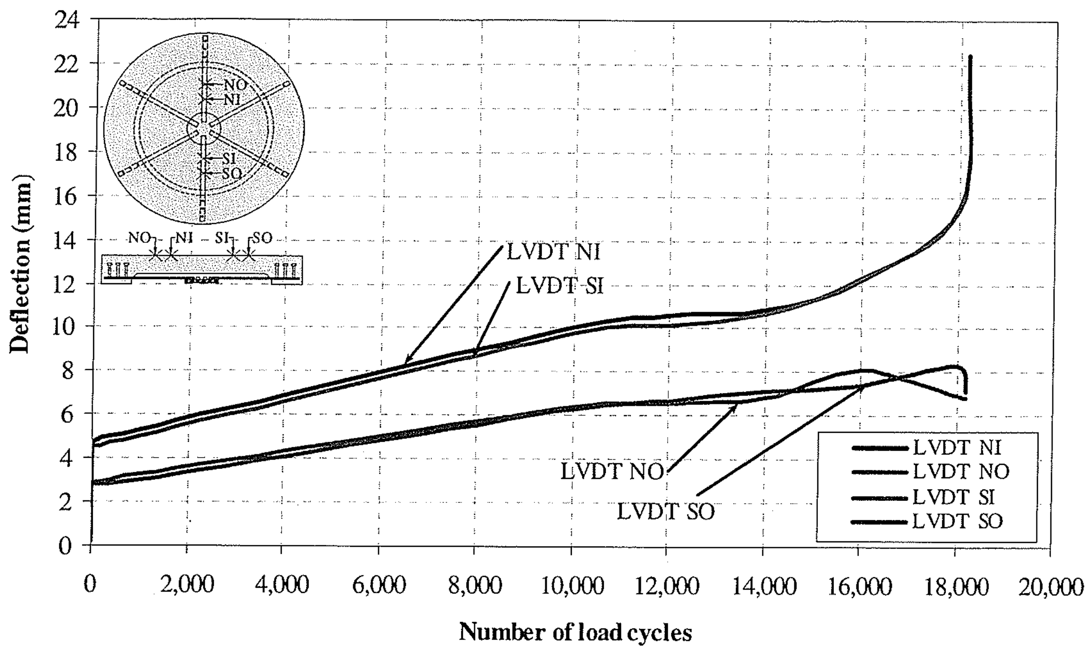

Figure 59: Deflection vs. number of load cycles behaviour of Slab-3

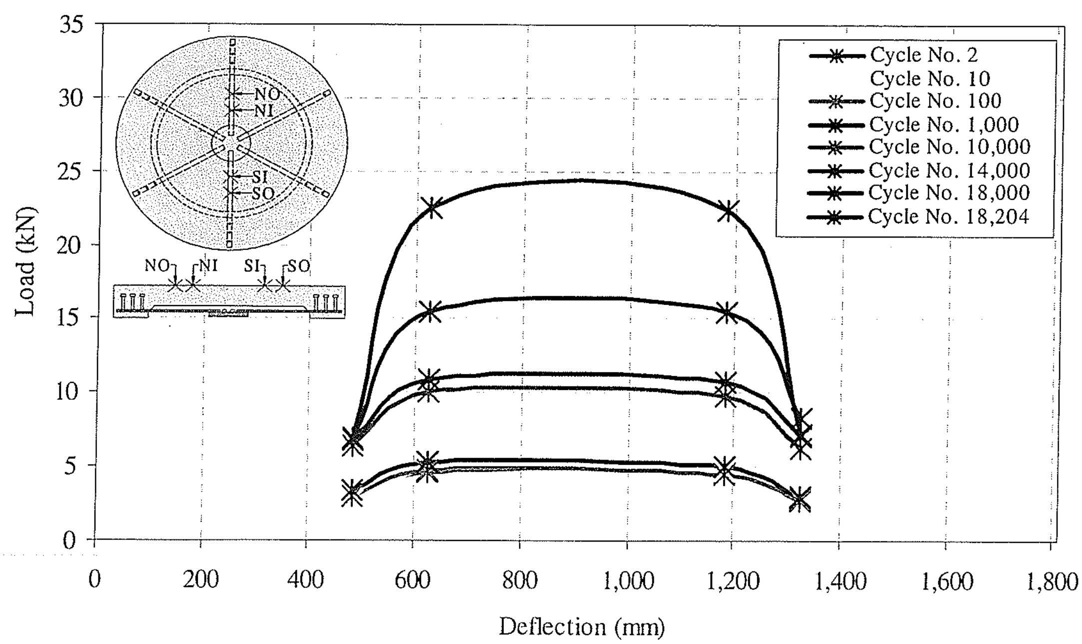

Figure 60: Deflection profile of Slab-3 along north-south centre line of the slab

Table 7: Deflection profile of Slab-3 along north-south centre-line of the slab

Number of load cycles \ Distance along deck (mm)	485	625	1185	1325
2	2.71	4.60	4.67	2.73
10	2.73	4.72	4.77	2.86
100	2.92	4.80	4.53	2.84
1,000	3.33	5.32	4.98	3.01
10,000	6.37	10.02	9.76	6.30
12,000	6.61	10.58	10.17	6.68
14,000	6.82	10.88	10.71	7.08
16,000	8.09	12.21	12.32	7.42
18,000	6.95	15.51	15.41	8.31
18,204	6.87	22.47	22.33	7.13

Note: All deflections are in millimetres

4.3.2 Strains in steel straps

A 25 mm electric strain gauge was installed at the mid-length of each steel straps to record the strains in the straps under fatigue loading. The recorded strains in the six steel straps are shown in load verses strain in steel straps curves (Figure 61, Figure 62, Figure 63, Figure 64, Figure 65 and Figure 66). The number of load cycles verses strain profile (Figure 67 and Table 8) suggested that the strain in all steel straps decreased with the increasing number of loading cycles and this trend continued in all steel straps up to cycle number 120,000. The lowest strain observed after 120,000 loading cycles was 527 $\mu\varepsilon$ at the steel strap spanning along the south-east direction. After 120,000 loading cycles, the strains in the steel straps spanning in north and south-west directions continued to decrease with some fluctuations. Whereas, the strains in the steel straps spanning along north-east, north-west, south and south-east directions increased gradually. After 18,204 loading cycles, the maximum strain of 1,079 με was recorded at the steel strap spanning the north-ease direction and the minimum strain of 530 με was recorded at the steel strap spanning the south-west direction.

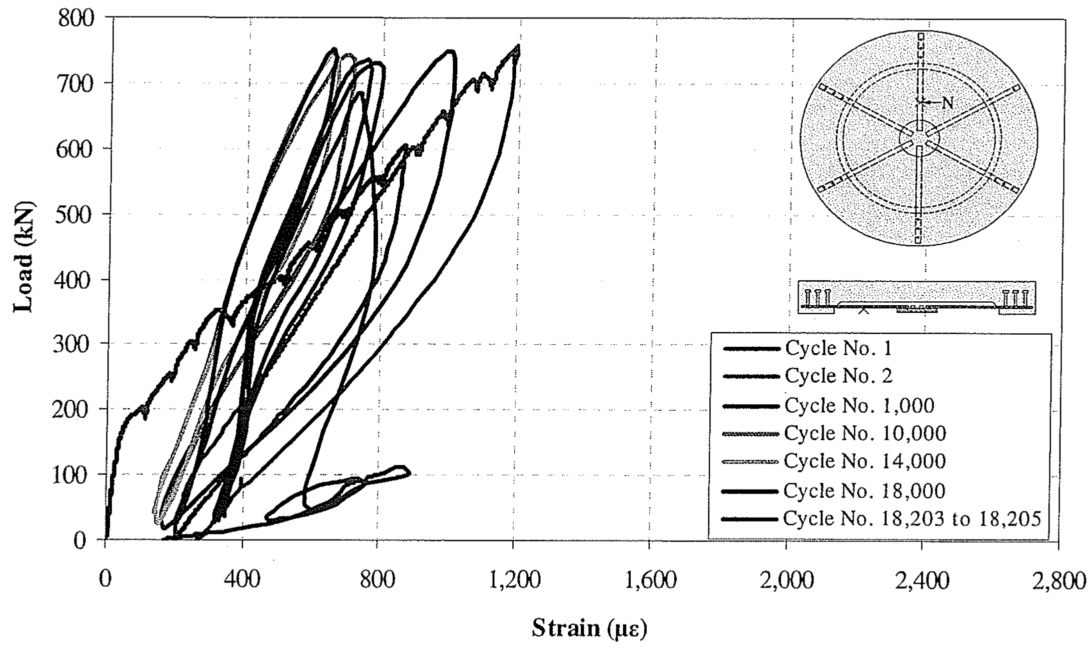

Figure 61: Load vs. strain behaviour in steel strap at ESG N location of Slab-3

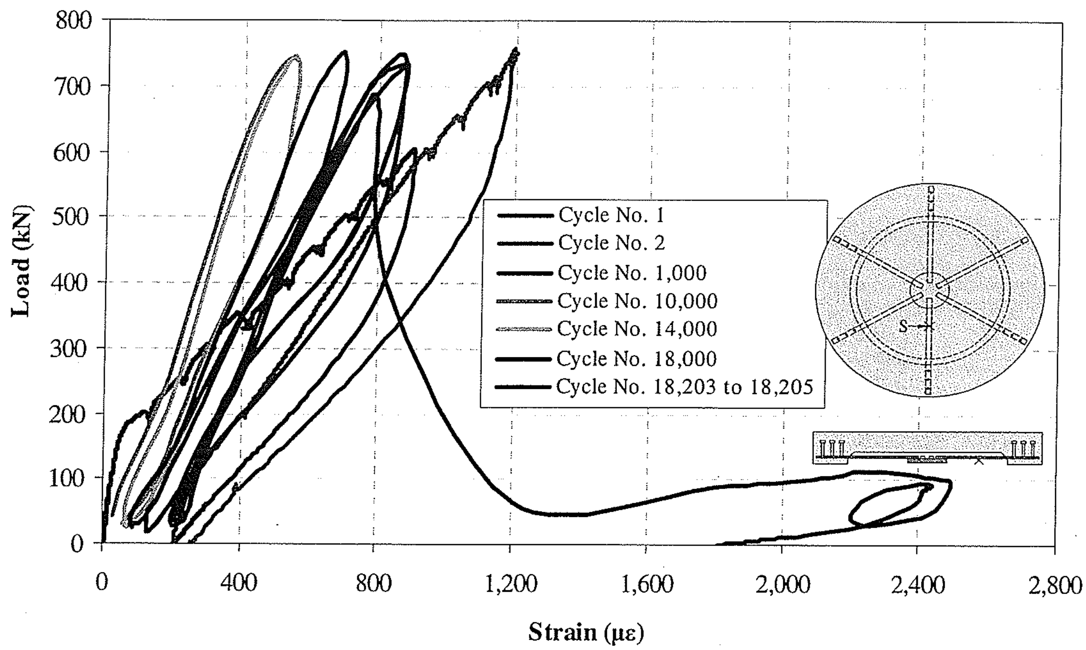

Figure 62: Load vs. strain behaviour in steel strap at ESG S location of Slab-3

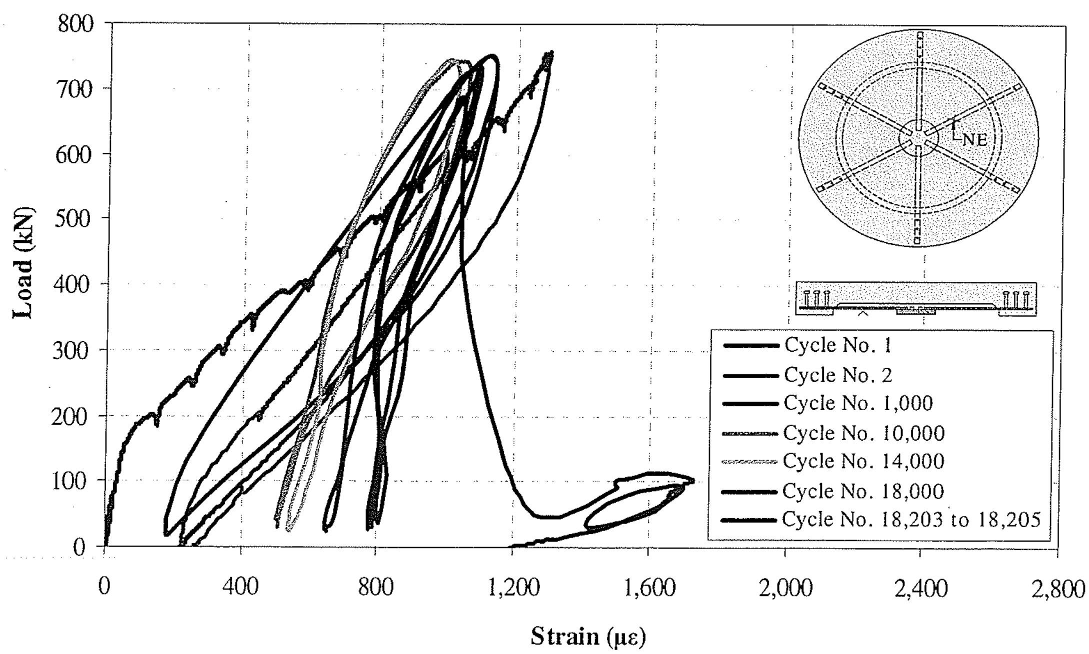

Figure 63: Load vs. strain behaviour in steel strap at ESG NE location of Slab-3

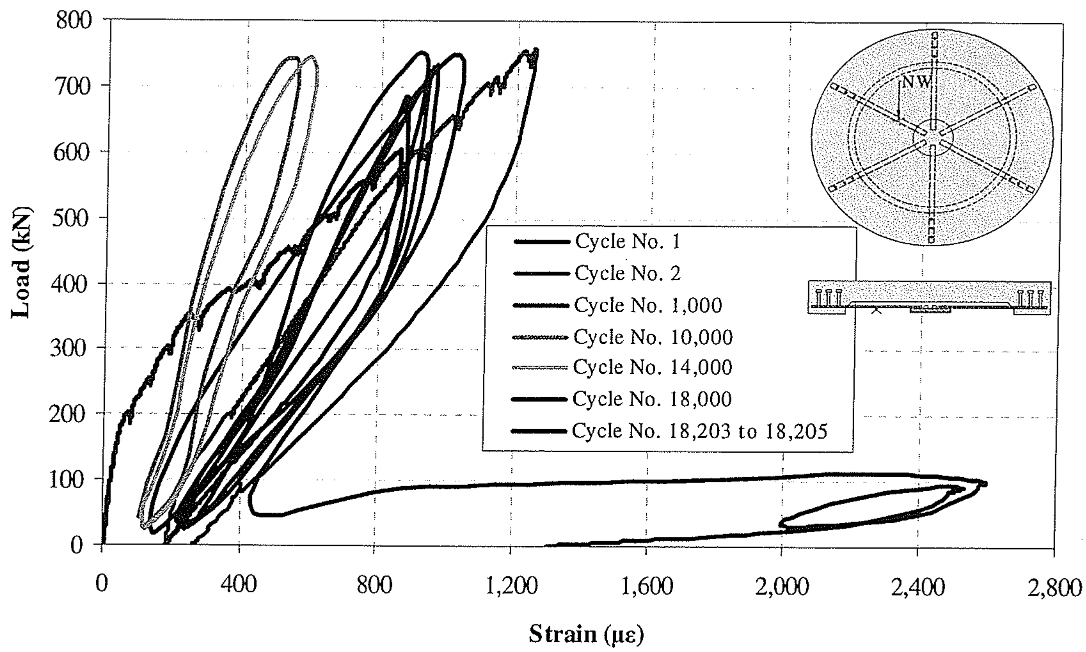

Figure 64: Load vs. strain behaviour in steel strap at ESG NW location of Slab-3

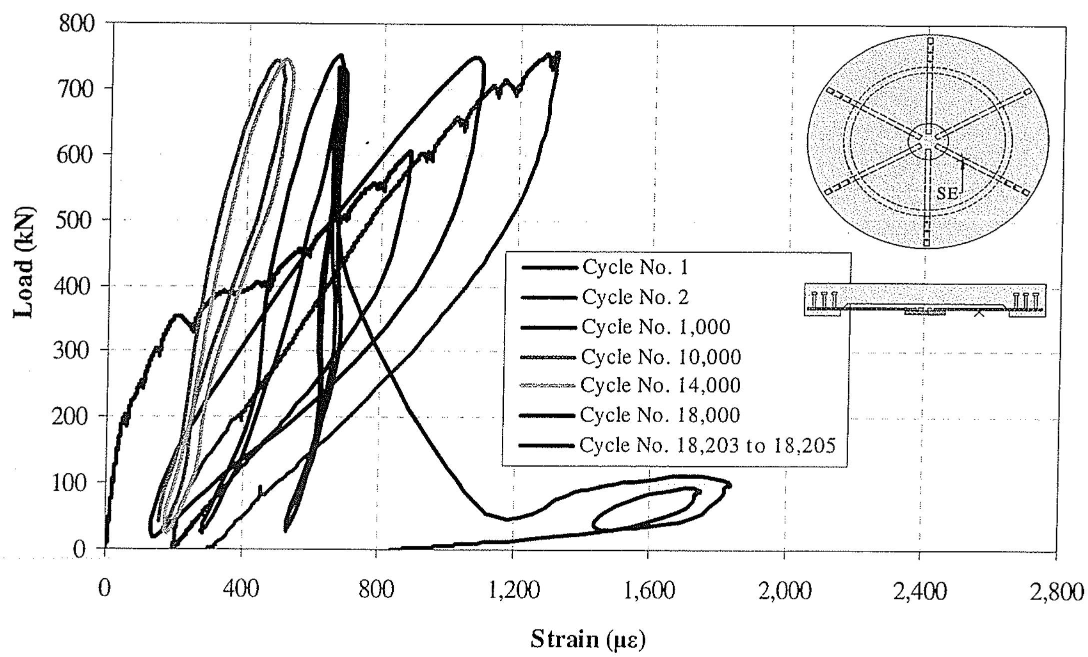

Figure 65: Load vs. strain behaviour in steel strap at ESG SE location of Slab-3

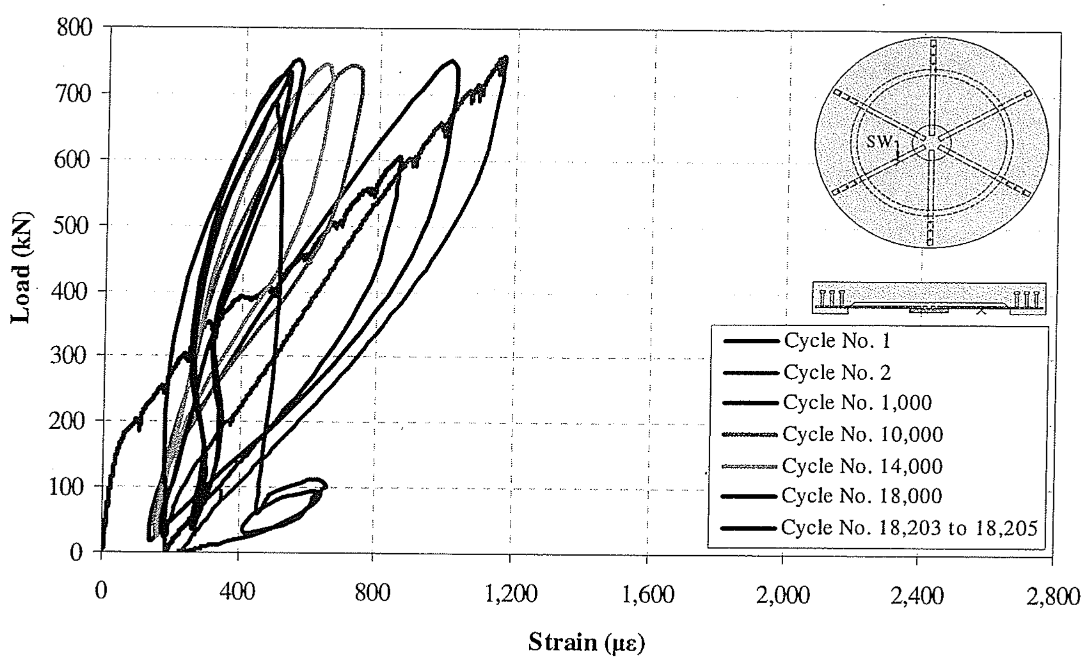

Figure 66: Load vs. strain behaviour in steel strap at ESG SW location of Slab-3

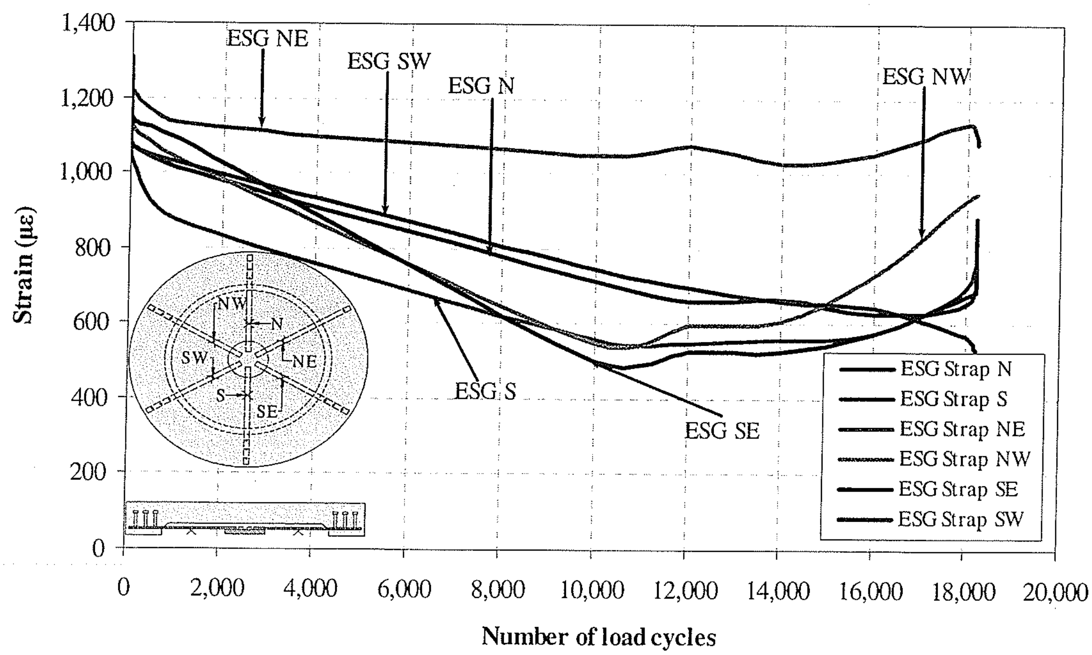

Figure 67: Strain in steel straps vs. number of load cycles behaviour of Slab-3

Table 8: Strain in steel straps vs. number of load cycles behaviour of Slab-3

Number of load cycles	Strain in steel straps (με)					
	ESG STRAP N	ESG STRAP S	ESG STRAP NE	ESG STRAP NW	ESG STRAP SE	ESG STRAP SW
1	1194	1197	1292	1249	1308	1162
10	1102	1102	1260	1188	1217	1099
100	1065	1018	1210	1113	1135	1065
1,000	1010	874	1133	1036	1090	1027
10,000	711	559	1051	550	502	744
12,000	660	550	1074	597	527	696
14,000	664	557	1025	608	528	660
16,000	629	576	1053	728	573	643
18,000	656	698	1135	930	674	568
18,204	795	881	1079	950	685	530

4.3.3 Crack width and crack mapping

In total four pi gauges were installed under the slab to record the width of radial cracks. The increase of crack widths with the increasing number of loading cycles are shown in the load verses crack width curves (Figure 68, Figure 69, Figure 70 and Figure 71). During the first loading cycle, radial cracks were first visible at around 200 kN on the bottom of the slab along the south-east, south-west and north-west directions. It was observed that, radial cracks spanned through all four pi gauges. The LVDT in the north-inner location (LVDT NI) was not functioning properly and for that reason the load was removed after reaching 600 kN to fix the problem with the LVDT. Thus the first loading cycle was completed. After checking all of the equipment and fixing the problem with the LVDT, loading was started again. The circumferential crack was first visible at the top of the slab at around 700 kN during the second loading cycle. The number of radial cracks increased with the increasing number of loading cycles. The number of load cycle verses crack width profile (Figure 72 and Table 9) shows that as the number of loading cycles increased, the width of the radial cracks increased gradually in all pi gauge locations. Unfortunately the pi gauge Pi-3 was not functioning properly after around 18,000 loading cycles. That is why the crack width data in the location of Pi-3 were unavailable after loading cycle 18,000. The deck failed after shear cracks formed at the bottom of the deck at 18,205 loading cycle. The widest radial crack observed during failure of the slab was under pi gauge Pi-1 and the width of that crack was 5.02 mm. The crack patterns of Slab-3 after failure are shown in Figure 74.

Schematic drawings of crack propagation at top and bottom of Slab-1 at different loading stages are shown in Figure 73. Photographs of the crack patterns of Slab-1after failure are shown in Figure 74.

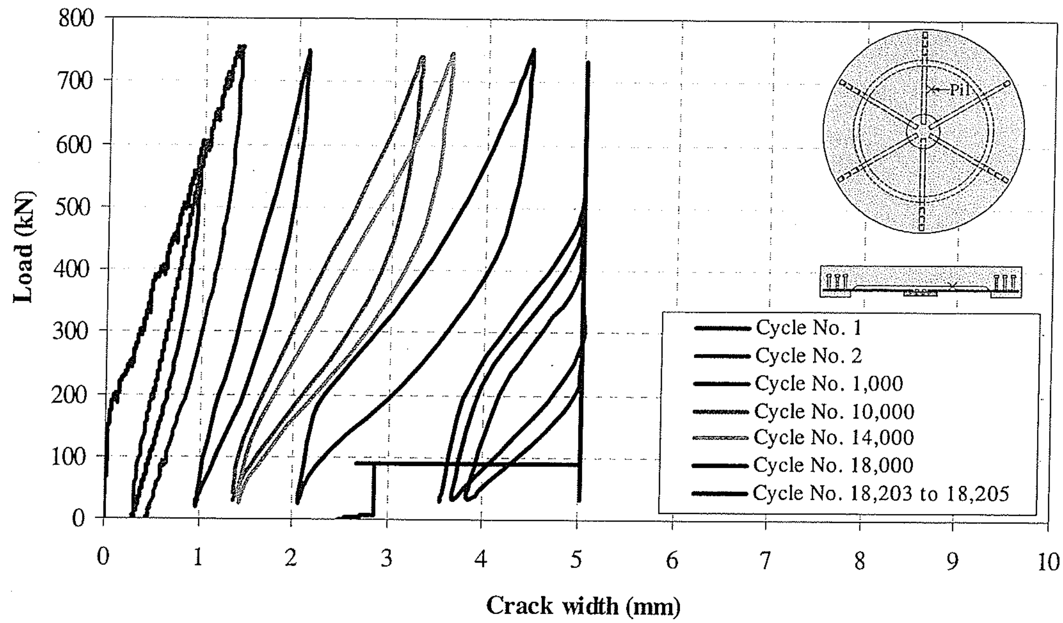

Figure 68: Load vs. crack width behaviour at Pi-1 location of Slab-3

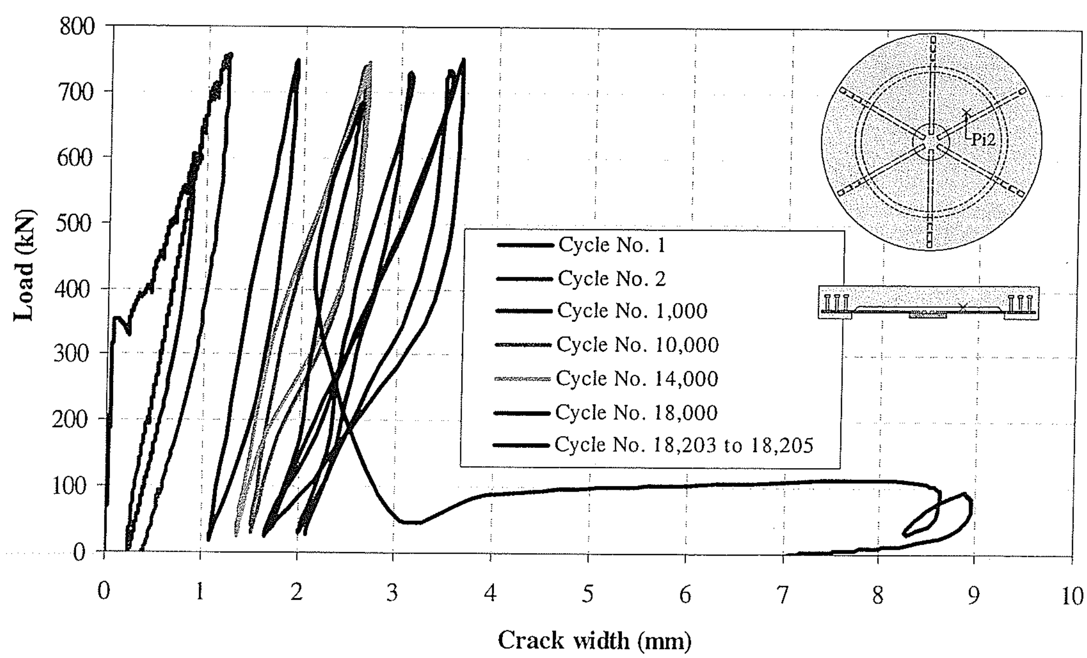

Figure 69: Load vs. crack width behaviour at Pi-2 location of Slab-3

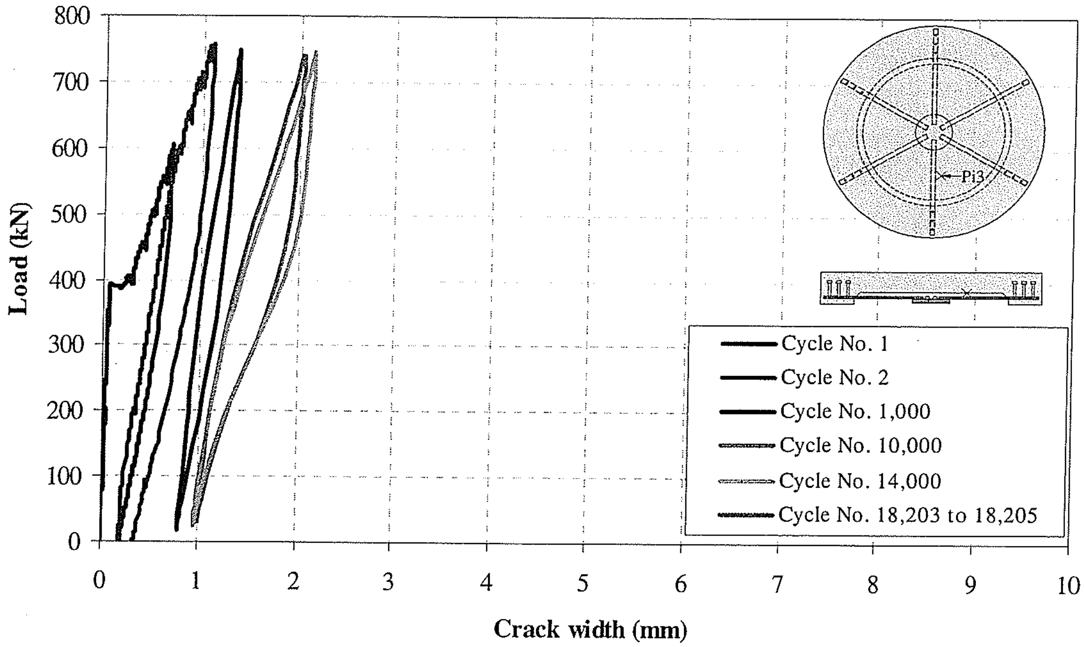

Figure 70: Load vs. crack width behaviour at Pi-3 location of Slab-3

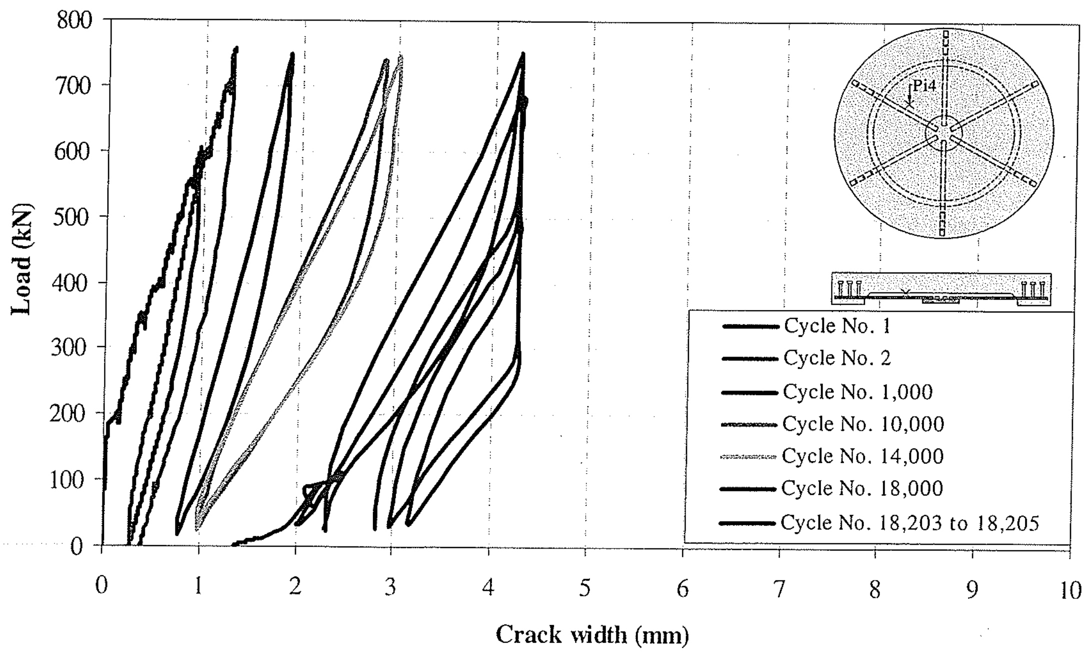

Figure 71: Load vs. crack width behaviour at Pi-4 location of Slab-3

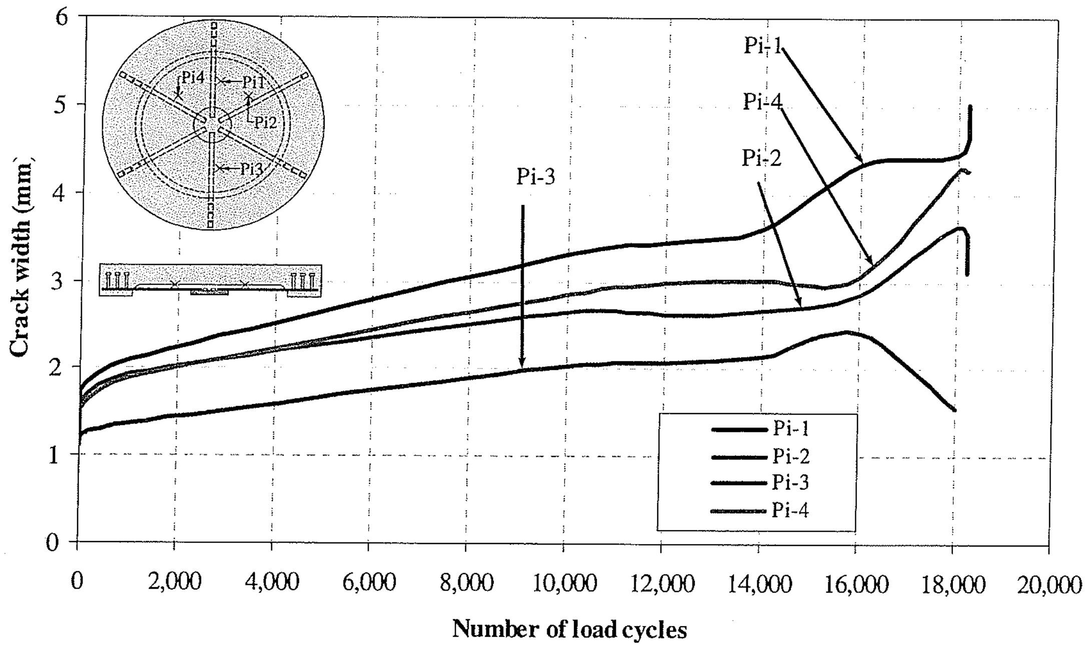

Figure 72: Crack width vs. number of load cycles behaviour of Slab-3

Table 9: Crack width vs. number of load cycles behaviour of Slab-3

Number of load cycles	Crack width (mm)			
	Pi-1	Pi-2	Pi-3	Pi-4
1	1.40	1.22	1.11	1.30
10	1.50	1.33	1.15	1.34
100	1.81	1.68	1.25	1.59
1,000	2.11	1.93	1.37	1.89
10,000	3.30	2.65	2.04	2.86
12,000	3.44	2.63	2.07	2.98
14,000	3.61	2.67	2.15	3.01
16,000	4.33	2.84	2.41	3.05
18,000	4.46	3.63	-	4.27
18,204	5.02	3.11	-	4.27

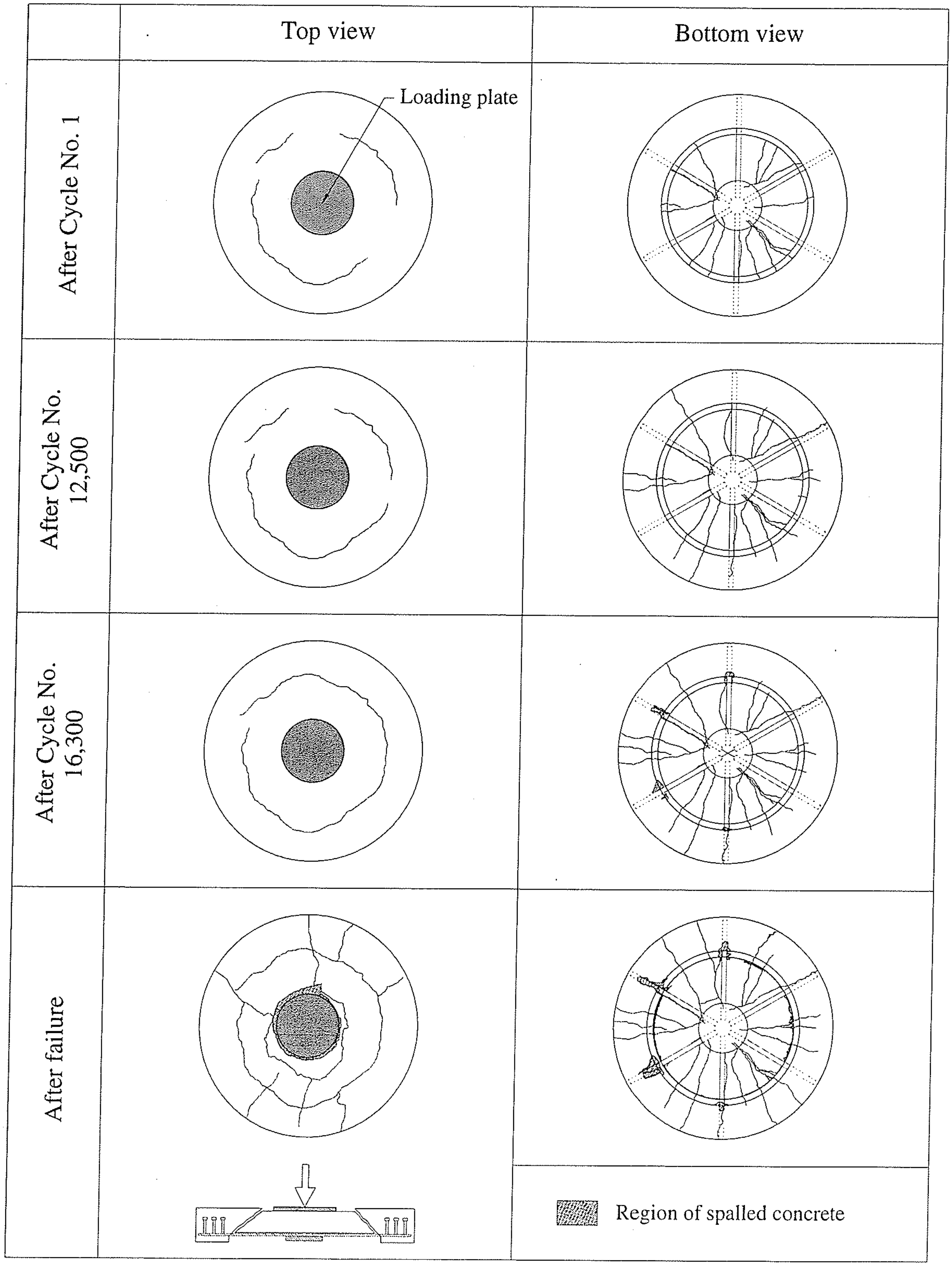

Figure 73: Crack patterns of Slab-3 at different stages of loading cycles

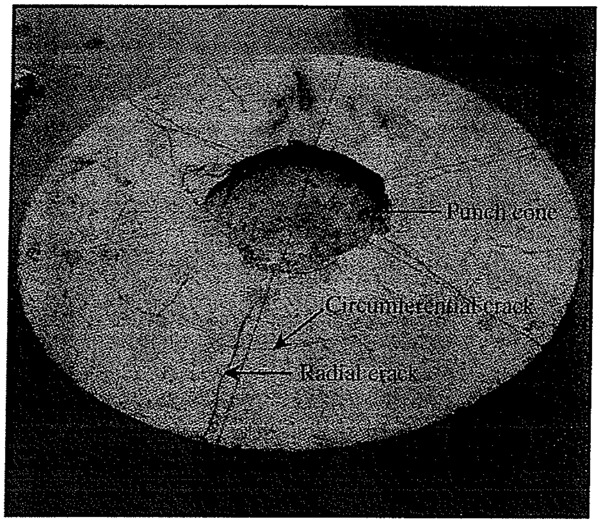

Top view

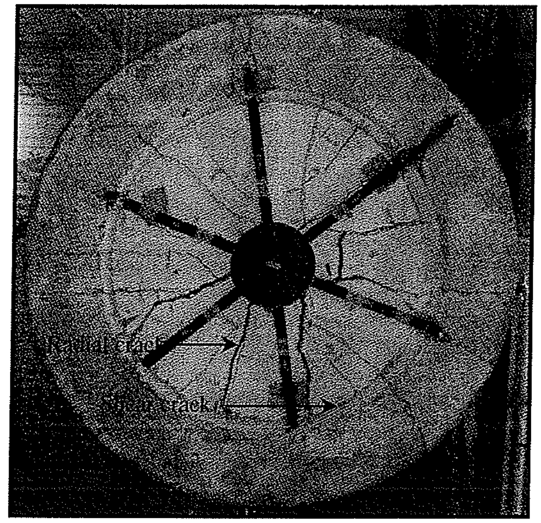

Bottom view

Figure 74 : Crack patterns of Slab-3 after failure

4.3.4 Strains in circumferencial CFRP wrap

The progressive increase in strains in the circumferential CFRP wrap with increase in the number of loading cycles are shown in load verses strain in CFRP wrap curves (Figure 75, Figure 76, Figure 77 and Figure 78). As shown in the strains in CFRP wrap vs. number of load cycles behaviour (Figure 79 and Table 10) the strains in the CFRP wrap increased steadily in all directions with increase in the number of loading cycles. It is worth noting that the strain in the radial steel straps decreased with increase in the loading cycles as described in section 4.3.2. This behaviour of strain in the radial steel-straps and strain in the circumferential CFRP wrap suggested that during the early stage of fatigue loading cycles, confinement provided to the circular steel-free concrete slab was governed by the radial steel straps. With the increase in the number of loading cycles confinement provided to the slab was governed by the circumferential CFRP wrap. The deterioration of the slab can be determined either by the decrease of strain in the radial steel straps or an increase in the strain in the circumferential CFRP wrap. The CFRP wrap experienced higher strains in the east and south corner of the circular slab. Finally, the slab failed at the 18,205 loading cycles in the punching failure mode, when the highest strain (4533 με) was recorded in the south location and the lowest strain (1957 με) was recorded in the north location of the CFRP wrap.

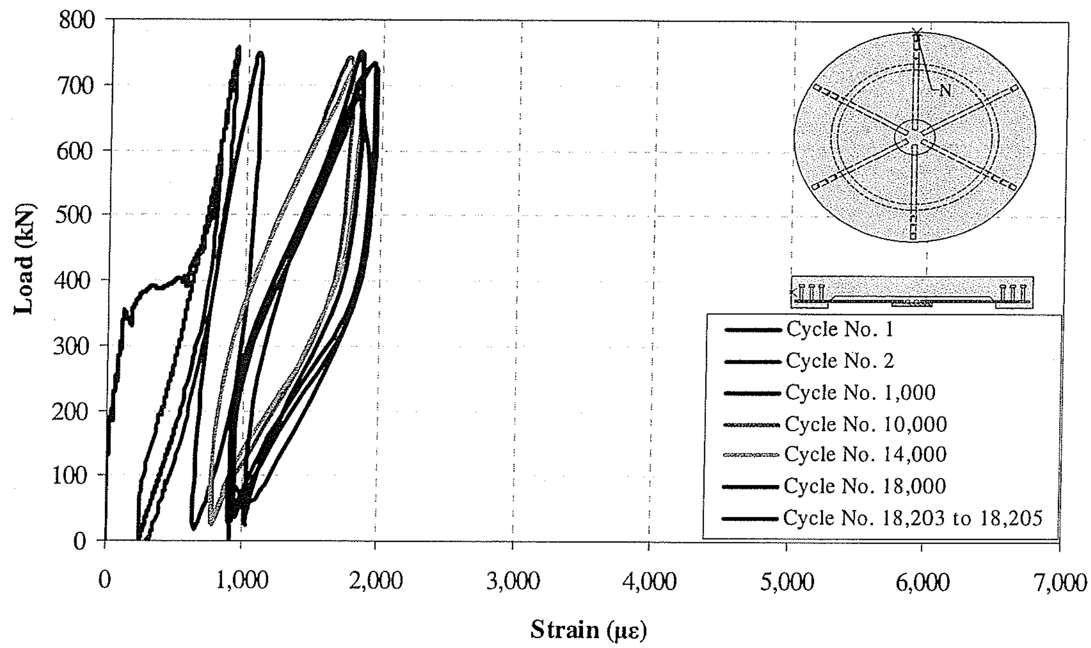

Figure 75: Load vs. strain behaviour in CFRP wrap at EGS CFRP N location of Slab-3

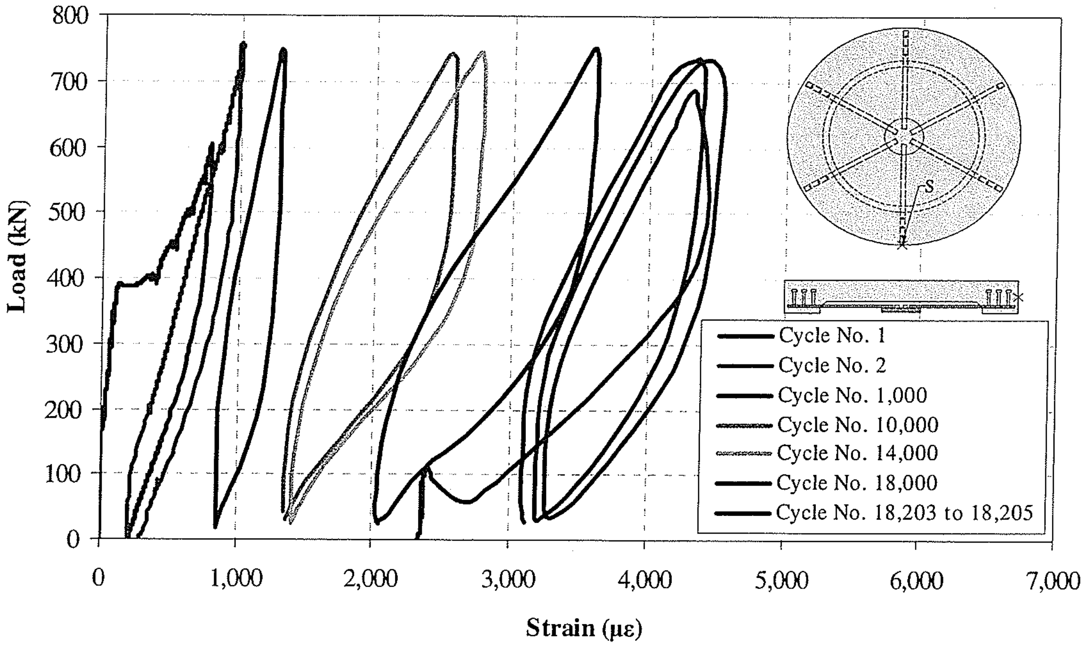

Figure 76: Load vs. strain behaviour in CFRP wrap at EGS CFRP S location of Slab-3

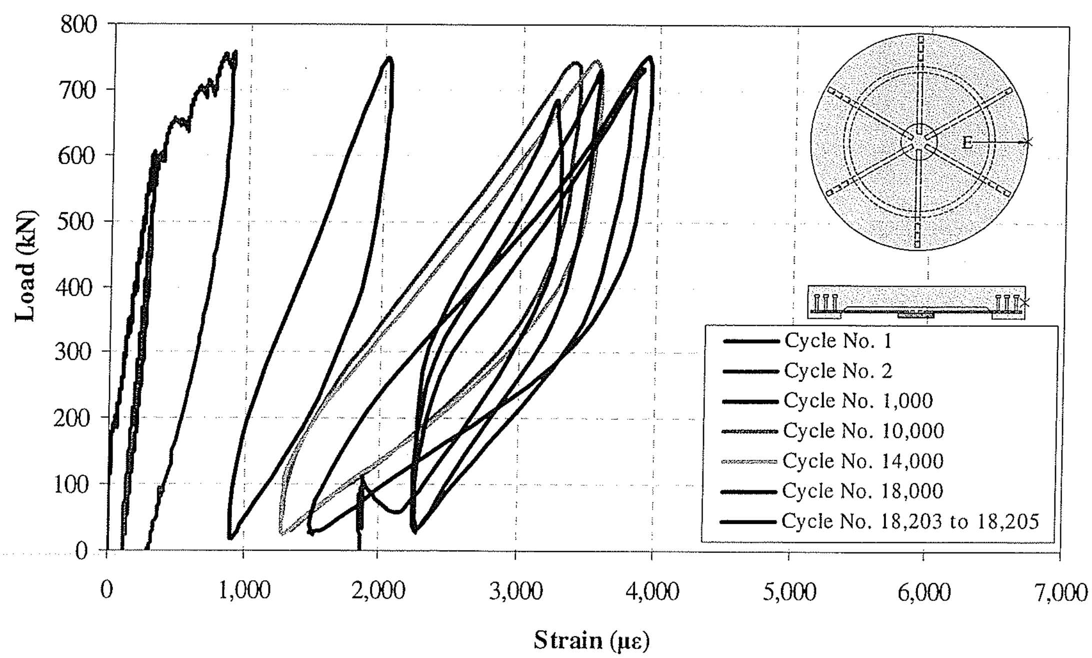

Figure 77: Load vs. strain behaviour in CFRP wrap at EGS CFRP E location of Slab-3

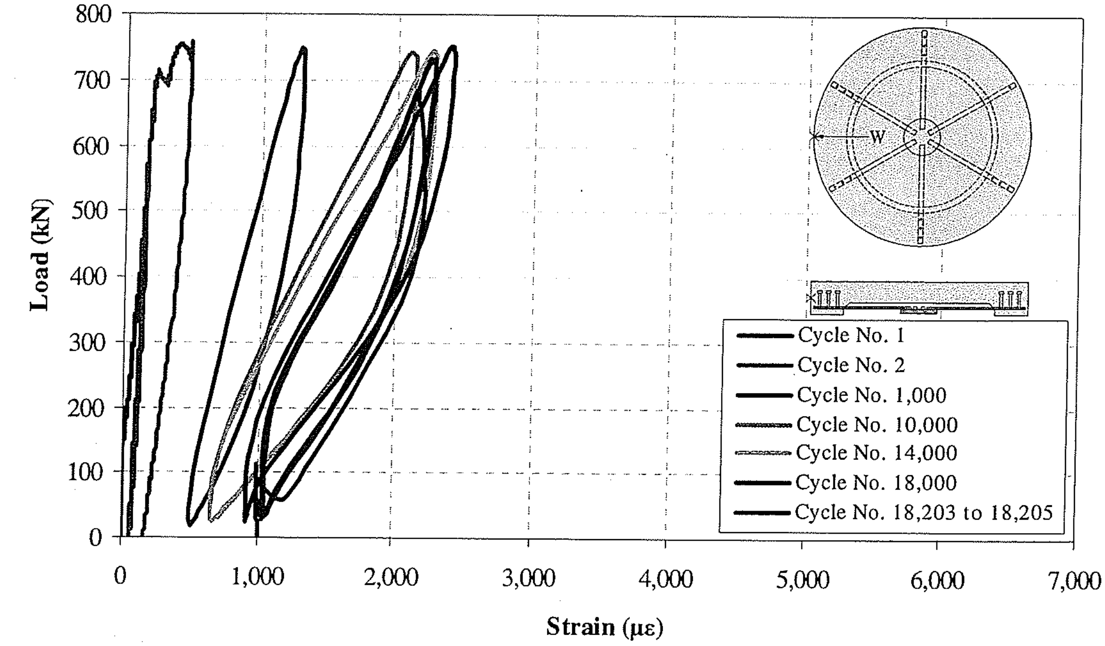

Figure 78: Load vs. strain behaviour in CFRP wrap at EGS CFRP W location of Slab-3

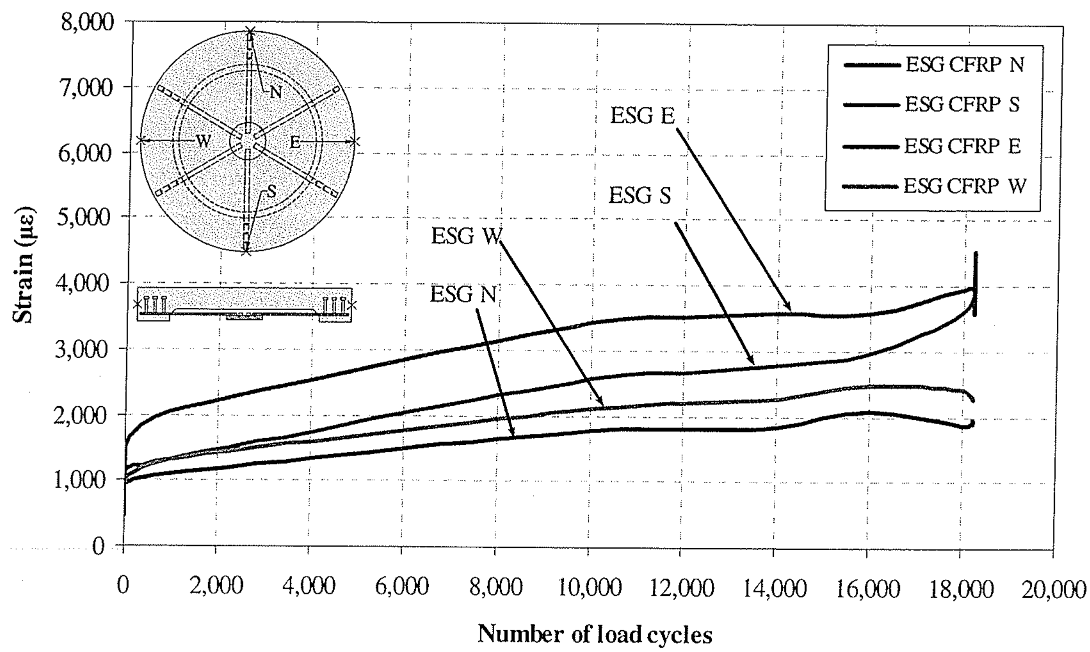

Figure 79: Strain in CFRP wrap vs. number of load cycles behaviour of Slab-3

Table 10: Strain in CFRP wrap vs. number of load cycles behaviour of Slab-3

	Strain in CFRP wrap (με)			
Number of load cycles	**ESG CFRP N**	**ESG CFRP S**	**ESG CFRP E**	**ESG CFRP W**
1	928	1012	885	466
10	959	985	1076	673
100	980	1184	1644	1070
1,000	1100	1305	2037	1298
10,000	1778	2575	3413	2121
12,000	1813	2652	3510	2198
14,000	1844	2777	3576	2271
16,000	2089	2949	3577	2477
18,000	1854	3608	3945	2400
18,200	1901	4229	3969	2261
18,204	1957	4533	3561	2258

4.3.5 Strains in concrete

A three dimensional array of twelve 25 mm electronic strain gauges were installed at the middle of the slab to record the three dimensional state of strains in concrete of the slab. Unfortunately after around 1,000 loading cycles all the strain data recorded by the strain gauges appeared abnormal, which indicated that none of the strain gauges were functioning properly after around 1,000 loading cycles and were damaged under fatigue load due to the friction between concrete and strain gauges.

4.4 Summary of test results

The test results of this research project are summarizes in Table 11.

Table 11: Summary of test results

	Slab-1	Slab-2	Slab-3
Number of radial steel straps	6	6	6
Confinement with circumferential CFRP wrap	No	Yes	Yes
Subjected to freeze-thaw cycle	No	Yes	Yes
Type of loading	Monotonic	Fatigue and static	Fatigue
Mode of failure	Flexure	Punching	Punching
Load at first radial crack (kN)	100	200	200
Load at circumferential crack (kN)	-	500	700
Maximum load (kN)	460	920	-
Amplitude of fatigue load cycles (kN)	-	-	750
Number of fatigue load cycles to fail the slab	-	-	18,204
Maximum deflection (mm)	4.6	16.5	22.47
Maximum crack width (mm)	2.63	8.11	5.02

The observations made from the test results presented in Table 11 can be summarized as below:

1. The first slabs (Slab-1) that was confined only with six radial steel straps failed in flexural mode of failure. Whereas, the slabs (Slab-2 and Slab-3) that were confined with both radial steel straps and circumferential CFRP wrap failed in punching. This indicates that the degree of confinement plays an important role in the mode of failure of circular steel-free concrete deck models.

2. The ultimate load for Slab-1 and Slab-2 are 460 kN and 9201 kN, respectively. This indicates that, increasing the degree of restraint (through providing circumferential CFRP wrap in Slab-2) increase the load required to fail the circular steel-free concrete slab.

3. The thickness of middle circular steel plate used to connect steel straps and the ultimate load of the similar slab (G2-6S) of previous research work

(Mediwake 2006) were 12 mm and 344 kN respectively. Whereas, for Slab-2, thickness of middle circular steel plate has increased to 38 mm and the ultimate load has also increased to 460 kN. This results indicates that increment of the thickness of middle circular steel plate used to connect steel straps in circular steel-free concrete deck slabs did not ensure punching failure but, did increased the degree of stiffness of the circular slab.

4. Load at first radial crack (kN) for Slab-1 is 100 kN and that for Slab-2 and Slab-3 is 200 kN. This indicates that, the increment of the degree of confinement through circumferential CFRP wrap in Slab-2 and Slab-3 did increase the amount of load required to produce radial crack.

5. With increment the degree of restraint (through providing circumferential CFRP wrap in Slab-2) the maximum deflection increased from 4.6 mm to 16.5 mm for Slab-1 and Slal-2 respectively.

6. With increment the degree of confinement (through providing circumferential CFRP wrap in Slab-2) the maximum radial crack width increased from 2.63 mm to 8.11 mm for Slab-1 and Slal-2 respectively.

4.5 Comparison between full-scale steel-free slab and circular steel-free slab

The experimental and theoretical results of the second circular steel-free concrete deck slab (Slab-2) of this research program are compared with that of a full-scale bridge deck slab tested by Thorburn *(Thorburn 1998)*. The comparisons between Thorburn's full-scale slab and the circular Slab-2 are demonstrated in Table 12.

The length of Thorburn's full-scale steel-free concrete slab was 1200 mm and it was rested over two W610×241 steel girders spaced at 2,000 mm centre-to-centre. In total eleven steel straps were welded to the girders at 1,000 mm intervals to transversely confine the slab. Static concentrated loads were applied over the slab using a 250 mm × 500 mm rectangular load plate. The slab failed at 911 kN load in the punching mode of failure and the deflection during failure was 14 mm. The slab was analyzed using the PUNCH program. The theoretical punching failure load obtained using PUNCH program was 814 kN and the deflection during failure was 14.54 mm. The analytical results matched reasonably with the experimental result.

The second circular slab (Slab-2), as described in this thesis report, was of 1,810 mm external diameter and 175 mm depth which was confined with four layers of circumferential CFRP wrap and six 20 mm × 40 mm radial steel straps. In total 616,026 cycles of fatigue load was applied on the slab and, after that, static load was applied over the slab until failure. The load was applied using a circular loading plate of 520 mm diameter. The slab failed in punching failure mode at 920 kN with deflection of 15.58 mm. The theoretical failure load of the slab obtained from analysis using PUNCH program was 962 kN and the maximum deflection during failure was 16.57 mm. Ignoring the residual deflection of the slab due to failure loading, the projected maximum deflection of the slab would be 12.1 mm. The analytical results match reasonably with the experimental result.

The comparisons between the full-scale steel-free concrete slab and circular steel-free concrete slab as presented in Table 11 suggested that the load-deflection behaviour and crack pattern for both full-scale steel-free deck model and circular steel-free concrete deck model were similar. Moreover, the punching behaviour of both the full-scale steel-free concrete deck model and circular steel-free concrete deck model excellently matched with the theoretical load-deflection behaviour provided by the PUNCH program. Last, but not the least, construction of the full-scale steel-free deck models are expensive and time consuming, whereas, the circular steel-free concrete deck models require less material and time to construct.

As the full-scale steel-free deck models and the circular steel-free concrete deck models are experimentally and theoretically similar, it can be concluded that, the circular steel-free concrete deck models can be used to understand the mechanics of behaviour of steel-free bridge deck concept which will save the cost and time to build full-scale deck models.

Table 12: Comparison between Thorburn's full-scale steel-free concrete slab *(Thorburn 1998)* and circular steel-free concrete slab 'Slab-2'

	Full-scale steel-free bride deck *(After Thorburn 1998)*	Circular steel-free deck (Slab-2)
Detail of steel-free deck slabs	Plan view; Section A-A	Bottom View; Section B-B

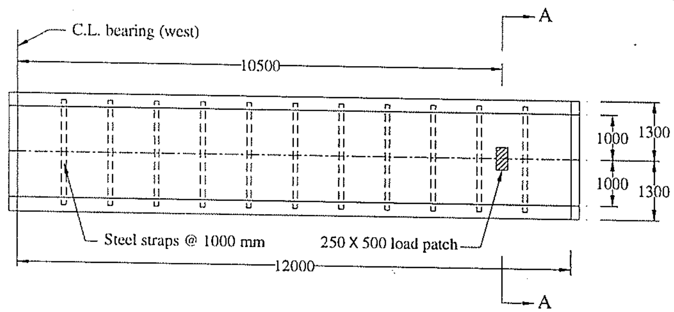

Plan view

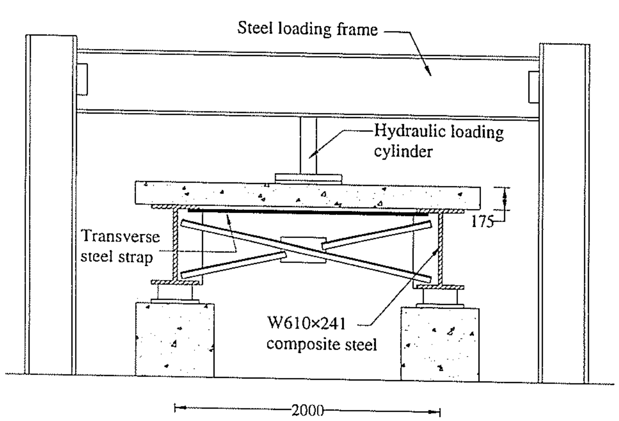

Section A-A

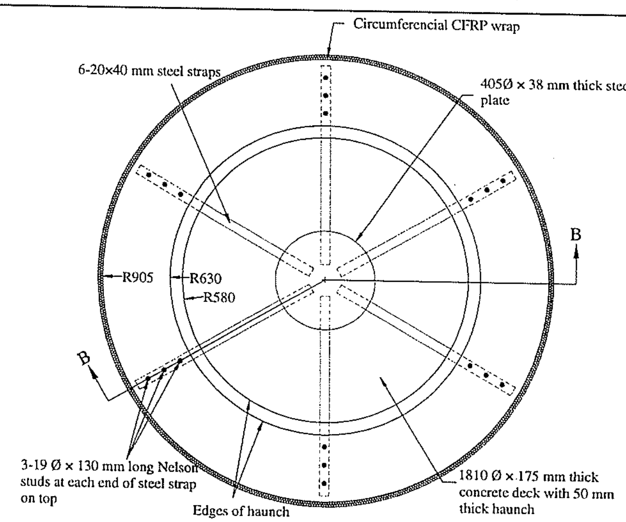

Bottom View

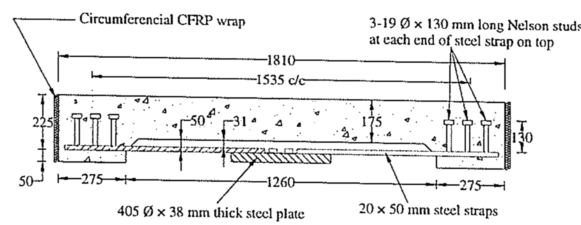

Section B-B

Crack pattern in concrete deck slabs under concentrated load

Full-scale steel-free bride deck *(After Thorburn 1998)*

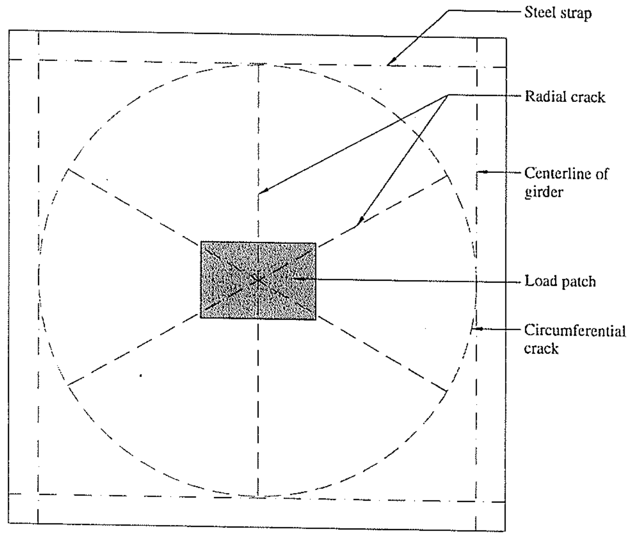

Plan view

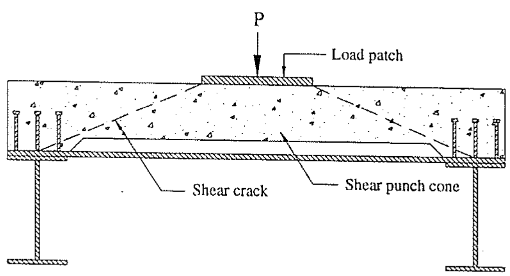

Cross section through strap

Circular steel-free deck (Slab-2)

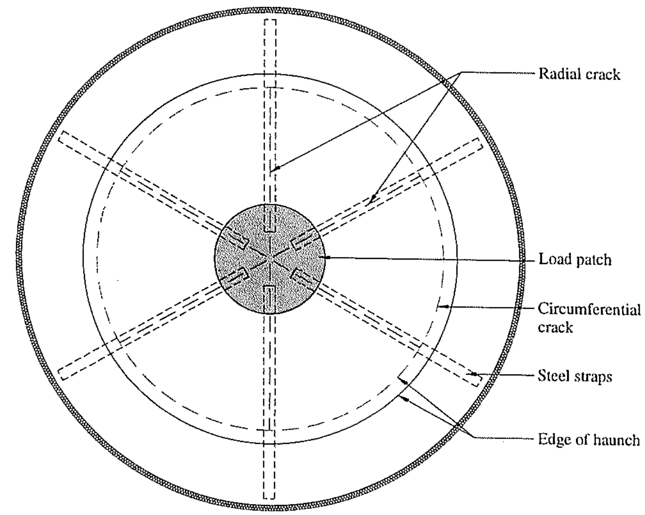

Plan view

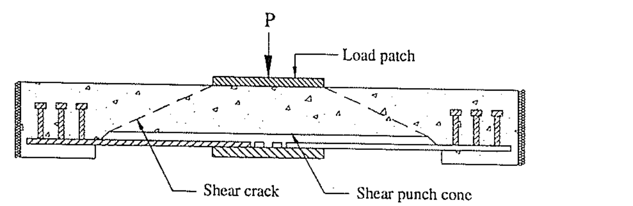

Cross section through strap

	Full-scale steel-free bride deck ***(After Thorburn 1998)***	**Circular steel-free deck (Slab-2)**
Load-deflection behaviour	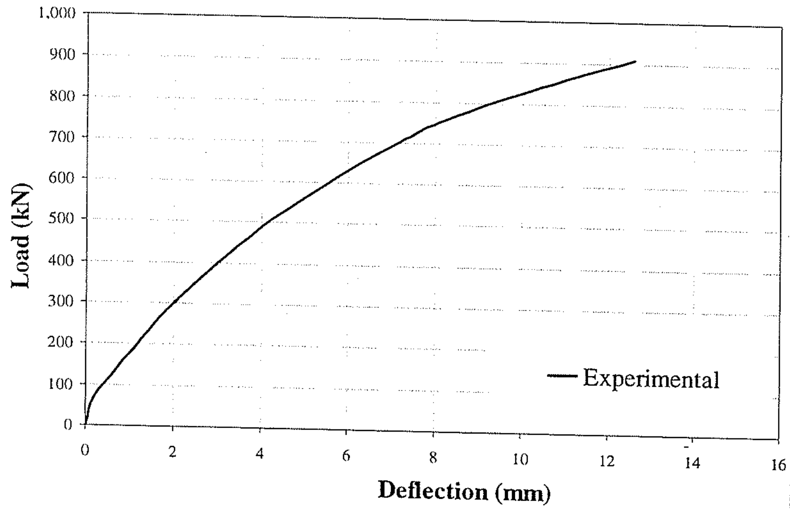	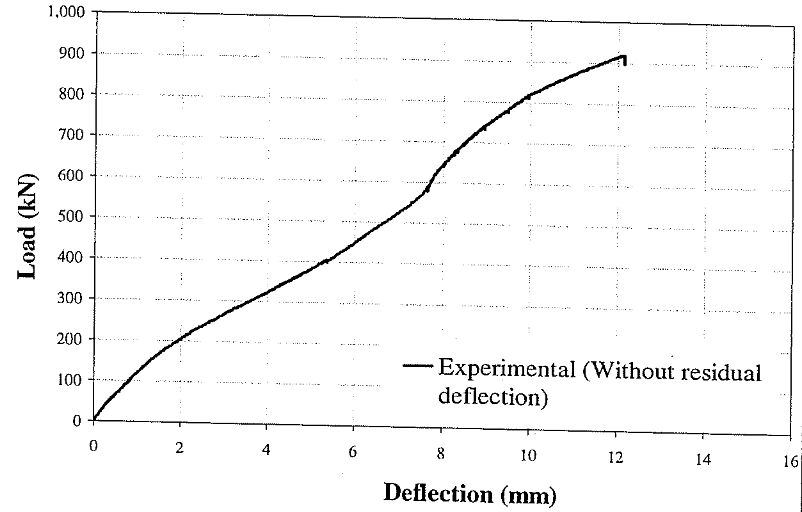
Comparison of experimental and theoretical results	Concrete confinement constant (K) = 370 N/mm/mm Experimental failure load ($P_{u,\ exp}$) = 911 kN Experimental deflection at failure load ($\delta_{u,\ exp}$) = 14 mm	Concrete confinement constant (K) = 330 N/mm/mm Experimental failure load ($P_{u,\ exp}$) = 920 kN Experimental deflection at failure load ($\delta_{u,\ exp}$) = 12.1 mm

Chapter 5

Conclusions and Recommendations

The effects of confinement from lateral restraints in circular steel-free concrete deck models, under static and fatigue loading, were experimentally investigated in this research project. Different aspects and behaviour of circular steel-free concrete bridge decks were also compared with that of full-scale steel-free concrete deck slabs to justify the logic behind using circular steel-free concrete bridge deck models to understand the mechanics of behaviour of the full-scale steel-free bridge deck concept. Several conclusions and recommendations for future work can be drawn from the experimental results obtained for the circular steel-free concrete deck slabs which are given in the following sections.

5.1 Conclusions

1. The mode of failure of circular steel-free concrete deck slabs, confined with both radial steel straps and circumferential CFRP wrap, was punching shear under both static and fatigue load.

2. Crack patterns and the failure mode of circular steel-free concrete slabs confined with both steel straps and circumferential CFRP wrap were similar to that of full-scale steel-free concrete slabs.

3. In absence of circumferential CFRP wrap, use of radial steel straps alone did not influenced triaxiality significantly to confirm punching failure, but straps combined with CFRP wrap did result in punching failure.

4. Degree of restraint provided has a significant effect on the ultimate load capacity and the mode of failure of circular steel-free concrete deck slabs.

5. Increment of the thickness of middle circular steel plate, used to connect steel straps in circular steel-free concrete deck slabs, did not ensure punching failure but, did increased the degree of stiffness of the circular slab.

6. The strains in the steel straps and circumferential CFRP wrap of Slab-2 and Slab-3 indicate that at the beginning of fatigue tests, both the radial steel straps and circumferential CFRP wrap provided the lateral restrain to the slab. With

progression of fatigue tests, the circumferential CFRP wrap rather than the radial steel straps provided the major confinement.

7. The similarity in experimental and theoretical results of circular steel-free concrete deck slabs with full-scale steel-free concrete deck models suggested that, the circular steel-free concrete deck models can be used to understand the mechanics of behaviour of the steel-free bridge deck concept which will save the cost and time to build full-scale steel-free deck models.

5.2 Recommendations for future research

1. More investigation in the behaviour of circular steel-free concrete deck slabs under fatigue load might be conducted to develop fatigue life curves (i.e. P-N curves).

2. More investigation in the effect of freeze-thaw cycles on fatigue load capacity of the circular steel-free concrete deck slabs might be conducted.

3. Investigation in the effects of impact and dynamic loading on the behaviour of circular steel-free concrete deck slabs might be conducted.

4. More effective instrumentation should be incorporated to investigate the three dimensional state of strains in concrete slabs under static and fatigue loading. One possible option might be to check the anchorage length of GFRP bras used to

build the cube to install strain gauges and select the length of GFRP bars accordingly.

References

AASHTO (2002). Standard Specifications for Design of Highway Bridges, 17th edition. *American Association of State Highway and Transportation Officials,* Washington, DC, USA.

AASHTO-LRFD (1998). Bridge Design Specifications, 2nd edition. *American Association of State Highway and Transportation Officials,* Washington, DC, USA.

ASTM (2001). Standard Test Method for Time of Flow of Fiber-Reinforced Concrete Through Inverted Slump Cone, ASTM C 995-01. *American Society for Testing and Materials,* West Conshohocken, Pennsylvania, USA.

ASTM (2003). Standard Test Method for Slump of Hydraulic-Cement Concrete, ASTM C 143/C 143 M-03. *American Society for Testing and Materials,* West Conshohocken, Pennsylvania, USA.

ASTM (2003-a). Standard Test Method for Resistance of Concrete to Rapid Freezing and Thawing, ASTM C 666/C 666 M-03. *American Society for Testing and Materials,* West Conshohocken, Pennsylvania, USA.

ASTM (2004). Standard Test Method for Splitting Tensile Strength of Cylindrical Concrete Specimen, ASTM C496/C 496M-04. (2004). *American Society for Testing and Materials,* West Conshohocken, Pennsylvania, USA.

ASTM (2005). Standard Test Method for Compressive Strength of Cylindrical Concrete Specimens, ASTM C39/C 39M-05e2. *American Society for Testing and Materials,* West Conshohocken, Pennsylvania, USA.

Bakht, B., and Agarwal, A.C. (1995). Deck Slabs of Skew Girder Bridges. *Canadian Journal of Civil Engineering,* Vol. 22, No. 3, pp. 514-523.

Bakht, B., and Mufti, A.A. (1998). Five Steel-Free Bridge Deck Slabs in Canada. *Structural Engineering International,* Vol. 8, No. 3, pp. 196-200.

CSA (2000). Canadian Highway Bridge Design Code, 1st Edition, CAN/CSA-S6-00. *Canadian Standard Association*, Toronto, Ontario, Canada.

CSA (2004). Method of Test to Determine Adhesion by Tensile Load, CAN/CSA-A23.2-6B. *Canadian Standard Association*, Toronto, Ontario, Canada.

Desai, Y.M., Mufti, A.A., and Tadros, G. (2002). User Manual for FEM PUNCH, *ISIS Canada Research Network*, Winnipeg, Manitoba, Canada.

Dorton, R.A., and Holowka, M. (1977). The Connestego River Bridge Design and Testing. *Canadian Journal of Civil Engineering,* Vol. 4, No. 18, pp. 18-39.

El-Ragaby, A., El-Salakawy, E., and Benmokrane, B. (2007). Fatigue Life Evaluation of Concrete Bridge Deck Slabs reinforced with Glass FRP Composite Bars. *Journal of Composites for Construction, ASCE,* Vol. 11, No. 3, pp. 258-268.

Green, M.F. (2007). FRP Repair of Concrete Structures: Performance in Cold Regions. *International Journal of Materials and Product Technology,* Vol. 28, No. 1-2, pp. 160-177.

Hewitt, B.E., and Batchelor, B.d. (1975). Punching Shear Strength of Restrained Slabs. *Journal of the Structural Division, ASCE,* Vol. 101, No. 9, pp. 1837-1853.

ISIS (2001). Strengthening Reinforced Concrete Structures with Externally-Bonded Fibre Reinforced Polymers. *Design Manual No. 4, ISIS-M04-01,* ISIS Canada Research Network, Winnipeg, Manitoba, Canad.

Klowak, C. (2007). Static & Fatigue Behaviour of Bridge Deck Cantilever Overhangs Subjected to a Concentrated Load. *M.Sc. Thesis*, Department of Civil Engineering, University of Manitoba, Canada.

Matsui, S., Tokai, D., Higashiyama, H., and Mizukoshi, M. (2001). Fatigue Durability of Fiber Reinforced Concrete Decks Under Running Wheel Load. *Proceedings, 3rd International Conference on Concrete Under Sever Conditions,* University of British Columbia, Vancouver, Canada, pp. 982-991.

Mediwake, G. (2006). Effect of Confinement from Lateral Restraints in Steel-Free Circular Deck Models Under Static Loading. *M.Sc. Thesis,* Department of Civil Engineering, University of Manitoba, Canada.

Memon, A.H. (2005). Comparative Fatigue Performance of Steel-Reinforced and Steel-Free Concreete Bridge Deck Slabs. *Ph.D. Thesis,* Department of Civil Engineering, University of Manitoba, Canada.

Mufti, A.A., Bakht, B., and Jaeger, L.G. (1991-a). Fibre RC Deck Slabs with Diminished Steel Reinforcement. *Proceedings, International Symposium on Interaction Between Constructuiion Technology and Design,* International Association for Bridge and Structural Engineering, Leningard, Russia, Vol. 64, pp. 388-389.

Mufti, A.A., Erki, M-A., and Jaeger, L.G (1991-b). Advanced Composite Materials With Application to Bridges. *Canadian Society of Civil Engineering*, Montreal, Quebec, Canada.

Mufti, A.A., Jaeger, L.G., Bakht, B., and Wegner, L.D. (1993). Experimental Investigation of Fibre-Reinforced Concrete Deck Slabs Without Internal Steel Reinforcement. *Canadian Journal of Civil Engineering*, Vol. 20, No. 3, pp. 398-406.

Mufti, A.A., Memon, A.H., Bakht, B., and Banthia, N. (2002). Fatigue Investigation of the Steel-Free Bridge Deck Slabs. *ACI International SP 206-4,* American Concrete Institute, pp. 61-70.

Newhook, J.P. (1997). The Behaviour of Steel-Free Concrete Bridge Deck Slabs Under Static Loading Conditions. *PhD Thesis,* Department of Civil Engineering, Technical University of Nova Scotia, Halifax, Nova Scotia, Canada.

Newhook, J.P., and Mufti, A.A. (2003). PUNCH User and Technical Manual, *ISIS Canada Research Network,* Winnipeg, Manitoba, Canada.

NeVille, A.M. (1995). Properties of concrete. *John Wiley & Sons, Inc.,* 4th Edition, New York, New York, U.S.A.

OHBDC (1979). Ontario Highway Bridge Design Code. *Ministry of Transportation of Ontario,* Downsview, Ontario, Canada.

Popovics, S. (1992). Concrete Materials: Properties, Specifications and Testing. *William Andrew Publishing,* 2nd Edition, Park Ridge, New Jersey, U.S.A.

Powers, T.C. (1945). A working Hypothesis for Future Studies of Frost Resistance of Concrete. *Proceedings, ACI Journal,* vol. 41, No. 1, pp. 245-272.

Powers, T.C., and Helmuth, R.A. (1953). Theory of Volume Changes in Hardened Portland Cement Paste During Freezing, *Proceedings, Highway Research Board 32*, pp. 285-297.

Sonoda, K., and Horikawa, T. (1982). Fatigue Strength of Reinforced Concrete Slabs Under Moving Loads. *Proceedings, IABSE Colloquium on Fatigue of Steel and Concrete Structures*, International Association for Bridge and Structural Engineering, Zurich, Switzerland, Vol. 37, pp. 455-462.

Thériault, M. and Neale, K.W. (2000). Design Equations for Axially Loaded Reinforced Concrete Columns Strengthened with Fibre Reinforced Polymer Wraps. *Canadian Journal of Civil Engineering*, Vol. 27, No. 5, pp. 1011-1020.

Thorburn, L.J. (1998). A study of Externally Reinforced Fibre-Reinforced Concrete Bridge Decks on Steel Girders. *PhD Thesis,* Department of Civil Engineering, Dalhousie University, Halifax, Nova Scotia, Canada.

Wobo MBrace (2008). Product data sheets. *BASF Construction Chemicals Asia Pacific.* http://www.basf-cc.com.sg, Shanghai, China.

Appendix A

Calculation related to design of Steel straps

In order to calculate the minimum cross sectional area of radial steel straps, required to confine the circular steel-free concrete deck slabs, the following values were used:

Factor considering inner panels (F_S) = 5

Spacing of the supporting beam (S) = 1.535 m

The maximum spacing of straps suggested by CHBDC, (S_l) = 1.25 m

Modulus of elasticity of the steel used for straps (E) = 200×10^6 MPa

Thickness of the slab (t) = 175 mm

Substituting the values in the equation provided by Canadian Highway Bridge Design Code *(CSA 2000)*, the minimum area of steel strap required to confine the circular steel-free concrete deck slab:

$$A_s = \frac{F_s \times S^2 \times S_l}{E \times t} \times 10^9 = \frac{5 \times (1.535\ \text{m})^2 \times (1.25\ \text{m})}{(200 \times 10^3\ \text{MPa}) \times (175\ \text{mm})} \times 10^9 = 421\ \text{mm}$$

Based on the above calculation, steel straps having cross section of 20 mm × 40 mm (800 mm^2) was selected to confine the circular steel-free concrete slab.

Calculation related to design of circumferential CFRP wrap

In order to calculate the number of CFRP sheet required to circumferentially confine the circular steel-free concrete deck slab, the following values were used:

Resistance factor for FRP (ϕ_{frp}) = 0.75

Tensile strength in FRP sheet (f_{frpu}) = 3800 MPa (Appendix B)

Thickness of one layer of FRP sheet (t_{frp}) = 0.33 mm (Appendix B)

External diameter of the circular slab (D_g) = 1810 mm

According to the *Thériault et al. (2000)*, the minimum confinement pressure (f_{lfrp}) from FRP confining wrap should be 4 MPa.

Substituting the above mentioned values in the equation provided by ISIS Canada Design Manual-4 (*ISIS 2001*), the number of CFRP sheet required to confine the circular steel-free concrete deck slab:

$$N_b = \frac{f_{lfrp} \times D_g}{2 \times \phi_{frp} \times f_{frpu} \times t_{frp}} = \frac{(4\text{MPa}) \times (1810\text{mm})}{2 \times (0.75) \times (3800\text{MPa}) \times (0.33\text{mm})} = 3.85 \approx 4$$

Based on the above calculation, the number of layers of CFRP sheet required to circumferentially confine the circular steel-free concrete slab was selected to be four.

Appendix B

Properties of Wobo®MBrace Primer *(Wobo MBrace 2008)*

Physical properties

Installed Thickness (approx)	= 0.075 mm
Density	= 1102 kg/m^3

Tensile properties

Yield Strength	= 14.5 MPa
Strain at yield	= 2.0 %
Elastic modulus	= 717 MPa
Ultimate strength	= 17.2 MPa
Poisson's ratio	= 0.48

Compressive properties

Yield Strength	= 26.2 MPa
Strain at yield	= 4 %
Elastic modulus	= 670 MPa
Ultimate strength	= 28.3 MPa
Rupture strain	= 10 %

Flexural properties

Yield Strength	= 24.1 MPa
Strain at yield	= 4 %
Elastic modulus	= 595 MPa
Ultimate strength	= 24.1 MPa

Functional properties

CTE	= 35.10^{-6}/°C
Thermal conductivity	= 0.20 W/m°K
Glass transition temp, T_g	= 77°C

Properties of Wobo®MBrace Putty *(Wobo MBrace 2008)*

Physical properties

Installed Thickness (approx)	=	0.075 mm

Tensile properties

Yield Strength	=	12 MPa
Strain at yield	=	1.5 %
Elastic modulus	=	1800 MPa
Ultimate strength	=	15.2 MPa
Rupture strain	=	7 %
Poisson's ratio	=	0.48

Compressive properties

Yield Strength	=	22.8 MPa
Strain at yield	=	4 %
Elastic modulus	=	1076 MPa
Ultimate strength	=	22.8 MPa
Rupture strain	=	10 %

Flexural properties

Yield Strength	= 26.2 MPa
Strain at yield	= 4 %
Elastic modulus	= 895 MPa
Ultimate strength	= 27.6 MPa
Rupture strain	= 7 %

Functional properties

CTE	= 35.10^{-6}/°C
Thermal conductivity	= 0.19 W/m°K
Glass transition temp, T_g	= 75°C

Properties of Wobo®MBrace Saturant *(Wobo MBrace 2008)*

Physical properties

Density	= 983 kg/m^3

Tensile properties

Yield Strength	= 54 MPa
Strain at yield	= 2.5 %
Elastic modulus	= 3034 MPa
Ultimate strength	= 55.2 MPa
Rupture strain	= 3.5 %
Poisson's ratio	= 0.40

Compressive properties

Yield Strength	= 86.2 MPa
Strain at yield	= 5 %
Elastic modulus	= 2620 MPa
Ultimate strength	= 86.2 MPa
Rupture strain	= 5 %

Flexural properties

Yield Strength	= 138 MPa
Strain at yield	= 3.8 %
Elastic modulus	= 3724 MPa
Ultimate strength	= 138 MPa
Rupture strain	= 5 %

Functional properties

CTE	= 35.10^{-6}/°C
Thermal conductivity	= 0.21 W/m°K
Glass transition temp, T_g	= 71°C

Properties of Wobo®MBrace CF 160 *(Wobo MBrace 2008)*

Physical properties

Fiber Material	=	High strength Carbon
Fiber tensile strength	=	4950 MPa
Areal weight	=	$600 g/m^2$
Fabric Width	=	500 mm
Nominal Thickness, T_f	=	0.33 mm/ply

0° tensile properties

Ultimate tensile strength, f^*_{fu}	=	3800 MPa
Tensile Modulus, E_f	=	227 GPa
Ultimate tensile strength per unit weight, $f^*_{pu}\ t_f$	=	1.25 kN/mm/ply
Tensile modulus per unit weight, $E_f\ t_f$	=	76 kN/mm/ply
Ultimate rupture strain, ε^*_{fu}	=	1.67 %

90° tensile properties

Ultimate tensile strength	=	0
Tensile modulus	=	0

Ultimate rupture strain	= n/a
Ultimate strength	= 86.2 MPa
Rupture strain	= 5 %

Flexural properties

Yield Strength	= 138 MPa
Strain at yield	= 3.8 %
Elastic modulus	= 3724 MPa
Ultimate strength	= 138 MPa
Rupture strain	= 5 %

Functional properties

CTE	= 35.10^{-6}/°C
Thermal conductivity	= 0.21 W/m°K
Glass transition temp, T_g	= 71°C

Appendix C

Concrete cylinder compression and tension test results

Table 13: Concrete cylinder compression and tension test results of slabs and supporting ring beam

Specimen designation	Age of cylinder (days)	Date of test	Compressive strength (MPa)	Tensile strength (MPa)
Slab-1	7	May 15, 07	30.69	-
	14	May 22, 07	36.17	-
	28	Jun 05, 07	40.00	3.43
	50 (Test day)	Jun 27, 07	41.98	3.58
Slab-2	7	Nov 15, 07	30.23	-
	14	Nov 22, 07	37.87	-
	28	Dec 06, 07	46.28	3.93
	510 (Test day)	Apr 01, 09	47.60	4.17
Slab-3	7	Feb 14, 08	18.94	-
	14	Feb 21, 08	24.11	-
	28	Mar 06, 08	32.90	3.35
	454 (Test day)	May 06, 09	30.36	2.62
Supporting ring beam	7	Aug 8, 07	37.27	-
	14	Aug 15, 07	45.41	-
	28	Aug 29, 07	50.41	-

Appendix D

Pull-off tests in Slab-2 and Slab-3

Test procedure

A series of adhesion tests on the circumferential CFRP wrap were conducted following CSA A23.2-6B standard specification *(CSA 2004)*. The pull-off equipment used for this test consisted of a mechanical driven pullout tester coupled to a calibrated dynamometer as shown in Figure 80. The counter pressure ring of the device was designed to accommodate specific 2″ (50.8 mm) square steel disks. The bottom of the steel disks were machined smooth and shoulder-cut to provide a plane surface to ensure a tensile force perpendicular to the bottom plane of the steel disks.

A peripheral bit was cut around each steel disk through the CFRP surface to a minimum depth of 10 mm into the underlying concrete using concrete drilling machine. The typical outside diameter of steel disc was slightly smaller than the inner dimension of the core bit. After drilling the bit, the upper surface of the CFRP sheet was cleaned by alcohol. Then the steel disks were bonded to the centre of the bits using DURAL® rapid curing epoxy compound adhesive. Different steps of preparing the surface of CFRP sheet are demonstrated in Figure 81.

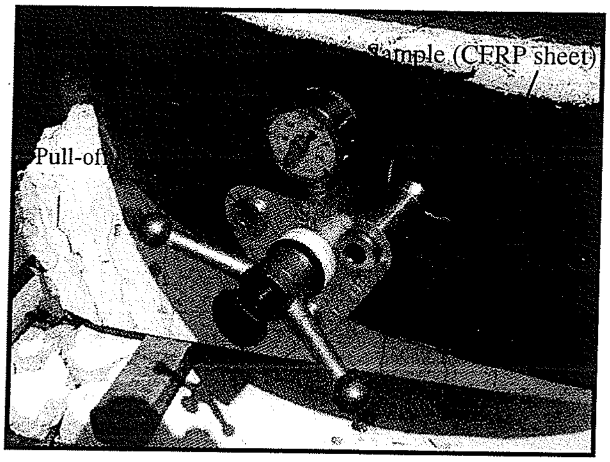

(a) **Pull-off equipment**

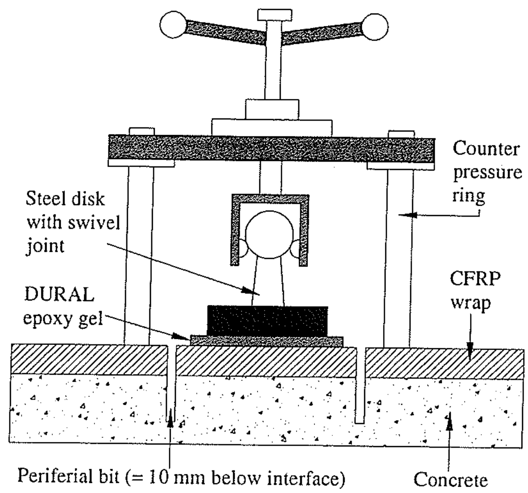

(b) Test specimen (side view)

Figure 80: Pull-off tester setup during testing

The pull-off tests were conducted in five locations at each of Slab-2 and Slab-3. The steel discs were installed along the outer surface of the circumferential CFRP wrap as shown in Figure 82.

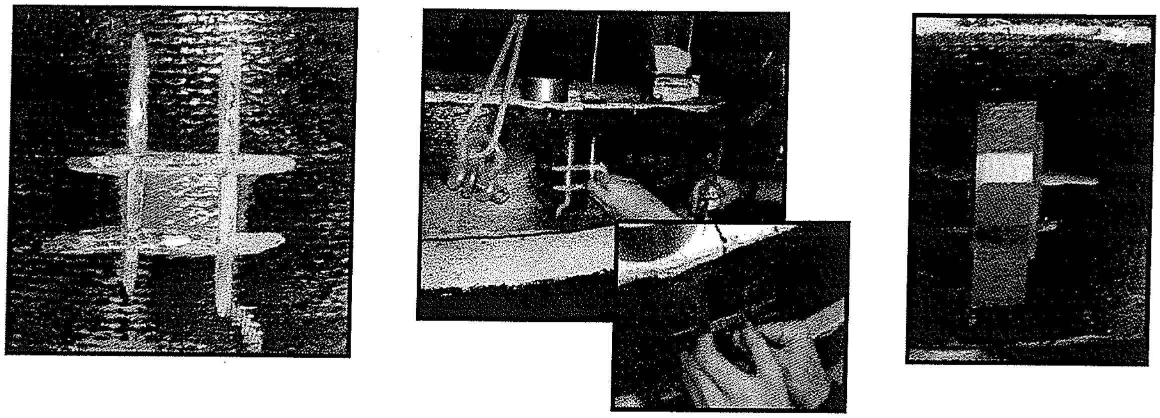

Step 1

Cutting of peripheral bit

Step 2

Cleaning and bonding of disc

Step 3

Curing of epoxy

Figure 81: Surface preparation for pull-off test

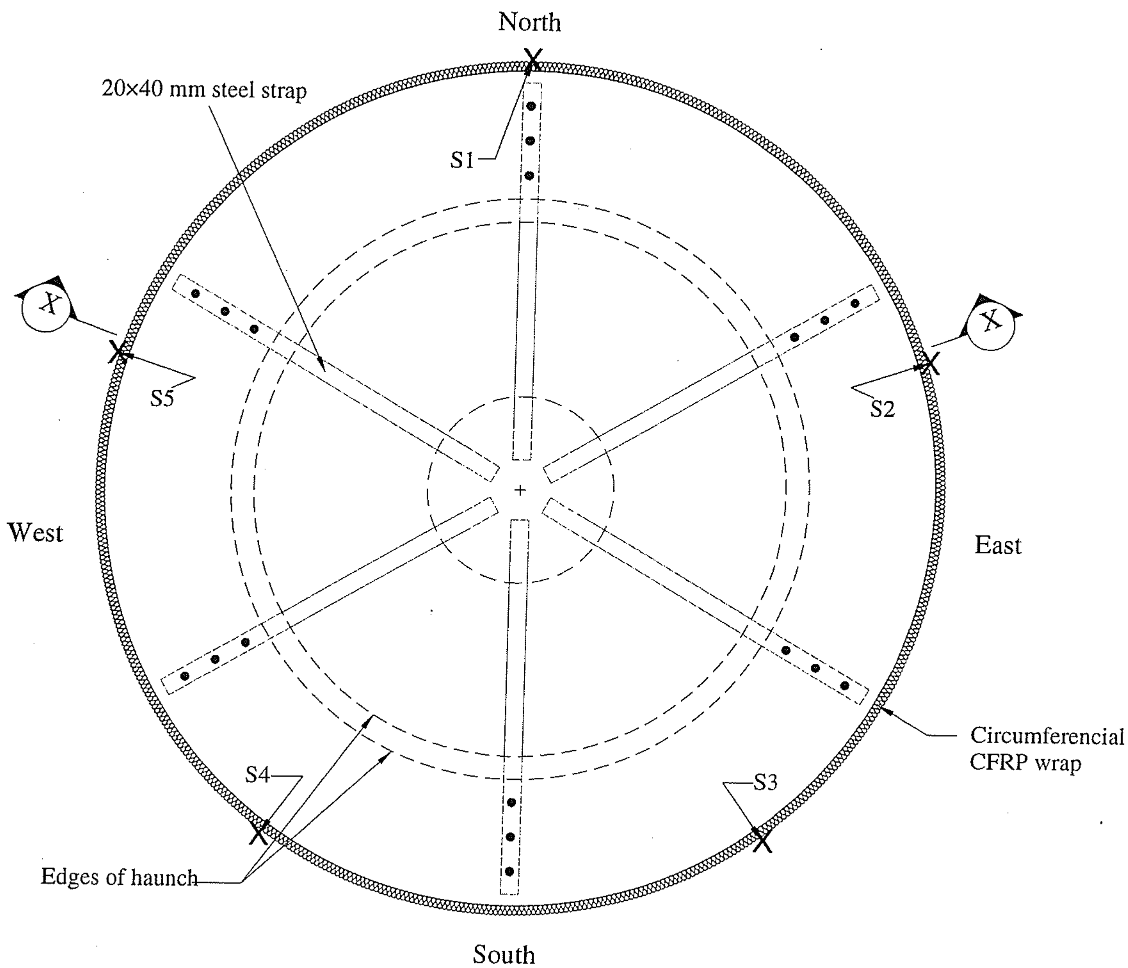

Bottom view

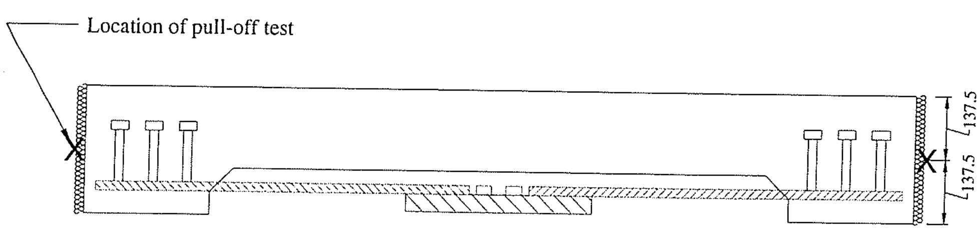

Section X-X

Figure 82: Locations of pull-off test (marked as "X")

Test results

The gauge readings, tensile bond strength and mode of failure obtained from pull-off tests are listed in Table 14. Different types of failure are demonstrated in Figure 83. The tensile bond strengths were calculated from the corresponding disk area over which the epoxy gel was applied to bond the fastening device to the CFRP surface.

Table 14: Pull-off test results

Circular slab	Disc label	Applied force (N)	Stress (MPa)	Mode of failure
Slab-2	S1	222.9	0.163	Partial bond failure & cohesive failure of existing concrete substrate
	S2	222.9	0.163	Partial bond failure & cohesive failure of existing concrete substrate
	S3	222.9	0.163	Cohesive failure of existing substrate
	S4	454.6	0.332	Partial bond failure & cohesive failure of existing concrete substrate
	S5	222.9	0.163	Cohesive failure of existing substrate
Slab-3	S1	222.9	0.154	Partial bond failure & cohesive failure of existing concrete substrate
	S2	222.9	0.172	Partial bond failure & cohesive failure of existing concrete substrate
	S3	222.9	0.154	Cohesive failure of existing substrate
	S4	222.9	0.154	Partial bond failure & cohesive failure of existing concrete substrate
	S5	222.9	0.163	Partial bond failure & cohesive failure of existing concrete substrate

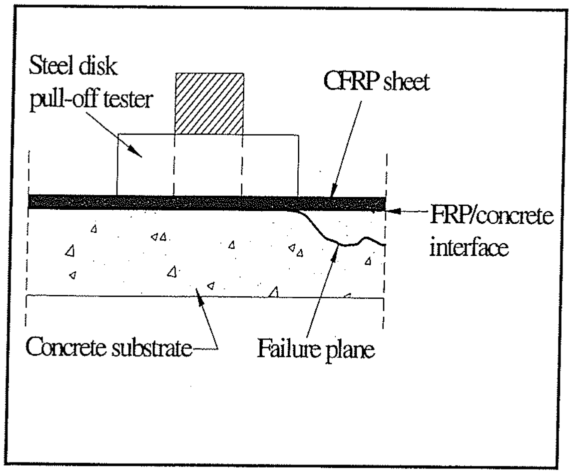

Failure type #1

Partial bond failure & cohesive failure of existing concrete substrate

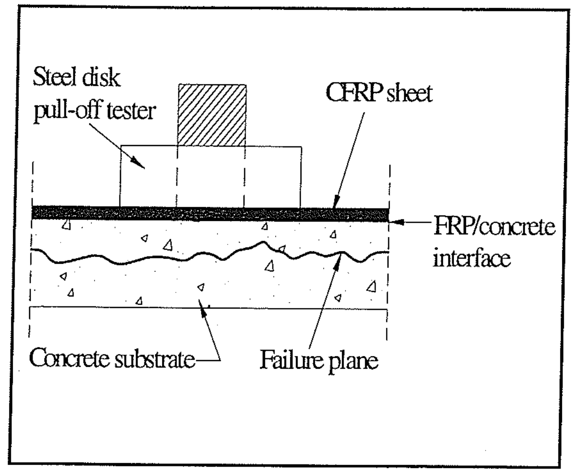

Failure type #2

Cohesive failure of existing substrate

Figure 83: Types of failure during pull-off test

For both Slab-2 and Slab-3 most of the discs were pulled-off because of partial bond failure and cohesive failure of existing concrete substrate at around 222.9 kN of applied force. Most of the failures had a portion of the plane going into the concrete substrate with a small portion only being at the interface between the concrete and FRP sheet. Photographs of CFRP sheets and concrete residue on steel plates after pull-off tests are shown in Figure 84. This failure mode dictated that the strength of concrete surface just below the CFRP wrap were weak due to crashing of concrete under cyclic load applied on the circular steel-free deck slabs.

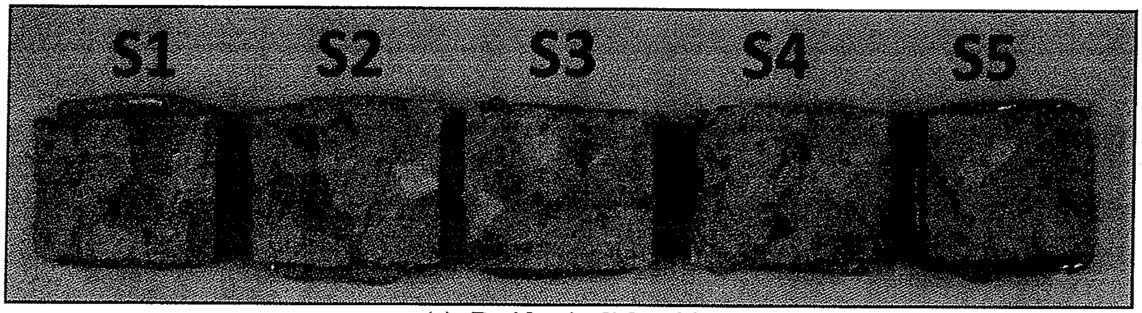

(a) **Residue in disks of Slab-2**

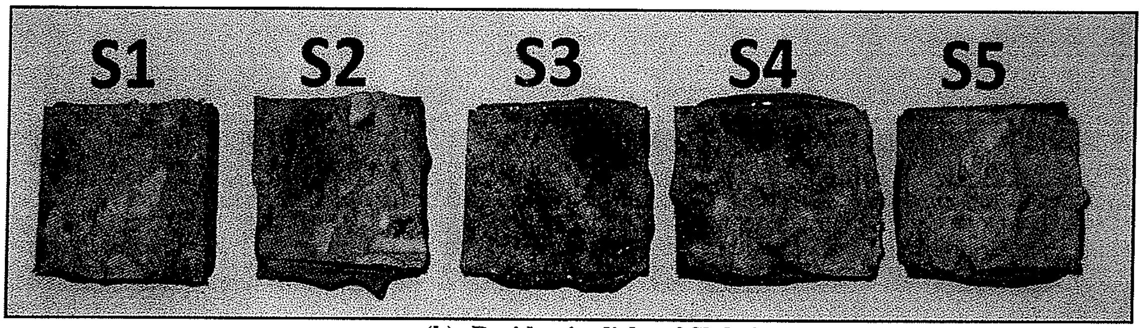

(b) **Residue in disks of Slab-3**

Figure 84: CFRP sheet and concrete residue on steel plates after pull-off

Appendix E

Design curves

Two computer programs named PUNCH program *(Newhook et al 2003)* and FEM PUNCH program *(Desai et al. 2002)* were developed to predict the punching behaviour of laterally restrained, concrete slab-on-girder bridge decks under wheel loading of heavy trucks. The PUNCH program was developed based on a simple rational model. On the other hand, the FEM PUNCH program was developed based on material three dimensional nonlinear finite element analyses in which three dimensional state of stress is considered. Both the programs require input of specific material and geometric properties of steel-free deck slab and produce load-deflection data.

A series of design curves can be produced using the analytical results of ultimate failure load obtained from these two programs. These design curves demonstrate the effect of deck thickness, girder spacing and transverse resistant stiffness (for PUNCH program) or linear spring constant (for FEM PUNCH program) on the punching failure load of the deck slabs. Such a series of design curves were produced for the full-scale steel-free concrete deck slab as shown in Figure 85. The input properties for the programs were similar to the design parameters of this full-scale steel-free concrete deck slab. Concrete strain of the deck was assumed to be 27 MPa and the yield strain of the steel straps was assumed to be 0.002.

The design curves produced using FEM PUNCH program are shown in Figure 86, Figure 87, Figure 88 and Figure 89 for deck depth of 150 mm, 175 mm, 200 mm and 225 mm respectively. These design curves provide the punching failure loads in 'kN' for a set of combinations of girder spacing in 'meter' and distributer linear spring constant (Spr) in 'N/mm'.

Design curves produced using PUNCH program are shown in Figure 90, Figure 91, Figure 92 and Figure 93 for deck depth of 150 mm, 175 mm, 200 mm and 225 mm respectively. These design curves provide the punching failure loads in 'kN' for a set of combinations of girder spacing in 'meter' and transverse resistant stiffness (k) in 'N/mm/mm'.

A steel-free deck model of similar design parameters of the slab as shown in Figure 85 was tested at Dalhousie University, Canada *(Thorburn 1998)*. The thickness of the slab was 175 mm. 1250 mm^2 steel straps at 1,000 mm spacing were used to transversely confine the slab. The deck slab was placed over two W610X241 composite steel girders spaced at 2,000 mm. The experimental punching failure load of the deck model was

923 kN. The calculated distributed linear spring constant (SprX and SprY) of the slab was 40,000 N/mm and transverse resistant stiffness (k) was 460 N/mm/mm.

The theoretical punching failure load of this slab can be determined using the design curves as shown in Figure 86 to Figure 93. According to the design curves produced using FEM PUNCH program (Figure 87), for deck depth of 175 mm and distributed linear spring constant (SprX and SprY) of 40,000 N/mm, the theoretical failure load of this slab is 870 kN. Similarly, from the design curved constructed using PUNCH program (Figure 91), for deck depth of 175 mm and transverse resistant stiffness (k) of 460 N/mm/mm, the theoretical failure load of this slab is 913 kN. These analytical results harmonize excellently with the experimental result.

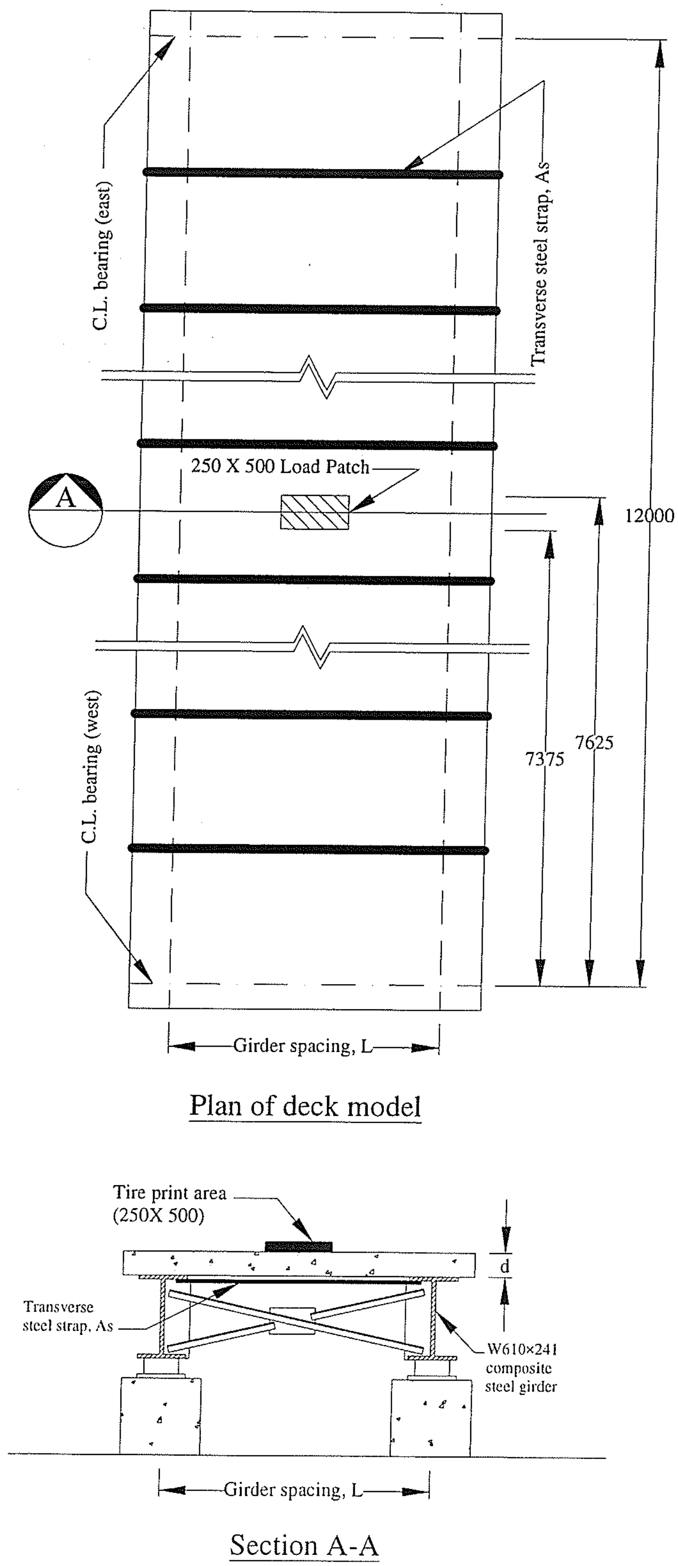

Figure 85: Detail of full-scale deck model used to construct design curves

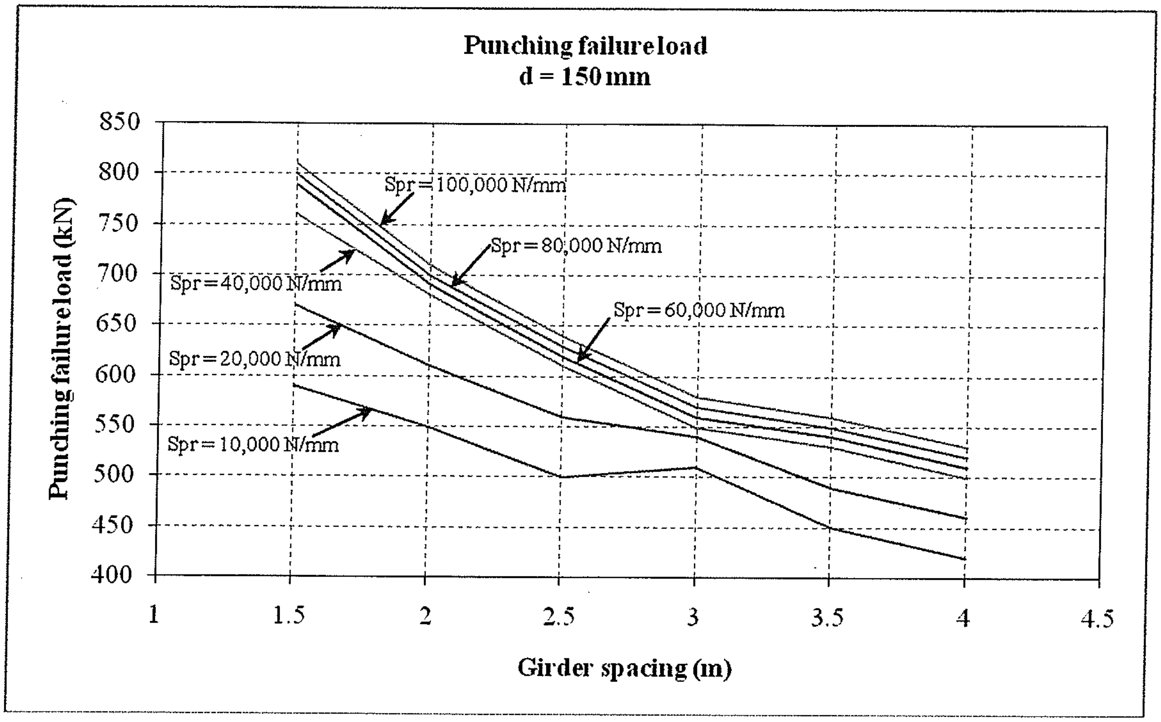

Figure 86: Punching failure curves using FEM PUNCH program for deck depth of 150 mm

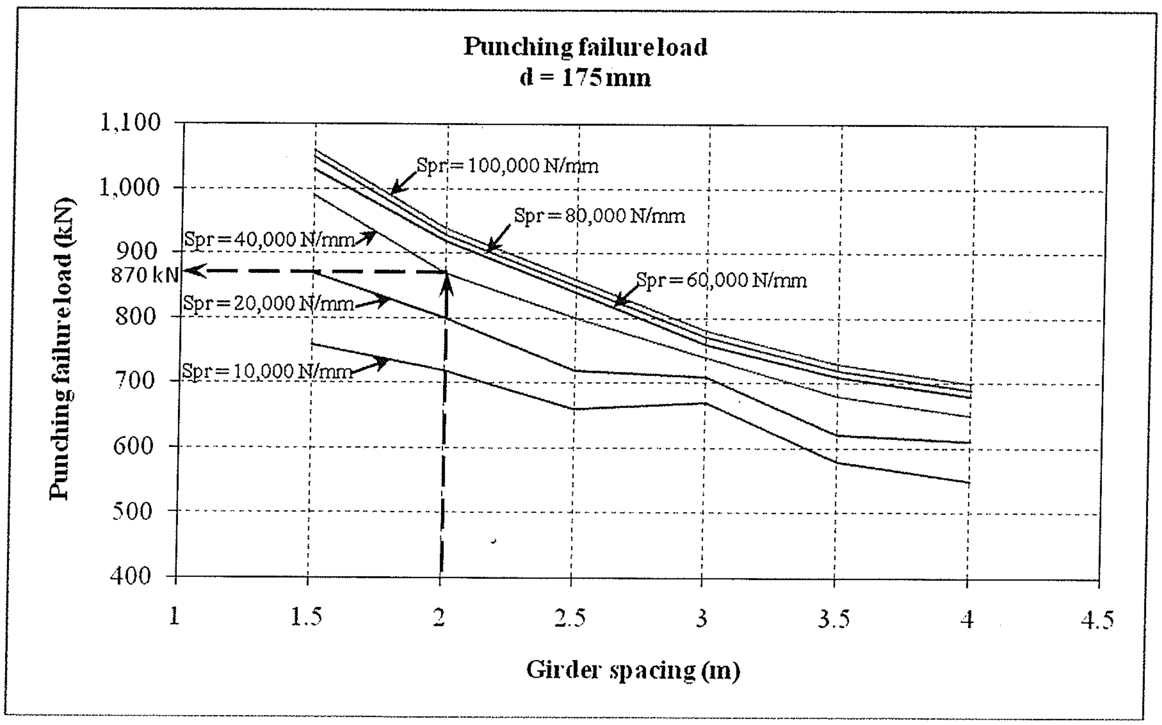

Figure 87: Punching failure curves using FEM PUNCH program for deck depth of 175 mm

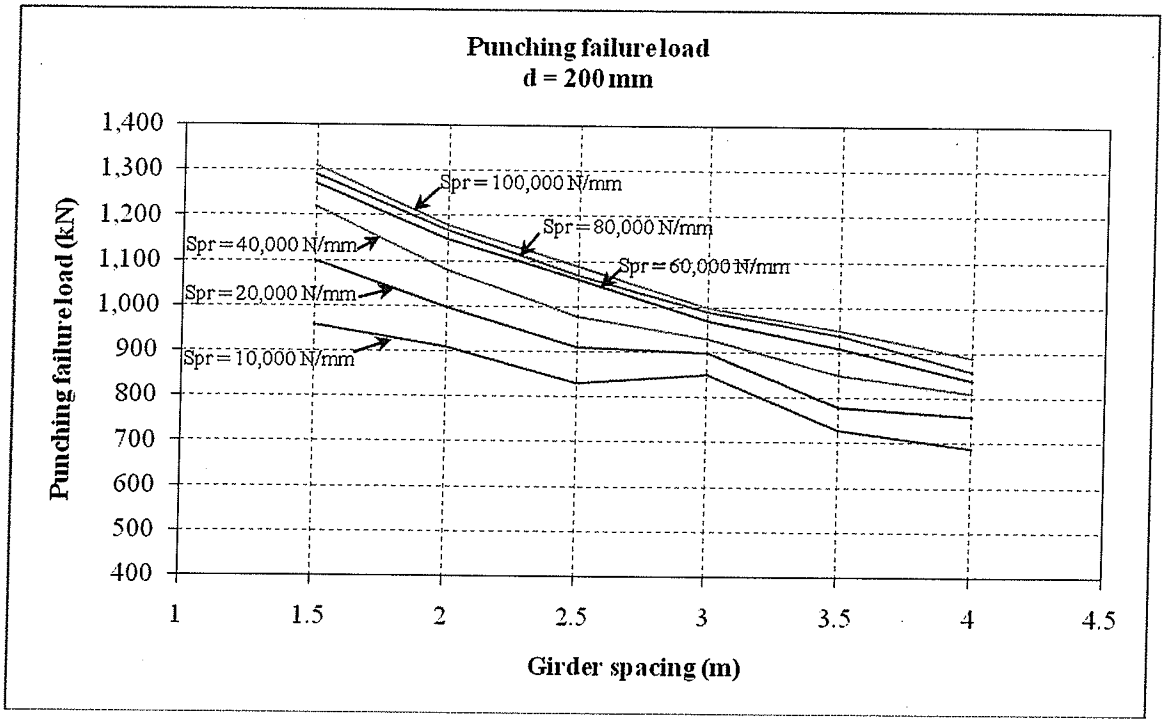

Figure 88: Punching failure curves using FEM PUNCH program for deck depth of 200 mm

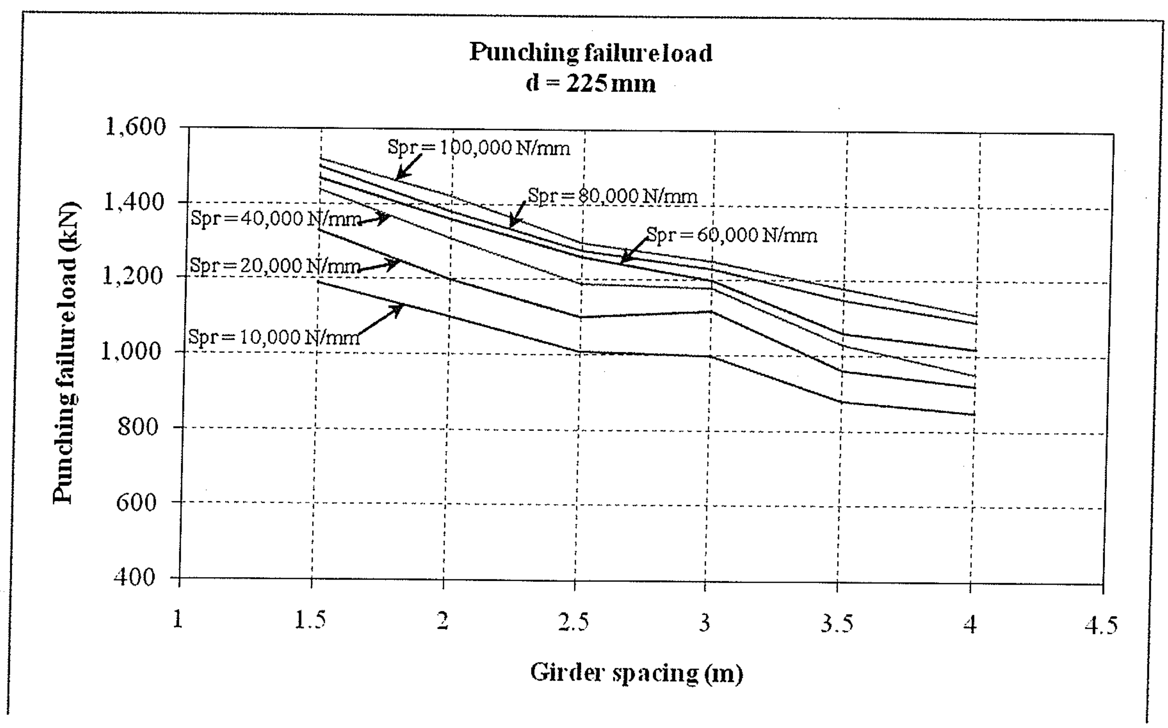

Figure 89: Punching failure curves using FEM PUNCH program for deck depth of 225 mm

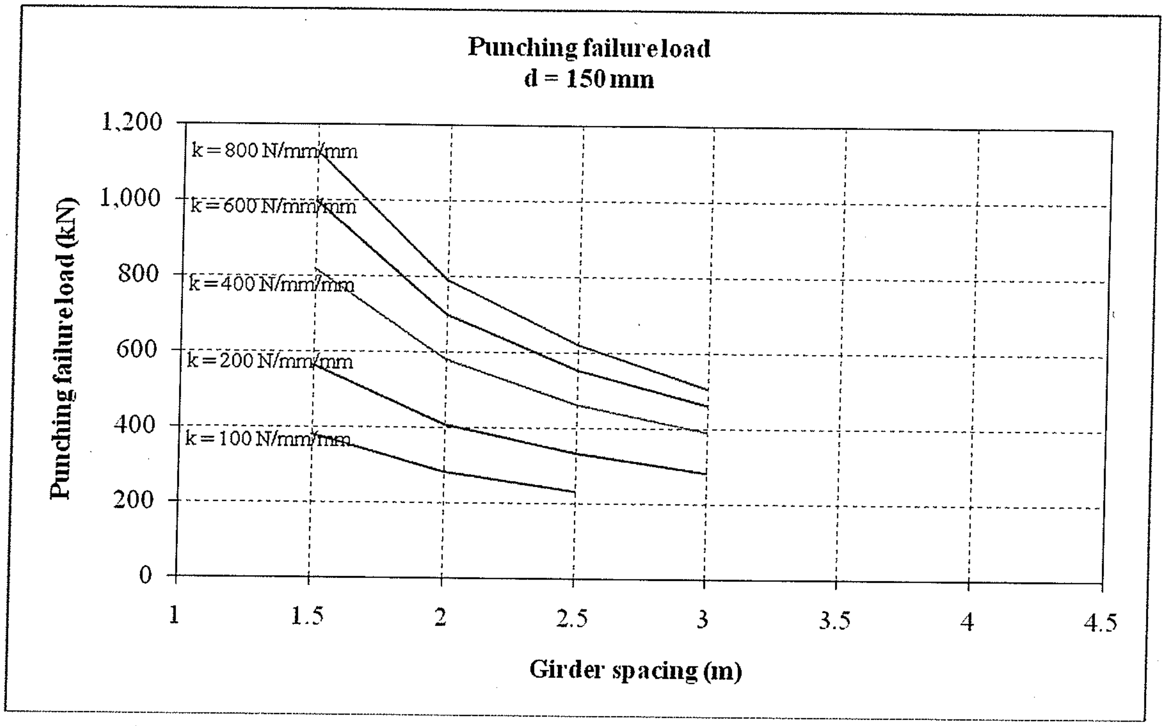

Figure 90: Punching failure curves using PUNCH program for deck depth of 150 mm

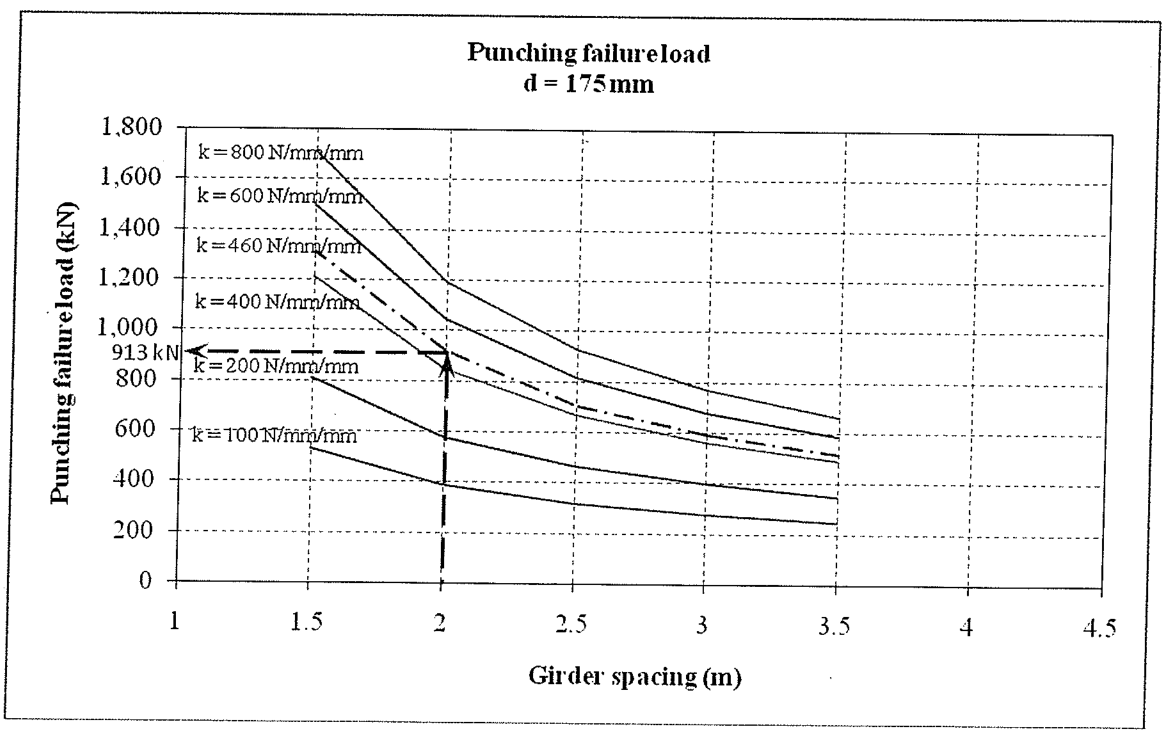

Figure 91: Punching failure curves using PUNCH program for deck depth of 175 mm

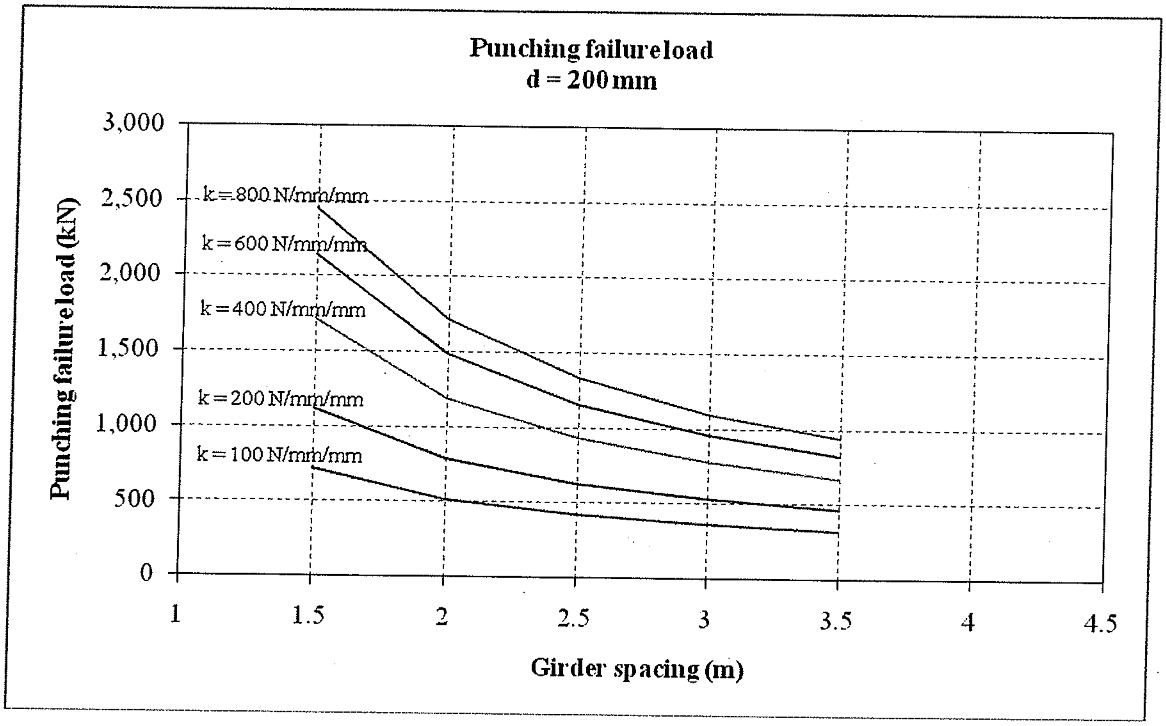

Figure 92: Punching failure curves using PUNCH program for deck depth of 200 mm

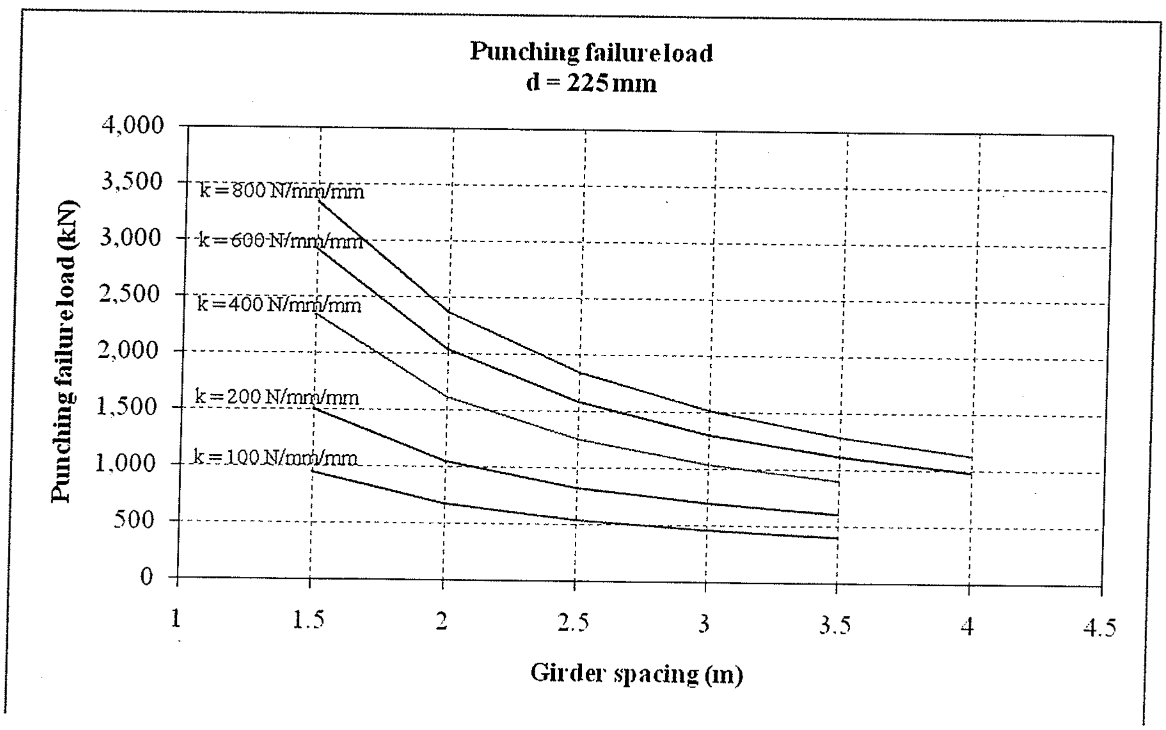

Figure 93: Punching failure curves using PUNCH program for deck depth of 225 mm

Appendix F

Comparison of experimental results with analytical models

The PUNCH and FEM PUNCH programs were used to predict the ultimate capacity of four half-scale steel-free deck models *(Mufti et al. 1993)*, one skewed steel-free deck slab *(Bakht et al. 1995)*, and seven full-scale steel-free bridge deck models *(Thorburn 1998, Newhook 1997)*. The comparison of the experimental punching failure load and analytical punching failure loads obtained using the PUNCH and FEM PUNCH programs are presented in Table 15. The analytical results suggested that both the PUNCH and FEM PUNCH programs can predict the punching failure load very accurately.

Table 15: Comparison of experimental and theoretical results

Test #	f'_c, MPa	Girder spacing, mm	Deck depth, mm	Straps, mm^2 @ mm (Total mm^2)	Experiment	PUNCH Program			FEM PUNCH Program		
					P_{exp}, kN	K, N/mm/mm	P_{Theor}, kN	P_{Theor} / P_{exp}	SprX & SprY , N/mm	P_{Theor}, kN	P_{Theor} / P_{exp}
Half-scale steel-free deck models											
1	46	1067	100	640 @ 457 (5120)	418	630	413	0.99	40,000	440	1.05
2	42	1067	100	640 @ 457 (5120)	418	630	407	0.97	40,000	410	0.98
3	43	1075	95	640 @ 457 (4480)	370, 388	630	354	0.96, 0.91	40,000	350	0.95, 0.90
4	51	1075	95	640 @ 610 (4480)	313	472	309	0.99	35,000	330	1.05
Skewed steel-free deck model											
5	55	800	80	608 @ 400 (3648)	323, 352	921	385	1.19, 1.09	10,000	370	1.14, 1.05
Full-scale steel-free deck models											
6	27	2000	175	2500 @ 1000 (18850)	1127	705	1127	1.00	40,000	840	0.75
7	27	2000	175	1250 @ 1000 (18850)	923	460	913	0.99	40,000	870	0.94
8	27	2000	175	950 @ 1000 (18850)	911	370	814	0.89	40,000	840	0.92
9	27	2000	175	650 @ 1000 (15055)	844	300	727	0.86	35,000	860	1.02
10	27	2000	175	650 @ 1000 (11030)	576	300	727	1.26	25,000	710	1.23
11	27	2000	175	650 @ 1000 (11030)	715	300	727	1.02	25,000	710	0.99
12	39	2700	300	1250 @ 1200 (11250)	1275	297	1274	1.00	18,000	1350	1.06